Measurement Point Selection and Damping Identification of Blisks

by

Darren E. Holland

A dissertation submitted in partial fulfillment
of the requirements for the degree of
Doctor of Philosophy
(Mechanical Engineering)
in The University of Michigan
2012

Doctoral Committee:

Associate Professor Bogdan Epureanu, Chair
Professor Steven L. Ceccio
Professor Carlos E. Cesnik
Professor Gregory M. Hulbert
Visiting Research Scholar Matthew P. Castanier

To my wife, my family, and everyone who helped me survive these years.

ACKNOWLEDGEMENTS

I would like to express my gratitude for the mentorship and direction provided by Professor Steven Ceccio, Professor Bogdan Epureanu, and Dr. Matthew Castanier. They all served as advisors throughout my graduate studies, providing me with needed support and guidance.

I am also thankful for the sponsor GE Aviation through the University Strategic Alliance (USA) program, with Steve Manwaring as the subsection manager and Dave Bulman as the section manager. In particular, Dr. Sergio Filippi provided useful insight and brought the perspective of industry to this work.

Also, I appreciate all the support of my colleagues in the lab and GCF. You have caused joy and happiness when I feared enjoying life was impossible. In particular, I would like to thank Andy Madden for his ability to put up with me, make me laugh, and for the necessary trips to find food.

Throughout this time, my wife has been incredibly supportive, patient, loving, and so helpful during my graduate studies. She deserves more gratitude than I can express. I would also like to thank my parents and two brothers for their encouragement and love which I felt continuously.

TABLE OF CONTENTS

DEDICATION ii

ACKNOWLEDGEMENTS iii

LIST OF FIGURES vii

LIST OF APPENDICES ix

CHAPTER

I. Introduction 1

1.1 Dissertation Objective 1
1.2 Dissertation Background 4
1.3 Dissertation Outline 7

II. Structural Damping Identification for Mistuned Bladed Disks and Blisks 10

2.1 Introduction 10
2.2 Methodology 12
2.2.1 Reduced-Order Modeling 14
2.2.2 Simple Case of Isolated Modes 16
2.2.3 Measurement Data Filtering 16
2.3 Damping Identification Results 17
2.4 Discussion and Conclusions 20

III. Measurement Point Selection and Modal Damping Identification for Bladed Disks 24

3.1 Introduction 24
3.2 MPS Extensions 26
3.2.1 EIDV and Cyclic Symmetry 27
3.2.2 Residual Weighting 30

3.2.3 Optimized MPS . . . 33
3.3 Modal Damping . . . 34
3.3.1 Modal Damping Model . . . 35
3.3.2 Modal Damping Identification . . . 36
3.3.3 Identification Filtering . . . 38
3.4 Results . . . 39
3.5 Conclusions . . . 44

IV. Hybrid Modal Damping Identification for Bladed Disks and Blisks . . . 46

4.1 Introduction . . . 46
4.2 Modal Damping . . . 48
4.3 Modal Damping Identification using Calibration . . . 49
4.4 Relative Modal Damping Identification . . . 52
4.5 Measurement Noise . . . 54
4.6 Modal Damping Identification Procedure . . . 56
4.7 Forcing Cases and Frequency Windowing . . . 56
4.8 Frequency Windowing Results . . . 61
4.9 Damping Identification Results . . . 64
4.10 Conclusions . . . 70

V. Component Damping Identification Methods for Mistuned Blisks . . . 72

5.1 Introduction . . . 72
5.2 Equations of Motion . . . 74
5.3 Component Damping Response . . . 76
5.4 Component Damping Identification . . . 79
5.5 Refinements for Cyclically Symmetric Structures . . . 83
5.6 Damping Solution . . . 84
5.7 Modal Sensitivity to Component Damping . . . 88
5.8 Damping Identification Results and Discussion . . . 90
5.9 Conclusions . . . 95

VI. Proportional Component Damping Hybrid Identification . . . 97

6.1 Introduction . . . 97
6.2 Proportional Component Damping Hybrid Identification . . . 99
6.3 Relative Structural Damping Identification using Calibration 101
6.4 Component Damping Constant . . . 102

VII. Conclusions and Future Work . . . 104

7.1 Contributions . . . 104

7.2 Future Research 107
7.2.1 Simultaneous ID Method 1 108
7.2.2 Simultaneous ID Method 2 111

APPENDICES 115

BIBLIOGRAPHY 122

LIST OF FIGURES

Figure

2.1 Identified (ID) structural damping for the validation blisk using data with 1% relative noise 18

2.2 Identified (ID) structural damping for the validation blisk using data with 5% relative noise 19

2.3 Relative error of the identified damping as the error in the relative forcing increases 20

3.1 Optimized MPS algorithm 33

3.2 Sample forced response for the 30 DOF system 40

3.3 Damping ID for a 30 DOF system 41

3.4 Damping ID for validation blisk 43

4.1 Frequency windowing procedure 57

4.2 Shown are, for each target mode, the frequency of the mode, the number of measurement sets in its measurement window, and the number of modes in its mode window 62

4.3 Mean identified (ID) damping for the validation blisk using data with 5% (a) and 10% (b) relative noise; mistuned modes are ordered by increasing frequency 66

4.4 Standard deviation (Std) of identified (ID) damping for the validation blisk using data with 5% (a) and 10% (b) relative noise; mistuned modes are ordered by increasing frequency 66

4.5 Mean identified (ID) damping for the two methods using data with 5% (a) and 10% (b) relative noise; mistuned modes are ordered by increasing frequency 68

4.6 Standard deviation (Std) of identified damping (ID) for the two methods using data with 5% (a) and 10% (b) relative noise; mistuned modes are ordered by increasing frequency 68

4.7 Variation in identified damping due to error in forcing 69

5.1 Algorithm for augmenting damping identification matrices 86

5.2 Mean values and standard deviations of the identified damping for the case of (a) 1% relative measurement noise and (b) 5% relative measurement noise 92

5.3 Relative (a) and normalized (b) error in the forced response predicted by using the identified damping for the case of 5% measurement noise 92

5.4 Mean values and standard deviations of the identified damping for the case of 1% relative, bias and absolute measurement noise 94

5.5 Modal damping identification of blisk with component damping . . 94

B.1 Mode window description 120

LIST OF APPENDICES

Appendix

A. Simple Case of Isolated Modes 116

B. Mode Window Calculation 120

CHAPTER I

Introduction

1.1 Dissertation Objective

System identification is an important precursor to predicting the dynamics of a structure. These predictions are important to structural design and health monitoring, because they indicate the behavior of the system under operating conditions. In turbomachinery, one important structure is an integrally bladed disk or blisk. These blisks have a complex geometry and are comprised of one piece of material. Capturing the motion of such complex structures can be very difficult and typically involves finite element models with a large number of degrees of freedom (DOFs). These models employ parameters which are often not well known, for example the actual mass and stiffness of the physical structure. Another such parameter is damping. Thus, identification techniques are needed to determine the actual damping. In addition, these methods require measurements of the vibratory response of the structure. In general, using more measurement points results in a more accurate identification. However, as the number of measurement locations increases, the cost of the experimental work increases greatly. This work introduces a measurement point selection method which will result in an accurate system identification with minimal experimental and computational cost.

Also, blisks can be subjected to harsh environments with a large number of cycles.

Therefore, due to wear or manufacturing, nominally cyclically symmetric blisks have slight variations in the mass or stiffness of their components known as mistuning. As a result, the cyclic symmetry is destroyed and vibration energy can be localized around certain regions of the system leading to a larger than expected forced response as compared to their analog cyclically symmetric (or tuned) structures. Therefore, the mistuned structure is more susceptible to high cycle fatigue and earlier failure than the tuned structure. Damping plays an important role in investigating the effects of localization, because damping affects the forced response of a mistuned system (in particular, it affects the maximum response amplitude).

Current damping identification methods assume that accurate measurement data has been measured, but they do not provide information on how this assumption is realized. The measurement locations may be one cause of current identification techniques' sensitivity to measurement noise. In addition, damping can be difficult to determine for regions of high modal density, requiring knowledge of complex eigenvalues and eigenvectors, or knowledge of the actual forcing that is applied to the structure.

The focus of this work is identification of damping in systems with high modal density (such as cyclically symmetric structures) exemplified by blisks and bladed disks. These systems contain eigenvalues which are very closely grouped, so multiple modes contribute to the off-resonant responses. For these systems, accurately determining the complex mode shapes for all contributing modes (as needed for some current damping identification methodologies) is impractical.

Other iterative damping identification procedures identify the mass, stiffness, and damping matrices simultaneously. For high modal density, such approaches lead to very high noise sensitivity because of the near-singular nature of the inverse problem. Moreover, many existing techniques for damping identification focus on measurements collected at resonant conditions. Such conditions are easily identified for low modal

densities. However, resonances are nearly impossible to identify from measurements in the case of high modal density. This difficulty occurs because large responses are observed between resonant or natural frequencies.

Most current damping identification techniques assume that damping has a certain form at a system level. For example, the damping in complex structures is often assumed to be viscous, modal, or structural. Such assumptions provide accurate results for structures with relatively simple geometries and low modal density. However, these approximations can be cumbersome or inaccurate for structures with complex geometry and high modal density. For such systems, using a component-oriented model can be more effective. In particular, component damping corresponds to a proportional or structural damping applied to individual components of a structure (i.e., each component has an associated material damping). For instance, each blade of a blisk can be modeled as a separate component with an associated damping parameter (which is to be identified). The resulting damping is only approximately modal, and the corresponding modal damping values vary with different component damping properties. As a result, the component damping can represent the physical attributes of the structure more closely and may require less effort than identifying the modal damping for a structure with a moderate number of components and a large number of modes in the frequency range of interest. This work aims to introduce damping identification methods

- For structural, viscous modal, and component damping models
- Which use a new measurement point selection method
- Which apply to mistuned systems
- Which avoid complications involved in measuring damped modal characteristics or applied forces

- Which accurately identify the damping using both full order models as well as reduced order models (ROMs)
- Which accurately identify the damping in the presence of measurement noise
- Which are equally effective for both low and high modal density cases
- Which identify the damping without knowledge of the absolute forcing
- Which capture the system dynamics.

1.2 Dissertation Background

Holland et al. [1] introduced a testing methodology for performing system identification of blisks. They included a procedure for choosing the order in which the blades are to be excited and the excitation (and measurement) frequencies so that the identification is accurate and requires as few measurements as possible. To choose measurement locations, the authors extended the effective independence distribution vector (EIDV) method to determine the minimum number and the best locations of the necessary measurements. The existing EIDV method [2] determines the amount of modal information provided by each point in a candidate set of measurement locations. However, this EIDV approach uses the full system model which requires a heavy computational effort. Thus, a novel extension that exploits the cyclic symmetry of blisks was developed in this research.

Applying a layer of material to the structure to induce or change the damping characteristics of the structure strongly affects its forced response. In an effort to minimize the effects of mistuning, this damping coating can be applied to a structure such as a mistuned blisk. However, Joshi et al. [3] found that the dynamics of the system can change to due variations in the thickness of the applied coating. To determine the effects of the damping coating, a damping identification technique is

needed which can determine the damping associated with individual components of a mistuned blisk before and after the coating is applied. Alternatively, as mistuning may significantly affect certain modes, the damping coatings should decrease the response of the desired modes.

The most basic methods represent the dynamics using a single DOF system [4–7]. Clearly, these methods have limited application to multi-DOF systems such as blisks. Another type of damping identification method is curve fitting. In 2005, Adhikari [8] proposed one such approach for the case of proportional damping. Other damping identification methods include wavelet analysis [9–12] and time-domain analysis [13, 14].

Still other methods use measurements of complex eigenvalues and complex eigenvectors. Some notable contributions to this type of identification come from Adhikari et al. [15–19], Minas and Inman [20], Ibrahim [21], Alvin et al. [22], Andrianne and Dimitriadis [23], Khalil et al. [24], and Pilkey and Inman [25]. The focus of this work is identification of damping in systems with high modal density (such as cyclically symmetric structures) exemplified by blisks. These systems contain eigenvalues which are very closely grouped, so multiple modes contribute to the off-resonant responses. For these systems, accurately determining the complex mode shapes for all contributing modes (as needed for these existing methodologies) is impractical.

Other methods utilize the full frequency response function (FRF), which requires the applied forcing to be known. Such methods include works by Chen et al. [26,27], Lee and Kim [28], Kim et al. [29], Fritzen [30], and Phani and Woodhouse [31].

Some current damping identification methods require energy measurements [32–34]. Statistical Energy Analysis (SEA) is one method for determining damping loss factors. In particular, this method is useful for high frequency ranges. However, this technique is limited as the damping is assumed to be known either from the power injection method (PIM) [32,33,35,36], power modulation [36] method, or wave

approach [37]. PIM and power modulation techniques require measuring energy for all the components which can be difficult or impossible to gather accurately. Wave theory only applies to periodic systems. Also, the SEA method can be time consuming if there are many components [36]. In addition, the accuracy of the SEA method depends on the modal density and the level of damping as is shown by Mace [38] and Yap and Woodhouse [39] respectively.

In general, the literature on the damping identification techniques considers low dimensional systems or systems with low modal density. Also, current methods do not use reduced order models (ROMs), and can be sensitive to measurement noise. Thus, current methods do not work well for damping identification for systems with regions of high modal density such as blisks.

There are three key observations which are applicable to damping identification of blisks. First, Holland et al. [1] provided a relative force calibration method based on reciprocity. Such calibration is necessary in cases where the applied forcing at a given frequency is only known relative to a reference forcing. In such cases, the actual magnitude of the reference forcing is unknown. The calibration method iteratively calibrates the excitation applied to each blade so that differences among the blade excitation magnitudes and phases can be minimized. Thus, the calibration ensures that the phases of the excitations applied to each of the blades can be accurately set for traveling wave excitation. The calibration algorithm uses the principle of reciprocity and involves solving a least squares problem to reduce the effects of measurement noise and uncertainty. Second, Yang and Griffin [40] found that slightly mistuned system modes can be well represented as a linear combination of tuned system modes within a region of high modal density. This relationship has been used in studying the effects of crack propagation [41–43] and multi-stage phenomena [44]. Therefore, it is reasonable to assume the optimal measurement locations for a set of tuned system modes of a blisk (in a frequency range of interest) are also the best locations for

the slightly mistuned blisk. Finally, mistuning identification methods [45–50] identify structural (mass and stiffness) variations, but must assume that either the damping can be ignored, is known, or can be solved simultaneously. In particular, the CMM method [48, 49] identifies the variation in the mass or stiffness matrix based on a finite element model without knowledge of the actual damping. Therefore, the mass and stiffness matrices for the mistuned system can be identified prior to the damping identification and the only unknown structural parameters to be identified are the damping coefficients.

1.3 Dissertation Outline

Chapter II introduces a general methodology for identifying (uniform) structural damping. This method uses undamped tuned system mode shapes. A minimum of two frequency responses must be measured. Next, a more general methodology is formulated, which incorporates stiffness mistuning and uses ROMs for enhanced robustness and fast calculations. Then, it is shown that the proposed method can reduce to the half-power method for isolated modes. Finally, two data filtering approaches are proposed to enhance the accuracy of the identification in the presence of measurement noise. The damping identification methodology is demonstrated together with the two measurement filters for a one-piece bladed disk with stiffness mistuning. Results of a study are presented which explore the damping identification sensitivity to forcing errors. The chapter finishes with a discussion regarding the proposed damping and other techniques that also identify one damping value per system.

Chapter III presents a measurement point selection (MPS) technique for blisks and applies it to a new modal damping identification method. First, a modified form of the original effective independence distribution vector (EIDV) method presented by Penny et al. [2] and adapted by Holland et al. [1] is discussed. Then, a residual

weighting is introduced to optimize the MPS technique by ranking individual measurement locations according to their noise sensitivity. In addition, an algorithm is presented which describes an effective procedure incorporating the MPS method into experiment preparation for complex structures.

Next, a new method to identify damping parameters for each mode in a frequency range of interest is presented. This method utilizes the proposed MPS technique to increase the accuracy of the identification. Measurement locations and modal damping results for a 30 degree of freedom system and a blisk with a complex geometry are presented. Then, the modal damping identification results using a numerical simulation of a low dimensional system and the University of Michigan validation blisk with respect to several ROMs of various sizes and various noise levels are presented. Finally, results utilizing the optimized MPS technique are provided.

Chapter IV introduces an alternate modal damping identification method. First, the damping identification is formulated using the frequency response matrix (FRM). This method identifies the damping by generalizing the FRM to retain only the measured degrees of freedom and the forcing which can be applied. Then, frequency windowing is introduced which can reduce the effects of measurement noise and also lower the number of required forcing cases. Next, the proposed method is extended to identify damping using the knowledge of the relative forcing instead of the actual forcing. The modal damping identification procedure is summarized followed by an example of the frequency windows. Then, results for a validation blisk are presented with respect to various measurement noise levels. A comparison of the proposed method with the alternative method in Chapter III is also presented. Finally, results of a study are presented which explore the damping identification sensitivity to forcing errors.

Chapter V presents a component damping identification technique which can be applied to mistuned systems and use ROMs for regions of low and/or high modal

density. First, the forced response equation is developed using Lagrange's equation with the addition of Rayleigh damping. Next, the component damping identification method is formulated for general systems. Then, specific forms of the identification equation are given for cases of structural damping, uniform damping, and cyclically symmetric structures. An identification procedure is introduced to reduce the effects of measurement noise and allow the identification to use smaller ROMs. Finally, results are provided for the University of Michigan validation blisk for various measurement noise levels.

Chapter VI introduces an alternate component damping identification method, which utilizes the reduced frequency response matrix and the known forcing. This method is extended by requiring only knowledge of the relative forcing.

Chapter VII summarizes the contributions of the work in this dissertation, offers suggestions for future work, and presents two potential methods for simultaneous mistuning and damping identification.

CHAPTER II

Structural Damping Identification for Mistuned Bladed Disks and Blisks

2.1 Introduction

To accurately predict the dynamics of most structures, a representation of damping must be used. This paper focuses on structural damping and the identification of structural damping for complex systems with cyclic symmetry such as bladed disks and integrated (one-piece) bladed disks (blisks) with mistuning. Mistuning represents variations in mass or stiffness (compared to the tuned system) which destroys cyclic symmetry and may cause localization of vibration energy. This localization leads to a larger response in portions of the structure. As a result, the mistuned structure is more susceptible to high cycle fatigue and earlier failure than the tuned structure. Mistuning identification methods [45–50] identify these structural variations, but must assume that the damping can be ignored, is known, or solve for the damping simultaneously. Furthermore, forced response predictions depend crucially on accurate knowledge of damping. These issues are particularly critical when damping coatings are used. Such coatings are increasingly used in turbomachinery applications. Applying a layer of material to the structure to induce or change the damping characteristics of the structure strongly affects its forced response. Hence,

to accurately determine the effects of the coatings, damping must be accurately identified.

Several methods are currently available for damping identification [6, 7, 14–20, 22, 26–29]. Notably, the steady-state and transient decay (such as Schroeder's integrated impulse [4, 33]) methods as well as the power injection method are available [32, 33]. Most of these techniques are designed for low dimensional systems or for systems with low modal density. Also, most of these techniques can be grouped into two types based on the nature of the system information that they require [31, 34]. The first type involves measuring damped eigenvalues and mode shapes, and does not require knowledge of the system excitation. The second type involves measuring the forces applied to the system and constructing (full) frequency response functions.

Herein, an alternate structural damping identification method specifically tailored for systems with high modal density (such as bladed disks and blisks) is presented. The approach is robust with respect to measurement noise and makes use of highly effective reduced order models (ROMs). In contrast to existing techniques, the proposed method also avoids complications involved in measuring damped modal characteristics (damped eigenvalues/eigenvectors) or applied forces, while identifying structural damping only from displacement or velocity measurements.

First, a novel, general methodology for identifying (uniform) structural damping is presented. This method uses undamped tuned system mode shapes and a minimum of two frequency responses must be measured. Next, a more general methodology is formulated, which incorporates stiffness mistuning and uses ROMs for enhanced robustness and fast calculations. Finally, two data filtering approaches are proposed to enhance the accuracy of the identification in the presence of measurement noise. The first filter applies to measurements which are approximately equal in amplitude and phase although they occur at different frequencies. The second filter removes measurements where the magnitude of the response is low.

2.2 Methodology

The equation of motion for a structure with uniform structural damping can be expressed as

$$-\omega_i^2 \mathbf{M}\mathbf{x}_i + (1 + j\gamma)\,\mathbf{K}\mathbf{x}_i = \mathbf{F}_i, \tag{2.1}$$

where $\mathbf{M}$ is the mass matrix, $\mathbf{K}$ is the stiffness matrix, $\gamma \in \Re$ is the structural damping, j is $\sqrt{-1}$, $\mathbf{x}_i$ is the displacement (vector), and $\mathbf{F}_i$ is the applied forcing (vector) for a harmonic excitation with index i and frequency ω_i.

The proposed damping identification approach assumes that the mass and stiffness matrices have already been identified and are known. This assumption implies that it is possible to identify the mistuning simultaneously with the damping or without knowledge of the damping. Three such methods, available for the mistuning identification, are the SNM method proposed by Griffin et al. [45–47], the CMM method of Lim et al. [48, 49], and a method proposed by Mignolet et al. [50]. In particular, the CMM method identifies the variation in the mass or stiffness matrix based on a finite element model (without knowledge of the damping). Therefore, the mass and stiffness matrices for the mistuned system can be known prior to the damping identification discussed herein.

Next, consider another excitation (of index k). Assuming that the applied forces $\mathbf{F}_i$ and $\mathbf{F}_k$ are harmonic and have the same spatial distribution (but can have different amplitudes, phases, and frequencies), one obtains $\mathbf{F}_i = \alpha_k \mathbf{F}_k$, and

$$-\alpha_k \omega_k^2 \mathbf{M}\mathbf{x}_k + \alpha_k\,(1 + j\gamma)\,\mathbf{K}\mathbf{x}_k = \alpha_k \mathbf{F}_k = \mathbf{F}_i, \tag{2.2}$$

where $\alpha_k \in \mathbb{C}$. Next, combining Eqns. (2.1) and (2.2), one obtains

$$-\omega_i^2 \mathbf{M}\mathbf{x}_i + (1 + j\gamma)\,\mathbf{K}\mathbf{x}_i = -\alpha_k \omega_k^2 \mathbf{M}\mathbf{x}_k + \alpha_k\,(1 + j\gamma)\,\mathbf{K}\mathbf{x}_k.$$

This equation sequentially leads to

$$(1+j\gamma)\,\mathbf{K}\left[\mathbf{x}_i-\alpha_k\mathbf{x}_k\right]=\mathbf{M}\left[\omega_i^2\mathbf{x}_i-\alpha_k\omega_k^2\mathbf{x}_k\right],$$
$$(1+j\gamma)\left[\mathbf{x}_i-\alpha_k\mathbf{x}_k\right]=\mathbf{K}^{-1}\mathbf{M}\left[\omega_i^2\mathbf{x}_i-\alpha_k\omega_k^2\mathbf{x}_k\right]. \tag{2.3}$$

Consider the physical to mistuned modal coordinate transformation matrix $\mathbf{\Phi\Psi}$, where $\mathbf{\Phi}$ is a matrix containing the tuned eigenvectors. $\mathbf{\Psi}$ is the transformation matrix from tuned coordinates to mistuned coordinates under the assumption that the mistuned modes are a linear combination of the tuned system modes. This assumption holds for systems with small mistuning [45, 48]. Note that $\mathbf{\Psi}=\mathbf{I}$ for a tuned system. Both $\mathbf{\Phi}$ and $\mathbf{\Psi}$ contain the *complete* set of eigenvectors of the entire structure (e.g., an entire blisk). The relationship between physical ($\mathbf{x}$) and modal ($\mathbf{p}$) coordinates is given by $\mathbf{x}=\mathbf{\Phi\Psi p}$. Note also that

$$\mathbf{\Phi}^T\mathbf{K\Phi}=\tilde{\mathbf{K}}\text{ and }\mathbf{\Phi}^T\mathbf{M\Phi}=\tilde{\mathbf{M}}, \tag{2.4}$$

so

$$\mathbf{K}^{-1}=\mathbf{\Phi\Psi}\tilde{\mathbf{K}}^{-1}\mathbf{\Psi}^T\mathbf{\Phi}^T\text{ and }\mathbf{M}=\mathbf{\Phi}^{-T}\mathbf{\Psi}^{-T}\tilde{\mathbf{M}}\mathbf{\Psi}^{-1}\mathbf{\Phi}^{-1},$$

where $\tilde{\mathbf{K}}$ and $\tilde{\mathbf{M}}$ are the modal stiffness and mass diagonal matrices, $^{-1}$ indicates the inverse, and $^{-T}$ is the inverse transpose. Substituting these terms into Eqns. (2.1) and (2.2), pre-multiplying by $\mathbf{\Psi}^{-1}\mathbf{\Phi}^{-1}$, and using $\mathbf{p}=\mathbf{\Psi}^{-1}\mathbf{\Phi}^{-1}\mathbf{x}$, one obtains

$$(1+j\gamma)\left[\mathbf{p}_i-\alpha_k\mathbf{p}_k\right]=\tilde{\mathbf{K}}^{-1}\tilde{\mathbf{M}}\left[\omega_i^2\mathbf{p}_i-\alpha_k\omega_k^2\mathbf{p}_k\right]. \tag{2.5}$$

Equation (2.5) can be interpreted as a least-squares problem of the form $\mathbf{a}\gamma=\mathbf{b}$ (with $\mathbf{a}$ and $\mathbf{b}$ being vectors and γ a scalar). Note that $\mathbf{p}_i$, $\mathbf{p}_k$ and α_k are (in general) complex numbers.

2.2.1 Reduced-Order Modeling

The methodology presented in the previous section uses all mode shapes and all (N) degrees of freedom (DOFs) of the system. This section presents the justification for using a ROM where the system is modeled by a truncated set of modes, and a truncated set of DOFs.

The structural response to forcing $\mathbf{F}_i$ can be expressed in modal coordinates as $\mathbf{p}_i = \left[\mathbf{p}_i^1 \ \ldots \mathbf{p}_i^v \ \ldots \mathbf{p}_i^N\right]^T$. Next, consider that the forcing $\mathbf{F}_i$ is in a frequency range where a particular mode v contributes very little to the response. Hence, $\mathbf{p}_i^v \approx 0$. Since $\tilde{\mathbf{K}}$ and $\tilde{\mathbf{M}}$ are diagonal, the entries of index v in these matrices can be replaced with zeros. Therefore, mode v may be removed along with the corresponding diagonal entries of $\tilde{\mathbf{K}}$ and $\tilde{\mathbf{M}}$. This process can be done for all modes which contribute little to the response in a given frequency range. So, $(\mathbf{\Phi\Psi})_{n\times m}\,(\tilde{\mathbf{p}}_i)_{m\times 1} \approx (\mathbf{x}_i)_{n\times 1}$, where n is the number of measurement DOFs and m is the number of responding modes. Then, for a ROM, $\mathbf{\Phi}$ is a matrix of size $n \times N$, and $\mathbf{\Psi}$ is of size $N \times m$. Next, assuming that the space spanned by the m mistuned eigenvectors in the frequency range of interest can be represented by the truncated set of q tuned system modes $\mathbf{\Phi}_{n\times q}$ [45, 48], the matrices $\mathbf{\Phi}_{n\times N}$ and $\mathbf{\Psi}_{N\times m}$ may be reduced to $\mathbf{\Phi}_{n\times q}$ and $\mathbf{\Psi}_{q\times m}$.

Solving the least squares problem in Eqn. (2.5) and taking the imaginary and real parts, the key equations used for a mistuned system modeled using a ROM can be expressed as

$$\gamma = Im\left\{\left([\mathbf{p}_i - \alpha_k\mathbf{p}_k]_{1\times m}^T\,[\mathbf{p}_i - \alpha_k\mathbf{p}_k]_{m\times 1}\right)^{-1}\ [\mathbf{p}_i - \alpha_k\mathbf{p}_k]_{m\times 1}^T\,\tilde{\mathbf{K}}_{mist_{m\times m}}^{-1}\ \left[\omega_i^2\mathbf{p}_i - \alpha_k\omega_k^2\mathbf{p}_k\right]_{m\times 1}\right\}, \tag{2.6}$$

$$1 = Re\left\{\left([\mathbf{p}_i - \alpha_k\mathbf{p}_k]_{1\times m}^T\,[\mathbf{p}_i - \alpha_k\mathbf{p}_k]_{m\times 1}\right)^{-1}\ [\mathbf{p}_i - \alpha_k\mathbf{p}_k]_{1\times m}^T\,\tilde{\mathbf{K}}_{mist_{m\times m}}^{-1}\ \left[\omega_i^2\mathbf{p}_i - \alpha_k\omega_k^2\mathbf{p}_k\right]_{m\times 1}\right\}, \tag{2.7}$$

where $\tilde{\mathbf{K}}^{-1}_{mist_{m\times m}}$ is the diagonal mistuned stiffness matrix in mistuned modal coordinates. Equation (2.6) can be used to determine γ. Equation (2.7) can serve to ascertain the accuracy of the model and that of the modal amplitudes $\mathbf{p}_i$ and $\mathbf{p}_k$.

For a system with stiffness mistuning, the stiffness matrix in tuned system modal coordinates is not diagonal, but full. This full matrix is denoted by $\bar{\mathbf{K}}_{mist_{N\times N}}$ such that $\mathbf{\Psi}^T_{m\times m}\bar{\mathbf{K}}_{mist_{N\times N}}\mathbf{\Psi}_{N\times N} = \tilde{\mathbf{K}}_{mist_{N\times N}}$. In general, $\mathbf{\Phi}_{N\times N}$ is mass normalized. Therefore, one obtains successively

$$\begin{aligned}\mathbf{\Psi}\bar{\mathbf{K}}^{-1}_{mist}\bar{\mathbf{M}}\mathbf{\Psi}^{-1} &= \mathbf{\Psi}\bar{\mathbf{K}}^{-1}_{mist}\mathbf{\Psi}^T\mathbf{\Psi}\mathbf{\Psi}^{-1}\\ &\approx \mathbf{\Psi}_{m\times m}\bar{\mathbf{K}}^{-1}_{mist_{m\times m}}\mathbf{\Psi}^T_{m\times m}\\ &\approx \tilde{\mathbf{K}}^{-1}_{mist_{m\times m}}.\end{aligned}$$

Solving the least squares problem in Eqn. (2.5) and taking the imaginary and real parts in tuned modal coordinates, where $\mathbf{p} = \mathbf{\Psi}^{-1}\mathbf{q}$ the key equations used for a mistuned system modeled using a ROM can be expressed as

$$\begin{aligned}\gamma \approx Im\Bigg\{\Big([\mathbf{q}_i - \alpha_k\mathbf{q}_k]^T_{1\times m}[\mathbf{q}_i - \alpha_k\mathbf{q}_k]_{m\times 1}\Big)^{-1}\ &[\mathbf{q}_i - \alpha_k\mathbf{q}_k]^T_{m\times 1}\tilde{\mathbf{K}}^{-1}_{mist_{m\times m}}\\ &\left[\omega_i^2\mathbf{q}_i - \alpha_k\omega_k^2\mathbf{q}_k\right]_{m\times 1}\Bigg\},\end{aligned} \tag{2.8}$$

$$\begin{aligned}1 \approx Re\Bigg\{\Big([\mathbf{q}_i - \alpha_k\mathbf{q}_k]^T_{1\times m}[\mathbf{q}_i - \alpha_k\mathbf{q}_k]_{m\times 1}\Big)^{-1}\ &[\mathbf{q}_i - \alpha_k\mathbf{q}_k]^T_{1\times m}\tilde{\mathbf{K}}^{-1}_{mist_{m\times m}}\\ &\left[\omega_i^2\mathbf{q}_i - \alpha_k\omega_k^2\mathbf{q}_k\right]_{m\times 1}\Bigg\},\end{aligned} \tag{2.9}$$

where $\mathbf{q}_i$ and $\mathbf{q}_k$ are the modal amplitudes at frequencies i and k respectively. The equation above highlights that the mistuned system modes $\mathbf{\Psi}$ are not required for the damping identification of a mistuned system in tuned modal coordinates.

The accuracy of the damping identification depends on the accuracy of the modal amplitudes $\mathbf{p}$ or $\mathbf{q}$ obtained from measurements. Therefore, methods for determining accurate $\mathbf{p}$ or $\mathbf{q}$ values from physical measurements must be used, such as those

proposed by Madden et al. [49].

2.2.2 Simple Case of Isolated Modes

A mode whose resonant response does not contain a response of any other mode is referred to as an isolated mode. An isolated mode is easily identifiable because its frequency is not near the frequencies of all the other modes. First, assume that the forced response for an isolated mode has been measured. Then, assume that measurements happen to be collected at the half-power frequencies for the isolated mode. Assuming that the forcing is constant and γ is small, the proposed method can be shown to reduce to the well-known half-power method for a single DOF system. See Appendix A for more information. Namely, for cases where γ is small, Eqn. (2.5) becomes

$$\gamma = \frac{\omega_2^2 - \omega_1^2}{2\ \omega_n^2} = \frac{\omega_2 - \omega_1}{\omega_n}\frac{\omega_2 + \omega_1}{2\omega_n} \approx \frac{\omega_2 - \omega_1}{\omega_n}. \tag{2.10}$$

2.2.3 Measurement Data Filtering

Examining Eqn. (2.6) reveals two types of measurement data where the damping identification may not be accurate. The first corresponds to cases where the two responses $\mathbf{x}_i$ and $\mathbf{x}_k$ appear to be very similar although they correspond to two different frequencies. This situation occurs when $\mathbf{x}_i - \alpha_k \mathbf{x}_k \approx 0$. For this case, measurement noise dominates the differences in the responses and causes an erroneous identification. To alleviate this issue, the data used as input to the identification is filtered. Measurement pairs removed from the identification (indicated by superscript *rem*) meet the following condition

$$||\mathbf{x}_i^{rem} - \alpha \mathbf{x}_k^{rem}|| \leq \frac{T_c}{100} max_{k=1,\ldots n, i=1\ldots n} ||\mathbf{x}_i^{rem} - \alpha \mathbf{x}_k^{rem}||,$$

where $||\cdot||$ denotes the 2-norm, and T_c is a given threshold (e.g. 25% for the blisk example in Sec. 2.3).

The second type of measurement data corresponds to cases where the magnitude of the response is low. Previous forced response studies have shown that low responding data cannot be adequately captured by ROMs [51]. Hence, the damping identification which uses that information will not be accurate. All measurements removed from the damping identification meet the following condition

$$max_{u=1...n} \left|\mathbf{x}_{i,u}^{rem}\right| \leq \frac{T_l}{100} max_{\omega,u=1...n} \left|\mathbf{x}_{i,u}^{rem}\right|,$$

where $|\cdot|$ denotes the absolute value, u is the u^{th} DOF, and T_l is a given threshold (e.g. 25% for the blisk example in Sec. 2.3). Note also that the modal amplitudes $\mathbf{p}_i$ and $\mathbf{p}_k$ are collected after an elaborate and complex process of measurement point selection, mode selection, and data filtering similar to the one used by Madden et al. [49] (and omitted for the sake of brevity).

The parameters T_c and T_l can be estimated to remove noisy and low responding data from the identification. The general guideline for choosing these parameters is that they should be consistent with the signal to noise ratio of the measurements used for the identification. If T_c and T_l are chosen to be too high, insufficient data may be retained for the identification. In such as case, T_c and T_l can be changed, and the identification can be performed again.

2.3 Damping Identification Results

This section contains damping identification results from numerical simulations. The results are obtained for the University of Michigan validation blisk, and assume that the relative forcing is calibrated. Therefore, the relative magnitude and phase are the same (i.e. $\alpha_k = 1$).

The validation blisk is a 141,120 DOF model, has an applied stiffness mistuning pattern with values between ±5%, a structural damping of 0.00015, and a cyclic modeling error [51] (CME) of approximately 5%. The validation blisk is described in detail in [52].

For a correct identification, Eqn. (2.7) is exactly satisfied. In general, the residual of this equation indirectly reflects the accuracy of the damping model, the accuracy of the physical to modal transformation, and the quality of the measurement data. In the following, the identified damping results are sorted by increasing relative residual value from Eqn. (2.7). The minimum and maximum values correspond to the most and least accurate identified damping values respectively.

Measurement data was generated for the first flex family by ANSYS. Relative noise was injected in the measurement data as follows $x_{ab}^{noise} = \left(1 + \frac{N_{level}}{100} r\right) x_{ab}$, where r is a uniform random number between +1 and -1, x_{ab} is the response of the a^{th} DOF at the b^{th} frequency, and N_{level} is the maximum noise level as a percentage. The identification uses the data filtering discussed in Sec. 2.2.3. Damping was identified using the prescribed mistuning and CME values.

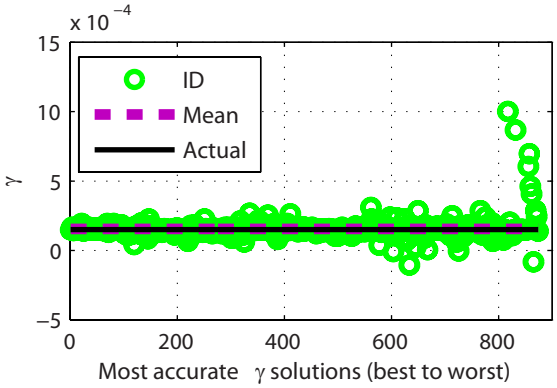

Figure 2.1: Identified (ID) structural damping for the validation blisk using data with 1% relative noise

Figures 2.1 and 2.2 show that the proposed method successfully identifies the blisk structural damping. Although the maximum relative errors are 420% and 568% for the 1% and 5% noise cases, the relative error of the average identified damping

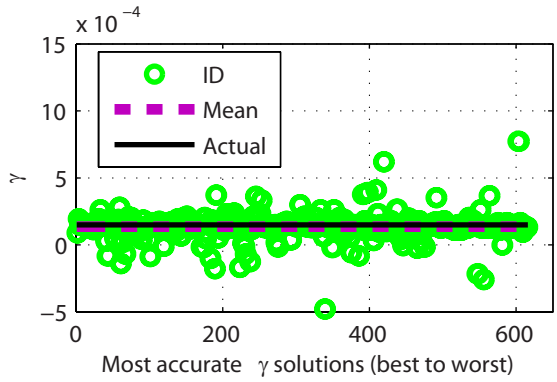

Figure 2.2: Identified (ID) structural damping for the validation blisk using data with 5% relative noise

is excellent, between 9.73% and 3.4% respectively. Note that the higher the residual in Eqn. (2.7) the more error is found in the identification. Thus, the proposed method can effectively establish (and rank) the quality of the results. Tighter measurement data filtering can improve accuracy and reduce the maximum relative errors by eliminating less accurate measurements. Overall, the proposed method accurately identifies the structural damping for the blisk. Similar results without noise and for 10% noise are included in [53].

Results for a smaller, 30 DOF system were also obtained and were presented previously [53]. It was found that the mean value of the identification cases provided accurate results when using a ROM and also with respect to measurement noise.

One of the assumptions of the damping identification method is that the relative forcing is known for a given frequency range. One way to obtain this information for a frequency band is to use the frequency transfer function for each speaker/magnet used for excitation, and assume that the force applied to the structure is proportional to the output of the speakers/magnets. To study the effects of errors in the transfer function or in the output of the speakers/magnets, the applied forcing was varied using $F(\omega) = 100[1 + \alpha_{error}/100 r_1(\omega)] + j\alpha_{error} r_2(\omega)$ (measured in mN), where $r_1(\omega)$ and $r_2(\omega)$ are random numbers drawn from a uniform distribution between -1 and 1. The nominal applied force is 100 mN. Therefore, the maximum amplitude errors

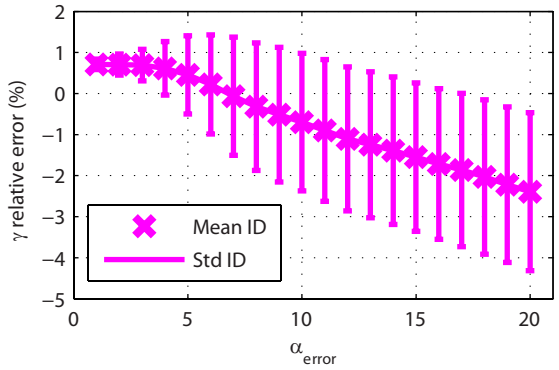

Figure 2.3: Relative error of the identified damping as the error in the relative forcing increases

considered are large, with values up to 22%. The maximum phase angle errors are also large, with values up to $\pm 14°$. 1000 realizations were calculated for α_{error} from 1 to 20.

Figure 4.7 shows the results for α_{error} from 1 to 20. The x-axis displays the α_{error} value, while the y-axis displays the relative error between the actual and the mean identified structural damping. The mean identification errors introduced by these simulated errors in α_k are below 2.4%. These low errors are for large errors up to 20% in the relative forcing coefficient. Surprisingly, Fig. 2.3 shows that the mean error in the identification decreases as α_{error} approaches 7%. It is believed that this trend is due to the removal of low responding data in the measurement filtering. The standard deviation of the predictions increases as α_{error} increases. The maximum standard deviation occurs at 20% variation in the relative forcing and is less than 2%. In general, the identification error caused by variations in the relative forcing is smaller than the error introduced by measurement noise.

2.4 Discussion and Conclusions

A structural damping identification procedure, which only requires knowledge of the undamped system modes, damped forced responses, and the relative frequency

dependence of the forcing was presented. Using the proposed method to identify structural damping allows for more accurate forced response and high-cycle fatigue predictions, especially when mistuning is present in blisks.

Moreover, numerical results for a blisk with complex geometry show that the novel method successfully identifies structural damping using ROMs. Noise and other effects such as temperature (on the excitation electronics) can cause the excitation to vary over time. Any such characteristics can be accounted for by using non-unitary values for α_k for certain (or all) measurements. Furthermore, even if one would choose to operate with measurements where $\alpha_k \neq 1$, one could simply plug in the α_k values and the proposed algorithm will work with the same level of performance. This strategy holds for both cases of zero and non-zero noise.

Many systems such as blisks have high modal density. These systems contain eigenvalues which are very closely grouped, so multiple modes contribute to the off-resonant responses. For these systems, accurately determining the complex mode shapes for all contributing modes (as needed for some current damping identification methodologies) would be nearly impossible. Other iterative procedures identify the mass, stiffness, and damping matrices. For high modal density, such approaches lead to very high noise sensitivity because of the near-singular nature of the inverse problem. In contrast, the proposed method gains robustness by exploiting the fact that the response of the system is a linear combination of the tuned system modes. Moreover, many existing techniques for damping identification focus on measurements collected at resonant conditions. Such conditions are easily identified for low modal densities. However, resonances are nearly impossible to identify from measurements in the case of high modal density. This difficulty occurs because large responses are observed between resonant or natural frequencies. Thus, a key advantage of the proposed method is that it does not require measurements precisely at resonance. Surely, large responses are preferable (because of their favorable signal to noise ratio),

but they are not required to be precisely at resonant conditions. Furthermore, the proposed method is equally effective for both low and high modal density cases. In fact, the proposed method reduces to the half-power method for isolated modes. In contrast, the blisk example provided is a very difficult case for other methodologies because most current techniques do not apply to systems with high modal density.

In acoustics, there is another damping methodology which assumes that all modes in a frequency range of interest have the same decay time. For viscous damping, this assumption is equivalent to assuming either the mode natural frequencies are the same (the system behaves like a SDOF system) or the natural frequency for a given mode is inversely proportional to the viscous damping for that mode. For structural damping, the assumption is also equivalent to assuming either the the system behaves like a SDOF system or the natural frequency for a given mode is inversely proportional to $\sqrt{1/2\left(\sqrt{1+\gamma^2}-1\right)}$ [54] for that mode. Now, assume that a forcing is applied and then removed so that the structural behavior is a free response. Then, the equation of motion can be written as

$$\mathbf{M}\ddot{\mathbf{x}} + (1 + j\gamma)\,\mathbf{K}\mathbf{x} = \mathbf{0}$$

Further, assume that the applied forcing is frequency filtered so that only modes in the frequency range of interest are forced.

In general, the similar damping identification methods assume that the modes which participate in the free response of the system have the same decay time [4]. This assumption is equivalent to fitting the exponential decay to a single-degree-of-freedom system or that the natural frequency of each mode is inversely proportional to a damping parameter (ζ for viscous damping and a function of γ for structural damping). Both of these assumptions are non-physical. Conversely, the proposed method allows for multiple time decays to occur in the response (as happens experimentally),

while identifying the damping. Therefore, the proposed method represents reality better than methods currently used in acoustics and the statistical energy analysis (SEA) subsystems. The benefit of the suggested methods is that the assumptions allow the energy loss to be identified without knowledge of natural frequencies or mode shapes. However, this method will become less accurate in two situations. The first corresponds to the frequency band containing a significant contribution from mode which is far from the centering frequency. The second situation occurs when the decay contains different decay times (as happens in actual systems). The proposed method does not have these limitations. In addition, both methods are limited to frequency bands where the damping and/or the frequency must be low enough to obtain a meaningful time decay.

It is found that the proposed method obtains more accurate results for energy loss identification and also has does not contain some of the limitations of the suggested techniques. However, it is recognized that the increase in accuracy (which is required for knowing the amplification of a mistuned system) and generalization results in a more complex methodology.

CHAPTER III

Measurement Point Selection and Modal Damping Identification for Bladed Disks

3.1 Introduction

Measuring the response of a structure is the first step in performing a system identification. Structures such as bladed disks and integrally bladed disks (blisks) have a complex geometry. Capturing the motion of such complex structures can be very difficult and typically involves finite element models with a large number of degrees of freedom (DOFs). Also, these models employ parameters which are often not well known; for example the actual mass and stiffness of the physical structure. Thus, identification techniques are needed to determine the actual system properties. Another such parameter and the focus of this work is damping. These identification techniques require measurements of the vibratory response of the structure. In general, increasing the number of measurement points increases the accuracy of the identification. However, as the number of measurement locations increases, the cost of the experimental work increases greatly. To address this issue, one may use the effective independence distribution vector (EIDV) method [2] which determines the amount of modal information provided by each point in a candidate set of measurement locations. Holland et al. [1] extended the EIDV method to determine the

minimum number and the best locations of the necessary measurements. This approach uses the full system model which requires a heavy computational effort. In this work, an optimized measurement point selection (MPS) technique is introduced to reduce the computational effort for blisks and to increase the robustness of the selection process.

Small sector-to-sector variations (mistuning) in the mass or stiffness of blisks can cause energy to be localized to certain regions of a blisk. This phenomenon results in an increase in the maximum vibration amplitudes and stresses compared to their analog cyclically symmetric (or tuned) structures. This difference can lead to high cycle fatigue failure. In an effort to minimize the effects of vibrations, damping coatings can be applied to these structures. As mistuning may significantly affect certain modes, the damping coatings should decrease the response of the desired modes. To determine the effectiveness of damping coatings, the modal damping of the system with and without the coating has to be determined. Current damping methods [4, 6, 7, 11, 12, 14–20, 22–24, 26–29] can be grouped into three categories. In general, the literature on these techniques considers low dimensional systems or systems with low modal density. The most basic methods represent the dynamics using a single DOF system [4]. The methods in the second category require measuring damped eigenvalues and mode shapes, and do not require measurements of the excitation. In contrast, the focus of this work is identification of damping in systems with high modal density (such as cyclically symmetric structures) exemplified by blisks. These systems contain eigenvalues which are very closely grouped, so multiple modes contribute to the off-resonant responses. For these systems, accurately determining the complex mode shapes for all contributing modes (as needed for these existing methodologies) is impractical. The methods in the third and last category require constructing (full) frequency response functions, and therefore require knowledge of the excitation. Herein, a novel modal damping identification method is presented

which accurately identifies the modal damping using noisy measurements, works well with both full order and reduced order models (ROMs) for (low and) high modal density cases, and only requires knowledge of how the *relative* forcing varies with frequency. Such forcing is obtained in many cases where the applied forcing at a given frequency is only known compared to a reference forcing, whereas the actual magnitude of the reference forcing is unknown.

Griffin et al. [40] found that slightly mistuned system modes can be well represented as a linear combination of tuned system modes. This relationship has been used to study the effects of crack propagation [41–43] and multi-stage phenomena [44]. Therefore, it is reasonable to assume that the optimized measurement locations for a set of tuned system modes of a blisk (in a frequency range of interest) are also the best locations for the slightly mistuned blisk. Moreover, the damping identification does not require cyclic symmetry. Therefore, the proposed MPS and damping methods apply to both cyclically symmetric and slightly mistuned systems.

3.2 MPS Extensions

Current damping identification methods assume that accurate measurement data has been measured, but they do not often provide information on how this assumption is realized. As such, the choice of measurement locations may be one cause of the sensitivity of current identification techniques to measurement noise.

In this section, the EIDV method [2] is extended in three different ways. First, the EIDV procedure is modified to take advantage of cyclic symmetry. Next, a residual weighting which considers the effects of noise is added to the EIDV method. Third, an algorithm is introduced to determine the measurement locations when the number of candidate DOF is very large.

3.2.1 EIDV and Cyclic Symmetry

The EIDV-based procedure presented by Holland et al. [1] uses the full tuned system modes to calculate the optimized measurement locations. When the model has many sectors with many candidate measurement locations, the matrices involved can become prohibitively large. For example, relatively small industrial blisks can easily lead to the need to handle matrices exceeding sizes of $10^4 \times 10^4$. However, using cyclic symmetry and exploiting the properties of the matrices involved in the EIDV procedure, one may redefine the minimum EIDV value and transform the method as to require only single sector calculations. As a result, the matrix sizes reduce from the total number of DOFs in all sectors of the system to the number of DOFs in a single sector. Therefore, the computational and memory costs are dramatically reduced. Next, we discuss such an EIDV-based method for structures with cyclic symmetry.

The EIDV vector [2] is defined as

$$\mathbf{EIDV}_a^{full} = diag\left(\mathbf{\Phi}\left[\mathbf{\Phi}^T\mathbf{\Phi}\right]^{-1}\mathbf{\Phi}^T\right), \tag{3.1}$$

where $\mathbf{\Phi}$ is a subset of tuned system modes in a frequency range of interest and *diag* refers to the diagonal entries of the enclosed matrix. Many such subsets can be chosen. To refer to one of these subsets, the subscript a is used to indicate the a^{th} subset.

Note that $\mathbf{\Phi}\left[\mathbf{\Phi}^T\mathbf{\Phi}\right]^{-1}\mathbf{\Phi}$ is idempotent and symmetric, and for a cyclically symmetric structure

$$\mathbf{\Phi} = (\mathbf{F} \otimes \mathbf{I}_{d\times d})\,\mathbf{\Phi}_{sec}, \tag{3.2}$$

where $\mathbf{F}$ is the real Fourier matrix [48] of size $s \times s$ (with s being the number of sectors in the system), d is the number of candidate DOFs in one sector, and $\mathbf{\Phi}_{sec}$ is a block diagonal matrix containing the a^{th} subset of tuned system modes for a single sector. For a blisk, each block in $\mathbf{\Phi}_{sec}$ corresponds to a different nodal diameter. Substituting

Eq. 3.2 into Eq. 3.1, one obtains

$$\mathbf{EIDV}_a^{full} = diag\left(\left[\mathbf{F}\otimes\mathbf{I}_{d\times d}\right]\mathbf{\Phi}_{sec}\left[\mathbf{\Phi}_{sec}^T\mathbf{\Phi}_{sec}\right]^{-1}\mathbf{\Phi}_{sec}^T\left[\mathbf{F}^T\otimes\mathbf{I}_{d\times d}\right]\right),$$

where $\mathbf{\Phi}_{sec}\left[\mathbf{\Phi}_{sec}^T\mathbf{\Phi}_{sec}\right]^{-1}\mathbf{\Phi}_{sec}^T$ is idempotent. The trace of any idempotent matrix is equal to its rank. This key observation [2] can be used to select as measurement DOFs the DOFs which correspond to the largest values on the diagonal of $\mathbf{EIDV}_a^{full}$. For a cyclically symmetric system, the entry of $\mathbf{EIDV}_a^{full}$ for a DOF on one sector is the same for all sectors. Hence, the same DOF that is chosen for one sector is also chosen as a measurement DOF for all the other sectors. Also, the rank of two matrices related through a similarity transformation is the same. Therefore, the cyclic expansion in Eq. 3.2 is not needed, and the first sector can provide all the required information. Now define

$$\mathbf{EIDV}_a^{sec} = diag\left(\mathbf{\Phi}_{sec}\left[\mathbf{\Phi}_{sec}^T\mathbf{\Phi}_{sec}\right]^{-1}\mathbf{\Phi}_{sec}^T\right).$$

Since $\mathbf{\Phi}_{sec}$ is block diagonal,

$$\mathbf{EIDV}_a^{sec} = diag\begin{bmatrix} \ddots & \mathbf{0} & \mathbf{0} \\ \mathbf{0} & \mathbf{A}_z\left[\mathbf{A}_z^T\mathbf{A}_z\right]^{-1}\mathbf{A}_z^T & \mathbf{0} \\ \mathbf{0} & \mathbf{0} & \ddots \end{bmatrix}, \tag{3.3}$$

where $\mathbf{A}_z$ is the z^{th} block of the a^{th} subset of tuned sector modes corresponding to the z^{th} nodal diameter. Each block of $\mathbf{EIDV}_a^{sec}$ is an idempotent matrix, where the diagonal values are the contribution of each DOF to the linear independence of that block of modes. Let

$$\mathbf{d}_{a,z} = diag\left(\mathbf{A}_z\left[\mathbf{A}_z^T\mathbf{A}_z\right]^{-1}\mathbf{A}_z^T\right). \tag{3.4}$$

The values in the vector $\mathbf{d}_{a,z}$ correspond to the candidate DOFs in one sector (for the

modes from $\mathbf{\Phi}_{sec}$) which have nodal diameter z. Therefore, one obtains

$$\mathbf{EIDV}_a^{sec} = \begin{bmatrix} \vdots \\ \mathbf{d}_{a,z} \\ \vdots \end{bmatrix}, \tag{3.5}$$

To further increase the efficiency of the method, one may note that only the diagonal entries in Eqn. (3.4) are retained. Therefore, the r^{th} diagonal entry is

$$d_{a,z}^r = diag\left(\mathbf{A}_z^T \tilde{\mathbf{A}}_z\right) = \sum_e A_z^{er} \tilde{A}_z^{er}, \tag{3.6}$$

where $\tilde{\mathbf{A}}_z = \left[\mathbf{A}_z^T \mathbf{A}_z\right]^{-1} \mathbf{A}_z^T$ and $\mathbf{A}_z^T$ are matrices of size $n \times d$, and n is the number of modes of nodal diameter z. The size of the largest matrix in the original EIDV method is $sd \times sd$, while the sector-level EIDV involves matrices of size $d \times \tilde{n}$ or less (where $\tilde{n}$ is the maximum number of modes over all z). Thus, one may express the reduction in memory required by the sector-level EIDV as

$$\%_{mem} = 100\left(1 - \frac{\tilde{n}}{s^2 d}\right). \tag{3.7}$$

For nodal diameters with mode pairs, $\mathbf{d}_{a,z}$ contains two values for each candidate DOF (otherwise $\mathbf{d}_{a,z}$ only contains one value per DOF). Therefore, let $\bar{\mathbf{d}}_{a,z}$ be a matrix where the b^{th} column contains the b^{th} occurrence of the candidate DOF in $\mathbf{d}_{a,z}$. If nodal diameter z has a single mode (not a pair), then $\bar{\mathbf{d}}_{a,z} = \mathbf{d}_{a,z}$. Hence, a key aspect is that the DOF corresponding to the minimum value of $\sum_b \bar{\mathbf{d}}_{a,z}^b$ contributes the least to the linear independence of the modes with nodal diameter z. Define the new EIDV value to be

$$\mathbf{EIDV}_a = \sum_z \sum_b \bar{\mathbf{d}}_{a,z}^b, \tag{3.8}$$

where b is a multiple of 2 for nodal diameters with mode pairs. Here, the sum of the

$\bar{\mathbf{d}}_{a,z}^{b}$ values is an indicator of the contribution of the candidate DOFs to the linear independence of the modes in the frequency range of interest. Similar to the original EIDV method [2], the new sector-level EIDV approach eliminates as a candidate DOF (one by one) the DOF (one on each sector) which corresponds to the lowest value in $\mathbf{EIDV}_a$.

The number of operations for the original EIDV method is $C_{orig} = 4m^2sd + 2s^2d^2m - m^2 - msd - s^2d^2$, where m is the number of modes in the frequency range of interest. At least one mode is included for each nodal diameter such that $z = 1...s$. Then, the computational cost for the sector-level EIDV method is $C_{sec} < m^2(2d-1) + 2dm^2 + d(m-s) + dm < 4m^2d + 2md$. Therefore, the reduction in the computational time is at least

$$\%_{time} = 100\left(1 - \frac{C_{sec}}{C_{orig}}\right) > 100\left(1 - \frac{2m+1}{s^2d\left(1-\frac{1}{2m}\right) + m\left(2s - \frac{1}{2d}\right) - \frac{s}{2}}\right). \quad (3.9)$$

Of course, one could also include the computational cost of the matrix inversion (for a given inversion method) in calculating $\tilde{\mathbf{A}}_z$ and the operations involved in creating and arranging the $\tilde{\mathbf{A}}_z$ matrices. Considering the inversion will increase the cost reduction, while including the cost of the matrix manipulations will decrease the cost reduction (as separate matrices for each nodal diameter are involved in the sector-level EIDV method).

3.2.2 Residual Weighting

To be robust and to provide accurate results, a MPS method must be insensitive to measurement noise. Therefore, we introduce a residual weighting which examines the error (associated with each measurement location) caused by noisy measurements. As damping identification depends on the modal transformation, this weighting considers the effect of the physical to modal and back to physical coordinate transformations

on noisy responses. The MPS (with residual weighting) is normally used for both mistuning identification [49] (not discussed here) as well as damping identification. First, a numerical forced response is performed at frequencies ω_y near the system natural frequencies. For increased computational efficiency, a ROM is used. To ensure that the selected measurement points are statistically optimized for any mistuning pattern (with some maximum mistuning in each blade), multiple forced responses are calculated. Each forced response is calculated for a random level of mistuning and cyclic modeling error [49] within model specific limits (e.g., between -5% and +5% mistuning). Noise is then injected into the calculated response to obtain surrogate data (one surrogate data set for each mistuning pattern and each noise realization) which mimic experimental data. The noise is modeled using

$$x^q_{noisy}(\omega_y) = x^q_{meas}(\omega_y) + N_p R^q_1 x^q_{meas}(\omega_y) + \frac{\sqrt{2}}{2} N_p R^q_2 \; max_{q=1\ldots DOF,y}\left(x^q_{meas}(\omega_y)\right), \tag{3.10}$$

where N_p is the maximum noise introduced, R^q_1 are randomly generated numbers drawn from a uniform distribution between -1 and 1, and R^q_2 are complex numbers composed of real and imaginary parts with values drawn from a uniform distribution between 0 and 1. R^q_1 introduces relative measurement noise, whereas R^q_2 introduces absolute and bias noise.

Let $x^q_{noisy}(\omega_y)$be the forced response of DOF q after noise has been injected into the actual (exact) response $x^q_{act}(\omega_y)$. Since the damping identification ignores low responding data, this data is removed from both the actual and the noisy data. Next, for each ω_y, the noisy responses of candidate DOF q are grouped in a vector $\mathbf{x}_{noisy}(\omega_y)$ for all q. Let $\mathbf{x}^a_{trans}(\omega_y) = \mathbf{\Phi}\left[\mathbf{\Phi}^T\mathbf{\Phi}\right]^{-1}\mathbf{\Phi}^T\mathbf{x}_{noisy}(\omega_y)$. The residual weighting for the

q^{th} candidate measurement DOF is defined as

$$Res_a^q = \frac{\epsilon + min_{q=1...DOF}\left(\sum_y \left|x_{act}^q(\omega_y) - x_{trans}^{a,q}(\omega_y)\right|\right)}{\epsilon + \sum_y \left|x_{act}^q(\omega_y) - x_{trans}^{a,q}(\omega_y)\right|}, \tag{3.11}$$

where $|\cdot|$ denotes the absolute value. The residual in Eq. 3.11 contains information about the sensitivity of the measurement locations to noise (when a specific ROM is used). Note that Res_a^q is a value between zero and 1. A low value of Res_a^q (close to zero) corresponds to a high sensitivity to noise. A high value of Res_a^q (close to 1) corresponds to a low sensitivity to noise.

In Eq. 3.11, the residual of the transformation from the physical to modal and back to physical coordinates $|x_{act}^q(\omega_y) - x_{trans}^{a,q}(\omega_y)|$ is calculated for each forced response case, and the mean value over the surrogate realizations is retained. As each sector contains the same measured DOFs, the final residual weighting value, $Res_{a,final}^q$ contains the minimum value of Res_a^q for DOF q over all the blades. This weighting cannot be done using sector-level calculations. However, as the residual is only calculated one time (for the set of all candidate DOFs) the residual weighting is less expensive computationally than the EIDV method.

The new MPS method combines the EIDV method with the residual weighting. Let

$$MPS_a^q = Res_{a,final}^q \; EIDV_a^q.$$

The minimum MPS_a^q corresponds to the DOF q (one on each blade) which contributes less to the linear independence of the modes and is more sensitive to noise than the other candidate locations. The best measurement locations for different ROMs can be easily obtained by determining MPS_a^q for $q = 1...DOF$ for the corresponding a^{th} set of modes in each ROM.

For DOFs with low residual weighting values, the MPS becomes dominated by

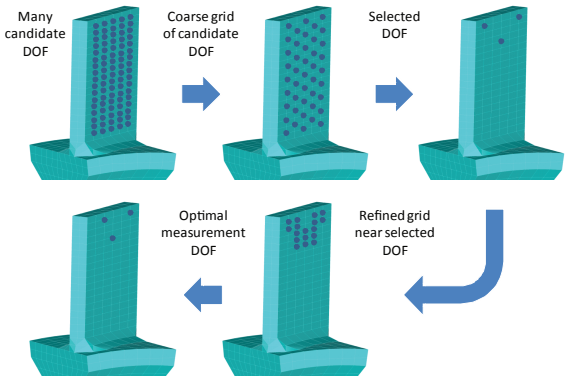

Figure 3.1: Optimized MPS algorithm

the residual weighting. For DOFs with high values in the residual weighting (close to 1), the MPS is dominated by the EIDV method. To achieve a balance between the noise sensitivity of each DOF and their contribution to the linear independence of the modes, ϵ is defined as

$$\epsilon = mean_{q=1...DOF,y} \left| x^q_{act} \left(\omega_y \right) \right| .$$

3.2.3 Optimized MPS

Next, the process of determining the best set of measurement points is described using an optimized MPS technique, as shown in Fig. 3.1. This algorithm is important even when using sector-level computations, and is particularly useful for structures with a large number of candidate DOF because additional reduction of the memory usage and the calculation cost are often necessary in such cases.

First, a set of candidate measurement locations is chosen. These locations should contain regions on the structure which are considered to be of interest and are physically possible to measure. Such locations may be chosen from a finite element model with a very fine mesh. Thus, it may be necessary to further sub-select from the candidate set. To do this sub-selection, the geometric information of the candidate points is used to choose a smaller set of locations where the reduced candidate measurement

locations are uniformly distributed over the structure. From the reduced candidate measurement locations, the MPS method determines an initial set of measurement locations. If desired, a local refinement step can be performed as follows. Taking all candidate locations (from the original set) that are in a region close to the previously chosen MPS points, one can define a new reduced set of candidate measurement locations. Applying the MPS method again on this new candidate set (containing only points near the previously chosen measurement points) provides a refined, optimized set of measurement locations.

3.3 Modal Damping

Mistuning identification methods [45–50] identify structural (mass and stiffness) variations, but must assume that either the damping can be ignored, is known, or can be solved simultaneously. In particular, the CMM method [48, 49] identifies the variation in the mass or stiffness matrix based on a finite element model without knowledge of the actual damping. Therefore, the damping identification approach herein assumes that mass and stiffness matrices for the mistuned system are identified prior to the damping identification and the only unknown structural parameters to be identified are the damping coefficients.

Next, a novel modal damping identification method is presented. This method identifies a damping parameter for each mode in a ROM. The formulation applies to both tuned and slightly mistuned systems as well as regions of low and high modal density. A key advantage of the proposed method is that it does not require measurements precisely at resonance. Large responses are preferable (because of their favorable signal to noise ratio), but they are not required to be precisely at resonant conditions.

3.3.1 Modal Damping Model

The equations of motion for a linear structure can be expressed as

$$\mathbf{M}\ddot{\bar{\mathbf{x}}} + \mathbf{C}\dot{\bar{\mathbf{x}}} + \mathbf{K}\bar{\mathbf{x}} = \bar{\mathbf{f}}, \tag{3.12}$$

where $\mathbf{M}$ is the mass matrix, $\mathbf{C}$ is the damping matrix, $\mathbf{K}$ is the stiffness matrix, $\bar{\mathbf{x}}$ is the response, and $\bar{\mathbf{f}}$ is the applied forcing. This forcing is assumed harmonic with amplitude $\mathbf{f}$ and frequency ω. Therefore, the physical response $\bar{\mathbf{x}}$ is harmonic and has a magnitude $\mathbf{x}$ given by

$$-\omega^2\mathbf{M}\mathbf{x} + j\omega\mathbf{C}\mathbf{x} + \mathbf{K}\mathbf{x} = \mathbf{f}, \tag{3.13}$$

where j is the imaginary unit.

Next, $\mathbf{x}$ is converted to tuned (or mistuned) modal coordinates p using $\mathbf{x} = \mathbf{\Phi\Psi p}$,where $\mathbf{\Phi}$ is a matrix containing the undamped tuned system normal modes. Note that for a mistuned system, $\mathbf{\Psi}$ is the transformation from tuned modal coordinates to mistuned coordinates under the assumption that the mistuned modes are a linear combination of tuned system modes [55]. For a tuned system $\mathbf{\Psi}$ is the identity matrix. Matrices $\mathbf{\Phi}$ and $\mathbf{\Psi}$ are of size $N \times N$, where $N$is the total number of DOF in the model (and is also the total number of system modes). Pre-multiplying Eq. 3.13 by $\mathbf{\Psi}^T\mathbf{\Phi}^T$, one obtains

$$-\omega^2\mathbf{p} + j\omega\mathbf{\Psi}^T\mathbf{\Phi}^T\mathbf{C}\mathbf{\Phi\Psi p} + \mathbf{\Lambda p} = \mathbf{\Psi}^T\mathbf{\Phi}^T\mathbf{f}, \tag{3.14}$$

where the tuned system modes are mass normalized, and $\mathbf{\Lambda} = \mathbf{\Psi}^T\mathbf{\Phi}^T\mathbf{K\Phi\Psi}$is a diagonal matrix containing the mistuned eigenvalues.

Let $\mathbf{C} = 2\mathbf{M\Phi\Psi}diag\left(\zeta_u/\omega_n^u\right)\mathbf{\Psi}^T\mathbf{\Phi}^T\mathbf{K}$, where $\zeta_u$is the viscous modal damping coefficient for mode u, and ω_n^u is the undamped natural frequency of mode u. For simplicity, let $\boldsymbol{\zeta} = diag\left(\zeta_u\omega_n^u\right)$. Next, assume that outside a given frequency range of

interest, $\mathbf{p}_v \approx 0$ for a known index set v. Then the columns of $\mathbf{\Phi\Psi}$ in set v can be ignored. So, $\mathbf{\Phi\Psi}$ reduces to a matrix of size $N \times m$,where m represents the number of modes in the frequency range of interest. These m modes are used to construct ROMs in the frequency range of interest. Also, for small mistuning the m mistuned modes are a linear combination of θtuned system modes in the frequency range of interest. Therefore, $\mathbf{\Phi}$ can be reduced to size $N \times \theta$ and $\mathbf{\Psi}$ can be reduced to size $\theta \times m$. The forced response can be obtained by solving

$$-\omega^2\mathbf{p} + 2j\omega\boldsymbol{\zeta}\mathbf{p} + \mathbf{\Lambda}\mathbf{p} = \mathbf{\Psi}^T\mathbf{\Phi}^T\mathbf{f} \tag{3.15}$$

for $\mathbf{p}$. Next, converting from $\mathbf{p}$ to $\mathbf{x}$, one obtains

$$\mathbf{x} = \mathbf{\Phi\Psi}\left[-\omega^2\mathbf{I} + 2j\omega\boldsymbol{\zeta} + \mathbf{\Lambda}\right]^{-1}\mathbf{\Psi}^T\mathbf{\Phi}^T\mathbf{f}. \tag{3.16}$$

3.3.2 Modal Damping Identification

When the forcing is applied (acoustically or magnetically) to a small area of the structure, the spatial forcing remains approximately the same at different frequencies. For excitations at frequencies ω_i and $\omega_k$such that $\mathbf{f}_i = \alpha_k\mathbf{f}_k$ (with known $\alpha_k \in \mathbb{C}$), Eq. 3.15 becomes

$$-\omega_i^2\mathbf{p}_i + 2j\omega_i\boldsymbol{\zeta}\mathbf{p}_i + \mathbf{\Lambda}\mathbf{p}_i = \mathbf{\Psi}^T\mathbf{\Phi}^T\mathbf{f}_i, \tag{3.17}$$

$$\text{and } -\omega_k^2\alpha_k\mathbf{p}_k + 2j\omega_k\boldsymbol{\zeta}\alpha_k\mathbf{p}_k + \mathbf{\Lambda}\alpha_k\mathbf{p}_k = \mathbf{\Psi}^T\mathbf{\Phi}^T\alpha_k\mathbf{f}_k. \tag{3.18}$$

Such forcing is obtained in many cases where the excitation applied at a given frequency is only known in relation to a reference forcing (at a different frequency), whereas the actual magnitude of the reference forcing is unknown. One way to approximate this relationship is to use the frequency transfer function for the speakers or magnets used to provide excitation. Then, one may assume that the force applied

to the structure is proportional to the excitation force for the given frequency band. Using Eq. 3.17, one obtains

$$2j\boldsymbol{\zeta}\left(\omega_i\mathbf{p}_i - \alpha_k\omega_k\mathbf{p}_k\right) = \omega_i^2\mathbf{p}_i - \omega_k^2\alpha_k\mathbf{p}_k - \boldsymbol{\Lambda}\left(\mathbf{p}_i - \alpha_k\mathbf{p}_k\right).$$

Rearranging $\boldsymbol{\zeta}\left(\omega_i\mathbf{p}_i - \alpha_k\omega_k\mathbf{p}_k\right)$ and recalling the definition of $\boldsymbol{\zeta}$, one obtains

$$2j\ diag\left(\omega_n^u\left[\omega_i p_{iu} - \alpha_k\omega_k p_{ku}\right]\right)\begin{bmatrix}\zeta_1\\ \vdots\\ \zeta_m\end{bmatrix} = \omega_i^2\mathbf{p}_i - \omega_k^2\alpha_k\mathbf{p}_k - \boldsymbol{\Lambda}\left(\mathbf{p}_i - \alpha_k\mathbf{p}_k\right), \quad (3.19)$$

where $diag\left(\omega_n^u\left[\omega_i p_{iu} - \alpha_k\omega_k p_{ku}\right]\right)$ is a diagonal matrix with the u^{th} diagonal entry given by $\omega_n^u\left[\omega_i p_{iu} - \alpha_k\omega_k p_{ku}\right]$. The viscous modal damping identification equation is then obtained as

$$\begin{bmatrix}\zeta_1\\ \vdots\\ \zeta_m\end{bmatrix} = Im\left\{diag\left(2\omega_n^u\left[\omega_i p_{iu} - \alpha_k\omega_k p_{ku}\right]\right)^{-1}\right. \\ \left.\left[\omega_i^2\mathbf{p}_i - \omega_k^2\alpha_k\mathbf{p}_k - \boldsymbol{\Lambda}\left(\mathbf{p}_i - \alpha_k\mathbf{p}_k\right)\right]\right\}, \quad (3.20)$$

and holds for all pairings of frequencies ω_i and ω_k as long as $\omega_i p_{iu} - \alpha_k\omega_k p_{ku} \neq 0$.

To eliminate zero-mean noise, the mean of Eq. 3.19 can be computed over all available frequency pairings measured. One obtains

$$\begin{bmatrix}\zeta_1\\ \vdots\\ \zeta_m\end{bmatrix} = Im\left\{diag\left(2\omega_n^u\left\langle\omega_i p_{iu} - \alpha_k\omega_k p_{ku}\right\rangle\right)^{-1}\right. \\ \left.\left[\left\langle\omega_i^2\mathbf{p}_i - \omega_k^2\alpha_k\mathbf{p}_k\right\rangle - \boldsymbol{\Lambda}\left\langle\mathbf{p}_i - \alpha_k\mathbf{p}_k\right\rangle\right]\right\}, \quad (3.21)$$

where $< \cdot >$ denotes the mean over all the frequency pairings (i, k). The modal

damping can be identified using Eq. 3.21. The next section provides data filters to increase the accuracy of this damping method.

3.3.3 Identification Filtering

To increase the accuracy of the modal damping identification, four identification filtering techniques are proposed. The first two filters eliminate measurement data that can cause erroneous solutions. The initial filter removes low responding data, which can be greatly affected by noise. Responses with magnitudes below a fraction T_l of the maximum response magnitude are removed. That is, measurements $x^q_{meas}(\omega_y)$ (collected at DOF q for an excitation with frequency ω_y) which satisfy

$$max_{q=1...DOF}|x^q_{meas}(\omega_y)| < T_l \; max_{q=1...DOF,y}|x^q_{meas}(\omega_y)|$$

are removed.

The physical to modal transformation is important for ensuring an accurate damping identification. Therefore, the second filter removes measurements which have a relative error greater than a desired threshold R_{thresh} in the transformation from physical to modal and back to physical coordinates. The measurements collected at frequencies ω_y for all $q = 1...DOF$ are grouped in a vector $\mathbf{x}_{meas}(\omega_y)$. Measurements $\mathbf{x}_{meas}(\omega_y)$ which satisfy

$$||\mathbf{\Phi}\left[\mathbf{\Phi}^T\mathbf{\Phi}\right]^{-1}\mathbf{\Phi}^T Re\left(\mathbf{x}_{meas}(\omega_y)\right) - Re\left(\mathbf{x}_{meas}(\omega_y)\right)||_2 > R_{thresh}||Re\left(\mathbf{x}_{meas}(\omega_y)\right)||_2 \text{ or}$$
$$||\mathbf{\Phi}\left[\mathbf{\Phi}^T\mathbf{\Phi}\right]^{-1}\mathbf{\Phi}^T Im\left(\mathbf{x}_{meas}(\omega_y)\right) - Im\left(\mathbf{x}_{meas}(\omega_y)\right)||_2 > R_{thresh}||Im\left(\mathbf{x}_{meas}(\omega_y)\right)||_2$$

are removed, where Re and Im denote real and imaginary parts, and $||\cdot||_2$ indicates the 2-norm.

The third and fourth filters prevent the identification of modes which either have low responses or have modal amplitudes which are difficult to determine using physical

measurements $\mathbf{x}$. The third filter is based on the modal response at frequency i resulting in negligible modal information. Responses which are too low (based on a maximum modal response threshold P_{thresh}) are considered to be too sensitive to noise. Thus, if mode u has an amplitude p_{iu} such that $|p_{iu}| \leq 0.5\, max_r|p_{ir}|$ (where $r = 1...m$), or $|p_{iu}| < P_{thresh}$, then mode u is ignored. The fourth and last filter prevents the damping identification for cases where the modal amplitudes at frequencies i and k are similar. Therefore, mode u is ignored for a pair of frequencies (i,k) when

$$|p_{iu} - \alpha_k p_{ku}| \leq P_{thresh}.$$

These four filters are used to increase the accuracy of the following results.

3.4 Results

The characteristics and validation of the measurement point selection and damping identification are presented for a 30 DOF system first. Then, the damping identification is validated for a more complex structure (the University of Michigan validation blisk). In this section, the benefits of the proposed damping identification with respect to using a ROM, the optimized MPS, a region of high modal density, and different noise levels are examined. The 30 DOF spring-mass system has mass and stiffness matrices defined as

$$\mathbf{M} = diag\left([1\ 2 \cdots 2\ 1]\right) kg,$$

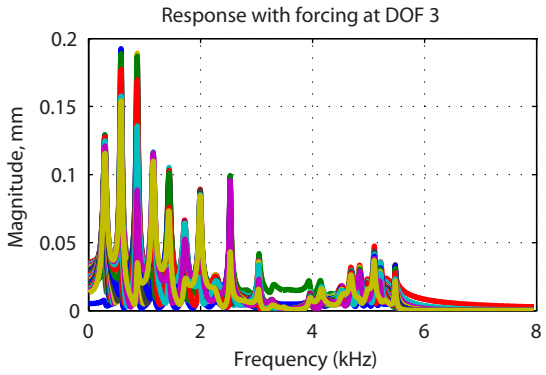

Figure 3.2: Sample forced response for the 30 DOF system

and

$$\mathbf{K} = \begin{bmatrix} 2.4 \cdot 10^9 & -0.6 \cdot 10^9 & & & & & \mathbf{0} \\ -0.6 \cdot 10^9 & 1.2 \cdot 10^9 & -0.6 \cdot 10^9 & & & & \\ & & \ddots & & & & \\ & & & & -0.6 \cdot 10^9 & 1.2 \cdot 10^9 & -0.6 \cdot 10^9 \\ \mathbf{0} & & & & & -0.6 \cdot 10^9 & 1.9 \cdot 10^9 \end{bmatrix} \frac{kg}{s^2},$$

where $diag([\cdot])$ indicates a diagonal matrix with entries given by the included vector $[\cdot]$. Figure 3.2 shows a sample forced response where the excitation was applied to DOF 3. Responses below 4 kHz are in a region of low modal density, whereas responses at frequencies higher than 4 kHz correspond to high modal density.

A ROM was created using modes 19 to 29 (ordered by frequency) with 20 DOF measured. These 11 modes were chosen since they are closely spaced, and therefore the damping is more challenging to identify. The values in the diagonal damping matrix $\mathbf{C}$ for this ROM are displayed in Fig. 3.3(a). A force of magnitude 10 N and phase of 0 was applied to each measured DOF near the natural frequency of each mode, and the physical response $x^q_{meas}(\omega_y)$ was recorded at frequencies ω_y for all measured DOF q. To simulate a physical experiment, measurement noise was injected using Eq. 3.10.

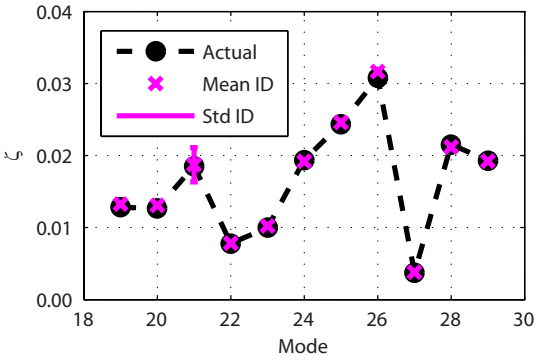

(a) Damping ID with 1% noise and optimized MPS

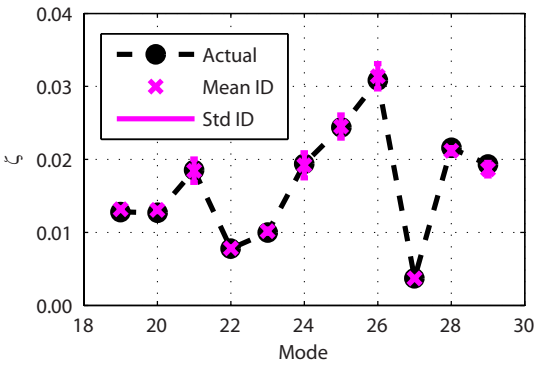

(b) Damping ID with 5% noise and optimized MPS

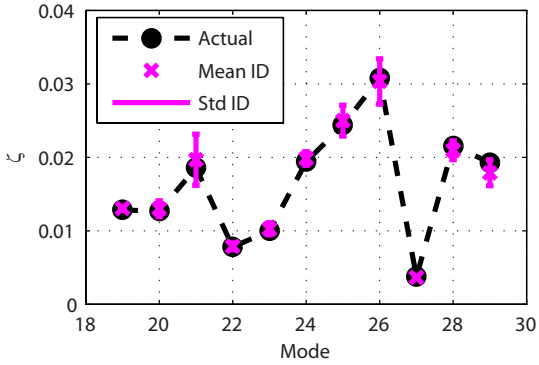

(c) Damping ID with 10% noise and non-optimized MPS

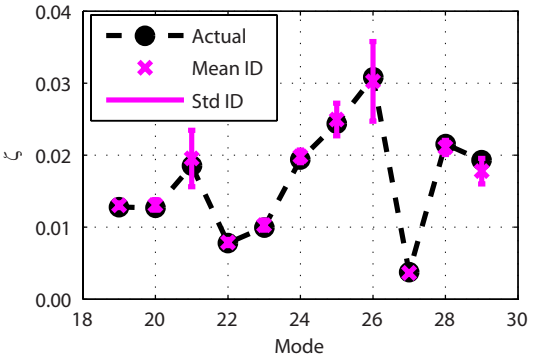

(d) Damping ID with 10% noise and optimized MPS

Figure 3.3: Damping ID for a 30 DOF system

These results in Fig. 3.3 include the mean and standard deviation of 1,000 identifications using different noisy measurement sets. The same 1,000 noise realizations (R_1^q and R_2^q separately chosen for each q DOF) were used to generate each of the graphs in Fig. 3.3. Standard deviation error bars are provided in the figures, and are denoted by Std. Also, the filtering thresholds in the identification are $R_{thresh} = 0.3$, $T_l = 0.35$, and $P_{thresh} = 10^{-5}$.

The results in Fig. 3.3 demonstrate that the 30 DOF damping identification is accurate using a ROM and for regions of high modal density. Figures 3.3(a) and 3.3(b) show that the identified damping values are accurate when the noise level is low. The non-optimized and optimized MPS chose the same measurement locations for both 1% and 5% noise. As the noise level increases, the results in Figs. 3.3(c) and

3.3(d) show the effect of the optimized MPS choosing two different locations as compared to the non-optimized MPS. The optimized MPS balances linear independence with sensitivity to noise. Therefore, the damping identified for the modes which are insensitive to noise may be less accurate than the damping identified using the non-optimized MPS, whereas the damping identified for modes which are more sensitive to noise should be more accurate. These effects on accuracy can be seen in the results in Figs. 3.3(c) and 3.3(d), where the damping values for modes 20, 23, and 28 are more accurately identified with the optimized MPS, but less accurately identified for modes 21, 25, and 26. Note that the standard deviation of most identified damping values is less than the level of the noise (e.g., the standard deviation is less than 10% for 10% noise in Figs. 3.3(c) and 3.3(d)). Modes 21 and 26 have a standard deviation greater than the level of the noise. Some of the mean damping values in Fig. 3.3(a) slightly exceed the 1% noise level. However, all of the mean values have errors below the corresponding noise levels in Figs. 3.3(b), 3.3(c), and 3.3(d). In general, the proposed method accurately identifies the modal damping with an error less than the corresponding noise level. Also, the optimized MPS improves the accuracy of the damping identification for modes which are sensitive to noise.

Care needs to be exercised when choosing the identification filtering parameters. If the filtering is too lax, the identification uses measurements that have less accurate modal coordinates due to a larger amount of noise in the response. Therefore, the identification becomes more contaminated by the noise effects. However, if the filtering is too strict, then the identification depends on too few measurements. As a result, the identification is also less accurate (since zero mean noise is not eliminated). The results presented are from the region of filtering which provides a balance between using measurements with less modal participation (of the modes for which the damping is to be identified) and elimination of zero mean noise. Note that different systems and measurements may require different values for R_{thresh}, T_l, and P_{thresh}.

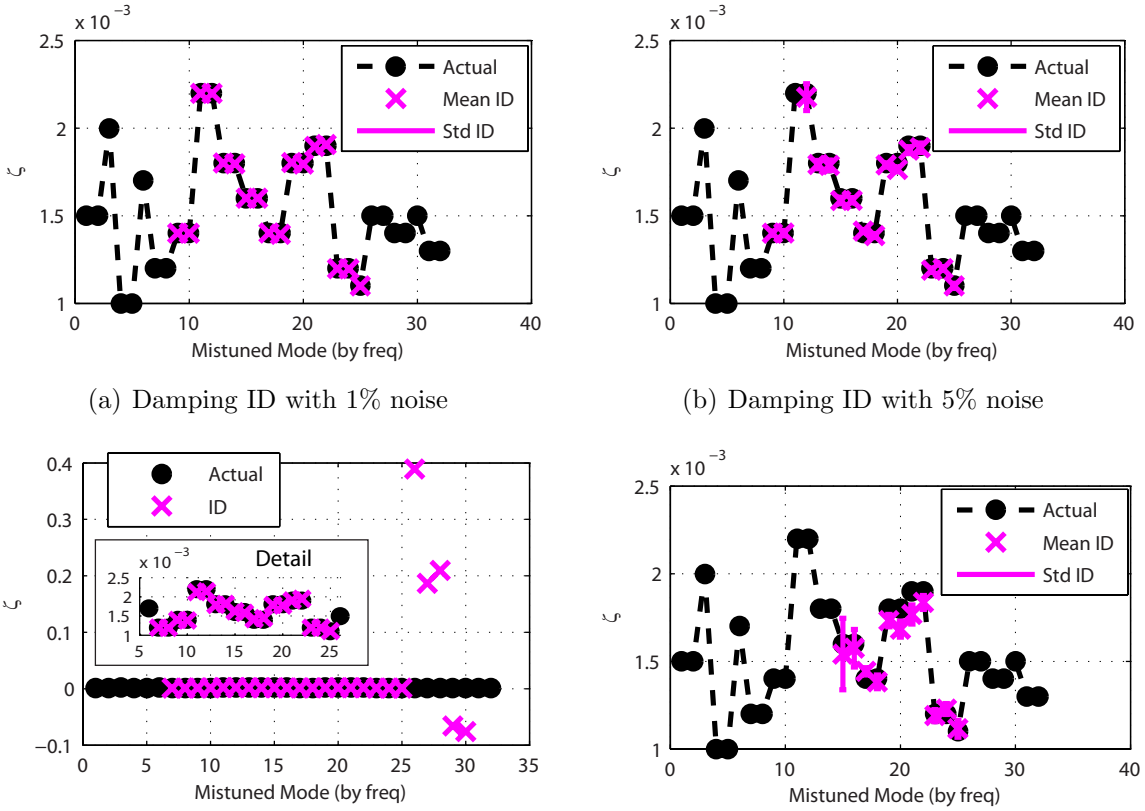

(a) Damping ID with 1% noise

(b) Damping ID with 5% noise

(c) Damping ID with 5% noise and 24 modes

(d) Damping ID with 10% noise

Figure 3.4: Damping ID for validation blisk

Next, results for a more complex structure in the form of the University of Michigan validation blisk [52] are presented. This blisk has mistuning of approximately 2% (composed of 1% zero mean mistuning and 1% cyclic modeling error [1]). The damping identification uses the actual mistuning to assess the accuracy of the proposed measurement point selection and damping identification methods. The following results show the mean and standard deviation of 100 identifications using different noisy response sets.

The results in Fig. 3.4 demonstrate that the mistuned validation blisk damping identification which uses a ROM is accurate for regions of high modal density and typically has an error less than the measurement noise level. Figures 3.4(a) and 3.4(b) display the identification results where 1% and 5% noise respectively have been injected into the numerically generated measurement data. For this figure, the

ROM contained 17 modes. Both the standard deviation and mean damping values in Figs. 3.4(a) and 3.4(b) are well below the corresponding noise level. Figure 3.4(d) displays the identification results for 10% noise. The standard deviations and mean damping values for all modes except mode 15 are below the 10% noise level. Note that some modes in Figs. 3.4(b) and 3.4(d) were not identified. The absence of identified values for a few modes is due to the increase in the noise level causing the identification filtering to either remove all the measurement data or determine that the missing modes would not be accurately identified.

If the motion of the structure occurs in a region or direction that is not measured, the damping identification should be less accurate. Figure 3.4(c) shows that. Specifically, using a larger ROM results in an inaccurate identification for the additional disk dominated modes. Modes 7 to 25 remain accurately identified. In particular, note that a ROM with greater size may require different measurement locations drawn from a larger candidate set in the MPS procedure. For this model, measurements on the disk are needed for the larger ROM.

This behavior of the ROMs has already been explored in the context of mistuning identification [49]. When introducing the concept of inverse ROMs (IROMs) for system identification, Madden et al. [49] noted that some ROMs can result in an inaccurate analysis. Madden et al. [49] presented an algorithm to test and select a subset of the full IROM for obtaining an accurate result. The methods proposed herein allow for the MPS and damping methods to be implemented in the same algorithm by individually defining the modal matrix for each IROM.

3.5 Conclusions

Two methods used for a new damping identification were proposed. The optimized measurement point selection (MPS) method improves robustness of the identification to noise. Also, by taking advantage of cyclic symmetry, the computational cost of

utilizing the MPS method is dramatically reduced. In addition, an algorithm was presented which describes an effective procedure incorporating the MPS method into experiment preparation for complex structures.

The second method involves identifying the damping associated with each system mode. The benefits of the proposed method include the ability to maintain accuracy despite reducing the order of the models used to predict the system response and despite the fact that regions of high modal density are encountered. The proposed method was shown to be relatively insensitive to noise, to apply to mistuned systems, and to require knowledge of only the forced response, the relative forcing, and a finite element model. As a result, the damping can be accurately identified for general structures such as blisks.

The novel modal damping identification method was demonstrated using a numerical simulation of a low dimensional system and a more complex system (the University of Michigan validation blisk). Results involving several reduced order models (ROMs) of various sizes and various noise levels were presented. To increase the accuracy of the proposed method, the optimized MPS technique was used. Results indicate that using the optimized MPS technique increases the accuracy of the identification for modes which are sensitive to measurement noise as compared to only using points chosen based on the (classical) EIDV method.

CHAPTER IV

Hybrid Modal Damping Identification for Bladed Disks and Blisks

4.1 Introduction

Due to wear or manufacturing, nominally cyclically symmetric structures such as bladed disks and integrally bladed disks (blisks) have slight variations in the mass or stiffness of their components known as mistuning. As a result, vibration energy can be localized around certain regions of the system leading to a larger than expected forced response. This increase can lead to high cycle fatigue. Damping plays an important role in investigating the effects of localization, because damping affects the forced response of a mistuned system (in particular, it affects the maximum response amplitude).

One approach to reduce the effects of mistuning is to apply a damping coating to the structure. As mistuning may adversely affect some modes more than others, it is important to increase as much as possible the damping of certain/desired modes. Joshi et al. [3] showed that an arbitrary damping coating does not always optimally decrease the maximum response of the desired modes as one might expect. Therefore, to assess the effects of a coating, damping must be identified before and after the coating is applied.

Current damping identification methods [4,6,7,11,12,14–20,22–24,26–29] use measurements of complex eigenvalues, complex eigenvectors, and the applied forcing, or energy measurements [32, 33]. Such measurements are difficult especially for systems with high modal density. Also, current methods do not use reduced order models (ROMs), and can be sensitive to measurement noise. Thus, current methods do not work well for damping identification for systems with regions of high modal density such as blisks. Recently, Holland et al. presented two different methods [55, 56] for damping identification which do not require knowledge of the applied forcing or energy. Instead, damping is identified using measurements of forced responses and information from a finite element model of the system. The forced responses are obtained from an excitation system which allows relative calibration [1], but does not provide the actual magnitude of the applied forces.

The work herein presents a novel modal damping identification technique for mistuned systems using ROMs in low or high modal density regions. This method makes use of forcing calibration [1] to decrease its sensitivity to noise. The new method identifies first modal damping values relative to each other, which makes these values known (only) up to a multiplicative constant. Then, to determine that constant the novel approach makes use of the method of Holland et al. [56]. Distinct from other identification methods based on frequency response functions, the proposed approach introduces a reduced frequency response matrix which can be constructed without requiring that all degrees of freedom (DOF) of the system model be both forced and measured. Thus, the new approach significantly reduces the amount of measurements needed for identifying damping. In addition, a frequency windowing technique is proposed to further reduce the size of the reduced frequency response matrix, while increasing the robustness of the resulting identification.

4.2 Modal Damping

This section summarizes the modeling approach used for modeling blisks with small mistuning and viscous modal damping. This description closely follows that of Holland et al. [56]. The starting point in modeling blisks is to exploit the fact that the mistuned modes for systems with small mistuning can be represented as a linear combination of tuned system modes [40]. Thus, $\mathbf{\Phi}_m = \mathbf{\Phi}\mathbf{\Psi}$, where $\mathbf{\Phi}_m$ is a mass-normalized matrix containing m mistuned modes in the frequency range of interest. Matrix $\mathbf{\Phi}$ is a mass-normalized matrix containing d undamped tuned system normal modes in the frequency range of interest. Matrix $\mathbf{\Psi}$ is the transformation from tuned modal coordinates to mistuned coordinates under the assumption that the m mistuned modes are a linear combination of the d tuned system modes [40]. For a tuned system, the full-order $\mathbf{\Psi}$ matrix is the identity matrix $\mathbf{I}$. Next, the equations of motion for the blisk can be expressed as

$$\mathbf{M}\ddot{\bar{\mathbf{x}}} + \mathbf{C}\dot{\bar{\mathbf{x}}} + \mathbf{K}\bar{\mathbf{x}} = \bar{\mathbf{f}}, \tag{4.1}$$

where $\mathbf{M}$ is the mass matrix, $\mathbf{C}$ is the damping matrix, $\mathbf{K}$ is the stiffness matrix, $\bar{\mathbf{x}}$ is the response, and $\bar{\mathbf{f}}$ is the applied forcing. This forcing is assumed harmonic with amplitude $\mathbf{f}$ and frequency ω. Then, the physical response $\bar{\mathbf{x}}$ is harmonic and has a magnitude $\mathbf{x}$. The response $\mathbf{x}$ can be converted to the reduced-order mistuned modal coordinates $\mathbf{p}$ by using $\mathbf{x} = \mathbf{\Phi}_m\mathbf{p} = \mathbf{\Phi}\mathbf{\Psi}\mathbf{p}$.

Assuming modal damping, $\mathbf{C}$ is diagonalized by $\mathbf{\Phi}_m$, i.e. $\mathbf{\Phi}_m^T\mathbf{C}\mathbf{\Phi}_m = 2diag\left(\zeta_u\omega_n^u\right)$, where ζ_u is the viscous modal damping coefficient for mode u, ω_n^u is the undamped natural frequency of mode u, and $diag\left(\cdot\right)$ denotes a diagonal matrix with entries corresponding to the included scalars. In the frequency range of interest, the damping matrix $\mathbf{C}$ can be replaced with matrix $\tilde{\mathbf{C}}$ given by $\tilde{\mathbf{C}} = 2\mathbf{M}\mathbf{\Phi}_m diag\left(\zeta_u/\omega_n^u\right)\mathbf{\Phi}_m^T\mathbf{K}$. This replacement is possible because $\mathbf{\Phi}_m^T\mathbf{M}\mathbf{\Phi}_m = \mathbf{I}$ and $\mathbf{\Phi}_m^T\mathbf{K}\mathbf{\Phi}_m = \mathbf{\Lambda}$, where $\mathbf{\Lambda}$ is a diagonal

matrix containing the mistuned eigenvalues $\lambda_n^u = \omega_n^{u2}$. Thus,

$$\begin{aligned}\boldsymbol{\Phi}_m^T \mathbf{C} \boldsymbol{\Phi}_m &= 2\boldsymbol{\Phi}_m^T \mathbf{M} \boldsymbol{\Phi}_m diag\left(\zeta_u/\omega_n^u\right) \boldsymbol{\Phi}_m^T \mathbf{K} \boldsymbol{\Phi}_m \\ &= 2diag\left(\zeta_u/\omega_n^u\right) \boldsymbol{\Lambda} = 2diag\left(\zeta_u/\omega_n^u\right) diag\left(\omega_n^{u2}\right) \\ &= 2diag\left(\zeta_u \omega_n^u\right).\end{aligned} \tag{4.2}$$

Equation (4.2) shows that the dynamics of the system with a damping of $\tilde{\mathbf{C}}$ is the same in the frequency range of interest as that of a system with a damping of $\mathbf{C}$. Thus, the forced response in the frequency range of interest can be obtained by replacing $\mathbf{C}$ with $\tilde{\mathbf{C}}$ and solving Eqn. (4.1) for $\mathbf{x}$. Substituting $\boldsymbol{\Phi}_m = \boldsymbol{\Phi}\boldsymbol{\Psi}$, one obtains

$$\mathbf{x} = \boldsymbol{\Phi}\boldsymbol{\Psi}\left[-\omega^2 \mathbf{I} + 2j\omega\ diag\left(\omega_n^u\right)\boldsymbol{\zeta} + \boldsymbol{\Lambda}\right]^{-1} \boldsymbol{\Psi}^T \boldsymbol{\Phi}^T \mathbf{f}, \tag{4.3}$$

where j is the imaginary unit, and $\boldsymbol{\zeta} = diag\left(\zeta_u\right)$.

4.3 Modal Damping Identification using Calibration

Acoustic and magnetic excitation, typically used in vibration testing of blisk, are hard or impossible to measure accurately. Thus, in this section we focus on a method that only requires forces to be known up to a multiplicative constant. The calibration method proposed by Holland et al. [1] uses reciprocity to ensure that an excitation system provides such forcing. Thus, only the relative forcing magnitude and phase are known at any given excitation frequency. Assume that such a force calibration has been performed on the excitation so that the relative magnitudes and phases of the excitations are known. Then, consider a forcing case (denoted as the g^{th} harmonic forcing) be applied with a relative distribution (magnitude and phase) $\tilde{\mathbf{G}}_g$ of forces for every DOF in the system. Note that not all DOFs have to be forced. The unforced DOFs are reflected by zero entries in $\tilde{\mathbf{G}}_g$. Also, define the diagonal matrix $\mathbf{F}$ such

that the u^{th} diagonal entry is the magnitude of the relative applied forcing (referenced to one of the forcing cases) so that $\mathbf{f}_g = c\tilde{\mathbf{G}}_g^T F_{gg}$. The constant $c \in \mathbb{C}$ is the known multiplicative constant relating the actual and relative forcing of the reference case.

If all the forcing cases are independent, then it is possible to group all vectors $\tilde{\mathbf{G}}_g$ into a matrix $\tilde{\mathbf{G}}$, which has a rank equal to the number of forcing cases y. Next, one may choose to represent $\tilde{\mathbf{G}}$ as a linear combination of a set of basis distributions $\mathbf{G}$ (such as single DOF forcing), so $\tilde{\mathbf{G}} = \mathbf{V}\mathbf{G}$, where $\mathbf{V}$ is a matrix of DOF participations in the excitation. Note that $\mathbf{G}$ must have a rank equal to the number of forcing cases. Substituting into Eqn. (4.1), and letting $\mathbf{H} = [-\omega^2\mathbf{M} + j\omega\mathbf{C} + \mathbf{K}]^{-1}$, one obtains $\mathbf{x} = c\mathbf{H}\tilde{\mathbf{G}}^T\mathbf{F} = c\ \mathbf{H}\mathbf{G}^T\mathbf{V}^T\mathbf{F}$. One may also choose the same DOFs to be measured for each forcing case. This choice is represented by using a matrix $\mathbf{R}$ which is a $N \times N$ diagonal matrix with a value of 1 for measured DOFs and 0 otherwise. N is the total number of DOFs in the system. Note that the rank of $\mathbf{R}$ is the number of measured DOF (n) and the rank of $\mathbf{G}$ is the number of forcing cases (y). The implications of these ranks are discussed in the Sec. 4.7. Pre-multiplying by $\mathbf{R}$ and defining the reduced frequency response matrix (RFRM) as $\tilde{\mathbf{H}} = \mathbf{R}\mathbf{H}\mathbf{G}^T$, one obtains

$$\mathbf{R}\mathbf{x} = c\ \mathbf{R}\mathbf{H}\mathbf{G}^T\mathbf{V}^T\mathbf{F} = c\ \tilde{\mathbf{H}}\mathbf{V}^T\mathbf{F}, \tag{4.4}$$

where $\mathbf{R}\mathbf{x}$ is a matrix containing only the measured DOF. Note that the RFRM ($\tilde{\mathbf{H}}$) only contains measured data taken at a few forcing cases. There is no requirement to measure or force all locations on the structure for damping identification. Taking the Moore-Penrose pseudoinverse of $\tilde{\mathbf{H}}$ and then pre-multiplying Eqn. (4.4) by $\mathbf{G}^T$, one obtains

$$\mathbf{G}^T\tilde{\mathbf{H}}^{-*}\mathbf{R}\mathbf{x} = c\ \mathbf{G}^T\mathbf{V}^T\mathbf{F} = \mathbf{f} = \left(-\omega^2\mathbf{M} + j\omega\mathbf{C} + \mathbf{K}\right)\mathbf{x}, \tag{4.5}$$

where $^{-*}$ denotes the Moore-Penrose pseudoinverse. Note that the left and right sides

of Eqn. 4.5 do not require knowledge of $\mathbf{V}$ or $\tilde{\mathbf{G}}$. Therefore, many different forms of $\mathbf{G}$ can be used as long as $\tilde{\mathbf{G}}$ can be well-represented as a linear combination of $\mathbf{G}$. Also, neither the matrix of participations ($\mathbf{V}$), nor the actual forcing distributions are required for the modal damping identification.

Equation 4.5 is in the form $\mathbf{Ax} = \mathbf{Bx}$, and must hold for all $\mathbf{x}$. Therefore, $\mathbf{A} = \mathbf{B}$. Converting to modal coordinates (as in Sec. 4.2) and pre-multiplying by $\mathbf{\Psi}^T\mathbf{\Phi}^T$, one obtains

$$\mathbf{\Psi}^T\mathbf{\Phi}^T\mathbf{G}^T\tilde{\mathbf{H}}^{-*}\mathbf{R\Phi\Psi} = -\omega^2\mathbf{I} + 2j\omega\ diag\left(\omega_n^u\right)\boldsymbol{\zeta} + \mathbf{\Lambda}. \tag{4.6}$$

Taking the imaginary part and solving for $\boldsymbol{\zeta}$, one obtains

$$\boldsymbol{\zeta} = \frac{1}{2\omega} diag\left(\omega_n^u\right)^{-1} Im\left\{\left(\mathbf{G\Phi\Psi}\right)^T \tilde{\mathbf{H}}^{-*}\mathbf{R\Phi\Psi}\right\}. \tag{4.7}$$

Note that $\mathbf{G\Phi\Psi}$ is a matrix containing the relative modal forcing, and $\mathbf{R\Phi\Psi}$ contains the mistuned mode shapes of the measured DOF. Recalling that $\mathbf{F}$ is diagonal (by construction) and post-multiplying Eqn. (4.4) by $\mathbf{F}^{-1}$, one obtains

$$\tilde{\mathbf{H}} = \frac{1}{c}\mathbf{RxF}^{-1}. \tag{4.8}$$

Substituting Eqn. (4.8) into Eqn. (4.7), one obtains

$$\boldsymbol{\zeta} = \frac{1}{2\omega} diag\left(\omega_n^u\right)^{-1} Im\left\{c\left(\mathbf{G\Phi\Psi}\right)^T\left(\mathbf{RxF}^{-1}\right)^{-*}\mathbf{R\Phi\Psi}\right\}. \tag{4.9}$$

The diagonal entries of $\boldsymbol{\zeta}$ in Eqn. (4.9) provide the values of the modal damping up to a multiplicative constant c. Note that if one uses an excitation system which can provide the (absolute, not relative) excitation magnitude, then c is known ($c = 1$). The types of excitation systems use for vibration testing of blisks typically do not provide the magnitude of the forcing, and hence c has to be determined by other means. The following section uses a modified version of the damping identification

method presented by Holland et al. [56] to solve for the unknown forcing coefficient. Note that the the phase of c embedded in the relative damping values, while the magnitude of c relates the relative damping to $\boldsymbol{\zeta}$.

4.4 Relative Modal Damping Identification

Applying the approach in Sect. 6.3, only relative forcing values are known. Thus, c must be found by an alternate technique. As two methods are required, the proposed approach herein is referred to as the hybrid damping identification method. Holland et al. [56] derived the following result

$$2j\bar{\boldsymbol{\zeta}}\left(\omega_i\mathbf{p}_i - \alpha_k\omega_k\mathbf{p}_k\right) = \omega_i^2\mathbf{p}_i - \omega_k^2\alpha_k\mathbf{p}_k - \boldsymbol{\Lambda}\left(\mathbf{p}_i - \alpha_k\mathbf{p}_k\right), \tag{4.10}$$

where $\mathbf{p}_i$ and $\mathbf{p}_k$ are the modal amplitudes of the response at frequencies ω_i and ω_k respectively, $\bar{\boldsymbol{\zeta}} = \boldsymbol{\zeta} diag\left(\omega_n^u\right)$, and α_k is the relative forcing coefficient which relates the forcing applied at frequency ω_i to the forcing applied at ω_k (both being known with respect to the forcing applied at a given reference frequency). As also discussed in [56], one way to extract α_k is to use the frequency transfer function for the speakers or magnets used for excitation, and assume that the force applied to the structure in a given frequency band is proportional to the signal applied to the speakers or magnets in that frequency band.

Solving Eqn. (4.6) for $\boldsymbol{\zeta}$, one obtains

$$\begin{aligned}\boldsymbol{\zeta} &= \frac{-j}{2} diag\left(\omega_n^u\right)^{-1}\left[\frac{c}{\omega}\left(\mathbf{G\Phi\Psi}\right)^T\left(\mathbf{RxF}^{-1}\right)^{-*}\mathbf{R\Phi\Psi} + \frac{1}{\omega}\left(\omega^2\mathbf{I} - \boldsymbol{\Lambda}\right)\right] \\ &= \frac{-j}{2} diag\left(\omega_n^u\right)^{-1}\left[c\mathbf{h}\left(\omega\right) + \mathbf{e}\left(\omega\right)\right],\end{aligned} \tag{4.11}$$

where $\mathbf{h}(\omega)$ and $\mathbf{e}(\omega)$ are defined as

$$\mathbf{h}(\omega) = \frac{1}{\omega}\left(\mathbf{G\Phi\Psi}\right)^T \left(\mathbf{RxF}^{-1}\right)^{-*} \mathbf{R\Phi\Psi} \quad \text{and} \quad \mathbf{e}(\omega) = \frac{1}{\omega}\left(\omega^2\mathbf{I} - \mathbf{\Lambda}\right). \tag{4.12}$$

Note that $\mathbf{h}(\omega)$ and $\mathbf{e}(\omega)$ depend on frequency ω, however their dependence on ω is such that $\boldsymbol{\zeta}$ given in Eqn. (4.11) does not depend on ω.

Thus, $\bar{\boldsymbol{\zeta}} = \frac{-j}{2} diag\left(\omega_n^u\right) diag\left(\omega_n^u\right)^{-1} \left[c\ \mathbf{h}(\omega) + \mathbf{e}(\omega)\right] = \frac{-j}{2}\left[c\ \mathbf{h}(\omega) + \mathbf{e}(\omega)\right]$, and Eqn. (4.10) becomes

$$\begin{aligned} &c\ \mathbf{h}(\omega)\left(\omega_i\mathbf{p}_i - \alpha_k\omega_k\mathbf{p}_k\right) \\ &\qquad = \omega_i^2\mathbf{p}_i - \omega_k^2\alpha_k\mathbf{p}_k - \mathbf{\Lambda}\left(\mathbf{p}_i - \alpha_k\mathbf{p}_k\right) - \mathbf{e}(\omega)\left(\omega_i\mathbf{p}_i - \alpha_k\omega_k\mathbf{p}_k\right). \end{aligned} \tag{4.13}$$

Pre-multiplying by $\left(\left(\omega_i\mathbf{p}_i - \alpha_k\omega_k\mathbf{p}_k\right)^\dagger \left(\omega_i\mathbf{p}_i - \alpha_k\omega_k\mathbf{p}_k\right)\right)^{-1} \left(\omega_i\mathbf{p}_i - \alpha_k\omega_k\mathbf{p}_k\right)^\dagger \mathbf{h}(\omega)^{-1}$, one obtains

$$\begin{aligned} c = &\left(\left(\omega_i\mathbf{p}_i - \alpha_k\omega_k\mathbf{p}_k\right)^\dagger \left(\omega_i\mathbf{p}_i - \alpha_k\omega_k\mathbf{p}_k\right)\right)^{-1} \left(\omega_i\mathbf{p}_i - \alpha_k\omega_k\mathbf{p}_k\right)^\dagger \\ &\mathbf{h}(\omega)^{-1}\left[\left(\omega_i^2\mathbf{p}_i - \omega_k^2\alpha_k\mathbf{p}_k\right) - \mathbf{\Lambda}\left(\mathbf{p}_i - \alpha_k\mathbf{p}_k\right) - \mathbf{e}(\omega)\left(\omega_i\mathbf{p}_i - \alpha_k\omega_k\mathbf{p}_k\right)\right], \end{aligned} \tag{4.14}$$

where † denotes the Hermitian. In essence, Eqn. (4.14) provides the value of c by exploiting combinations of measurements at different frequencies (in the modal space). Once c is known and $\mathbf{h}(\omega)$ is substituted into Eqn. (4.9), one obtains

$$\boldsymbol{\zeta} = \frac{1}{2} diag\left(\omega_n^u\right)^{-1} Im\left\{c\ \mathbf{h}(\omega)\right\}. \tag{4.15}$$

Note that solving for c allows the forcing to be identified if the forcing distribution $\tilde{\mathbf{G}}$ is known. The forcing is given by $\mathbf{f} = c\ \tilde{\mathbf{G}}^T\mathbf{F}$.

4.5 Measurement Noise

Solving Eqn. (4.14) requires the frequency pairs (i,k) to be for the same forcing case (i.e. for the same blades being excited). Thus, for frequency pair (i,k) and forcing case b, Eqn. (4.13) can be expressed as $\mathbf{V}_{i,k}^{b}\ c_{i,k}^{b} = \mathbf{W}_{i,k}^{b}$, where $\mathbf{V}_{i,k}^{b} = \mathbf{h}(\omega)(\omega_i \mathbf{p}_i - \alpha_k \omega_k \mathbf{p}_k)$ and $\mathbf{W}_{i,k}^{b} = \omega_i^2 \mathbf{p}_i - \omega_k^2 \alpha_k \mathbf{p}_k - \mathbf{\Lambda}(\mathbf{p}_i - \alpha_k \mathbf{p}_k) - \mathbf{e}(\omega)(\omega_i \mathbf{p}_i - \alpha_k \omega_k \mathbf{p}_k)$. Therefore, one obtains

$$c_{i,k}^{b} = \frac{\mathbf{V}_{i,k}^{b}{}^{\dagger}\mathbf{W}_{i,k}^{b}}{\mathbf{V}_{i,k}^{b}{}^{\dagger}\mathbf{V}_{i,k}^{b}}. \tag{4.16}$$

In the absence of measurement noise all $c_{i,k}^{b}$ would be identical and equal to the desired value c. Note that in general c is a complex number.

To increase the accuracy of identifying c, the effects of zero mean noise can be reduced by averaging the values $c_{i,k}^{b}$ obtained for all frequency pairs (i,k) and all forcing cases b. One obtains

$$c = \frac{1}{y}\sum_{b=1}^{y}\left[\frac{1}{q}\sum_{(i,k)}\frac{\mathbf{V}_{i,k}^{b}{}^{\dagger}\mathbf{W}_{i,k}^{b}}{\mathbf{V}_{i,k}^{b}{}^{\dagger}\mathbf{V}_{i,k}^{b}}\right], \tag{4.17}$$

where y is the number of independent forcing cases measured, and q is the number of frequency pairs measured for forcing case b.

Solving for the magnitude $\bar{c}$ and phase θ_c of c in Eqn. (4.17), one obtains

$$\bar{c} = \left|\frac{1}{y}\sum_{b=1}^{y}\left[\frac{1}{q}\sum_{(i,k)}\frac{\mathbf{V}_{i,k}^{b}{}^{\dagger}\mathbf{W}_{i,k}^{b}}{\mathbf{V}_{i,k}^{b}{}^{\dagger}\mathbf{V}_{i,k}^{b}}\right]\right|, \tag{4.18}$$

$$\theta_c = \theta_c^{avg} = \frac{1}{y}\sum_{b=1}^{y}\frac{1}{q}\sum_{(i,k)} -\theta_{h,u} - \theta_{p,u,b}^{i,k} + \theta_{w,u,b}^{i,k}, \text{ and} \tag{4.19}$$

$$\theta_{wp,u}^{avg} = \frac{1}{y}\sum_{b=1}^{y}\frac{1}{q}\sum_{(i,k)} -\theta_{p,u,b}^{i,k} + \theta_{w,u,b}^{i,k} = \theta_c^{avg} + \theta_{h,u}$$

where $|\cdot|$ denotes magnitude, $\theta_{h,u}$ is the phase of the u^{th} diagonal entry of $\mathbf{h}(\omega)$, $\theta_{p,u,b}^{i,k}$

is the phase of the u^{th} entry of vector $\omega_i \mathbf{p}_i - \alpha_k \omega_k \mathbf{p}_k$, and $\theta^{i,k}_{w,u,b}$ is the phase of the u^{th} entry of vector $\mathbf{W}^b_{i,k}$.

Note that, $\boldsymbol{\zeta}$ and $\mathbf{e}(\omega)$ are real, diagonal matrices. However, in general $\mathbf{h}(\omega)$ is a complex diagonal matrix. Thus, the real part of Eqn. (4.6) can be expressed as

$$Re\left(c\tilde{\mathbf{h}}(\omega)\right) = -\tilde{\mathbf{e}}(\omega), \tag{4.20}$$

where $\tilde{\mathbf{h}}(\omega)$ and $\tilde{\mathbf{e}}(\omega)$ are vectors of size $m \times 1$ containing the diagonal entries of matrices $\mathbf{h}(\omega)$ and $\mathbf{e}(\omega)$. While the forcing coefficient and damping can be identified using Eqns. (4.18), (4.19), and (4.15), the effect of measurement noise can be decreased using Eqn. (4.20). In terms of the magnitude and the phase of c, one obtains

$$cos\left(\theta_c + \theta_{h,u}\right) = \frac{-\tilde{\mathbf{e}}_u(\omega)}{\bar{c}\bar{\mathbf{h}}_u(\omega)}. \tag{4.21}$$

Substituting $\theta^{avg}_{c,u}$ from Eqn. (4.19), one obtains

$$\theta^{avg}_{wp,u} = cos^{-1}\left(\frac{-\tilde{\mathbf{e}}_u(\omega)}{\bar{c}\bar{\mathbf{h}}_u(\omega)}\right). \tag{4.22}$$

Solving for $\theta^{avg}_{wp,u}$ using Eqn. (4.22) instead of directly using Eqn. (4.16) ensures that the identified damping values are real and reduces the effects of the measurement noise on the involved phases. Note that cosine is used on the interval 0 to π, but both $\theta^{avg}_{wp,u}$ and $-\theta^{avg}_{wp,u}$ are solutions to Eqn. (4.22). Therefore, the sign of $\theta^{avg}_{wp,u}$ should be updated after substituting $\theta^{avg}_{wp,u}$ into Eqn. (4.19) and comparing the sign of $\theta^{avg}_c + \theta_{h,u}$ with the value of $\theta_c + \theta_{h,u}$ obtained from the phases in Eqn. (4.17). Also, measurement noise can cause the right hand side of Eqn. (4.21) to be outside of the interval $[-1, 1]$. To avoid this issue, any values less than -1 or greater than 1 are replaced with -1 and 1 respectively. After calculating $\theta^{avg}_{wp,u}$ from Eqn. (4.22), θ^{avg}_c can be calculated using Eqn. (4.19).

4.6 Modal Damping Identification Procedure

There are several different types of mistuning identification techniques [45–50]. These methods identify the damping together with the mistuning, ignore the damping, or assume that the damping is known. The damping identification method herein can be used in conjunction with the component mode mistuning (CMM) [48,49] method. In CMM, the stiffness mistuning is determined *prior* to the damping identification. Therefore, herein the mistuned eigenvalues in $\mathbf{\Lambda}$, and the transformation matrix $\mathbf{\Psi}$ from tuned to mistuned coordinates are considered known.

The procedure for identifying the modal damping can be summarized as follows. First, the forced response is measured for different forcing cases with various blade-to-blade distributions ($\mathbf{G}$) in the frequency range of interest. Also, the relative applied forcing $\mathbf{F}$ (with respect to a reference case) is known for a given frequency (after a calibration procedure [1] has been applied). Next, Eqn. (4.12) uses this data to calculate $\mathbf{h}(\omega)$ and $\mathbf{e}(\omega)$.

There are four steps for determining the forcing coefficient. First, the magnitude $\bar{c}$ of c is determined by solving Eqn. (4.18). Then, Eqn. (4.22) is used to solve for $\theta_{wp,u}^{avg}$. The sign of this phase is checked against the phase determined by Eqn. (4.17) and changed if necessary. The phase of c is then obtained using Eqn. (4.19).

4.7 Forcing Cases and Frequency Windowing

One important requirement of the modal damping identification is that the rank of matrices $\mathbf{F}$ and $\tilde{\mathbf{H}}$ must be greater or equal to the number of damping values to be identified. Let z be the number of damping values to be identified, m the number of (mistuned) modes in the frequency range of interest, and n the number of measured DOF. Then, to achieve an accurate identification $z \leq m \leq n$ and $z \leq y$. In general, the value of the damping for each mode is desired, and therefore, $z = m$.

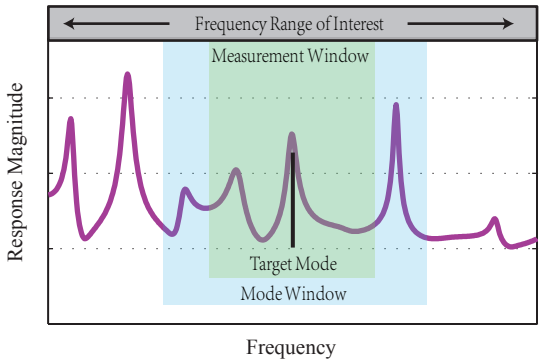

Figure 4.1: Frequency windowing procedure

The frequency range of interest may include many modes, and so m may be large. For a blisk, m is normally equal to or slightly greater than the number of blades. Therefore, more than one point per blade must be measured so that the number of measurements n is greater or equal to m. The last requirement ($z \leq y$) is for the number of forcing cases to be greater than the number of damping values to be identified (which may be equal to the number of modes). In general, meeting this requirement would require forcing multiple distinct locations on at least one or a few blades to obtain independent forcing distributions. As an example, the 0 to 3 kHz frequency range of interest for the University of Michigan validation blisk includes 32 modes ($m = 32$). This blisk has 24 blades, so identifying the modal damping for all 32 modes ($z = 32$) would require at least 2 measurement locations per blade ($n = 48$) [56] and $y = 32$ forcing cases (which would require multiple forcing locations on at least one or a few blades). However, this is impractical for blisks. A solution to this challenge is presented next.

To reduce the number of forcing cases and the number of required measurements, a frequency windowing method is introduced. This procedure is summarized in Fig. 4.1. There, a target mode (indicated by a vertical black line) is any one mode (one at a time) from the frequency range of interest. The goal of the frequency windowing is to capture the motion of the target mode with the minimal amount of modes and

measurements necessary for the damping identification. There are two key observations which can be made about the forced response. First, the participation of the target mode in measurements outside of a certain range (denoted the measurement window, and located within the inner, shaded rectangle of Fig. (4.1)) is low. Thus, the modal amplitude of the target mode is low outside the measurement window. Therefore, measurements outside the measurement window are not used when identifying the damping of the target mode. Also, for a target mode, $\mathbf{h}(\omega)$ and $\mathbf{e}(\omega)$ will be more accurate at a frequency where the modal participation for the target mode is largest. Therefore, ω is chosen to be the frequency inside of the measurement window with the largest participation of the target mode over all forcing cases. Second, the participation of modes which are outside of a certain frequency range (denoted the mode window, and indicated by the outer, shaded rectangle) is low for the responses in the measurement window. Therefore, modes within the mode window are needed to capture responses in the measurement window and to identify the damping of the target mode. An additional benefit of the windowing is an increase in the accuracy of the identification as measurements with low contributions to the target mode are excluded (and those measurements can result in an inaccurate damping identification). Note that the measurement *locations* are chosen using the method of Holland et al. [56] (based on the frequency range of interest). Finally, note that the frequency windowing is particularly useful identifying $\mathbf{h}(\omega)$ and $\mathbf{e}(\omega)$, and is not needed for the identification of c (although it can be beneficial for noise rejection).

While more complicated methods may be used to calculate these windows, to minimize the computational cost the following estimates are suggested. For a mistuned system, the damping identification depends on knowledge of the mistuned system. As all mistuning identification techniques contain some level of error, any of the actual mistuned natural frequencies will lie within a narrow frequency range. This range can be used to define the measurement window. A measurement window $[\omega_l^t, \omega_u^t]$ is

defined for target mode t based on these parameters as

$$\omega_l^t = \omega_n^t \left(1 - \sqrt{\delta\omega_n^2}\right) \text{ and } \omega_u^t = \omega_n^t \left(1 + \sqrt{\delta\omega_n^2}\right), \tag{4.23}$$

where $\delta\omega_n^2$ is the maximum estimated error of the mistuned eigenvalues.

To adequately represent measurements in the range $[\omega_l^t, \omega_u^t]$ by using ROMs based on tuned modes, the mode window must contain all modes which participate significantly in the responses in the measurement window. Therefore, a mode window is defined by examining how far in frequency a mode should be from the range $[\omega_l^t, \omega_u^t]$ as to not contribute to the maximum response of any DOF more than $T_x\%$ of the maximum response of all DOF in the measurement window. Consider that the maximum response magnitude observed in the measurement window is $|X_{in}|$, below ω_l^t is $|X_{out}^l|$, and above ω_u^t is $|X_{out}^u|$. Then, one can choose the mode window so that all modes (below or above) that window contribute to the response in the range $[\omega_l^t, \omega_u^t]$ less than $T_x|X_{in}|$. Two non-dimensional scalars can then be defined as $r_l = |X_{out}^l|/(T_x|X_{in}|)$ and $r_u = |X_{out}^u|/(T_x|X_{in}|)$. Then, the mode window $[\omega_{m,l}^t, \omega_{m,u}^t]$ is given by

$$\omega_{m,l}^t = \omega_l^t \sqrt{1 - 2\zeta_e\sqrt{r_l^2 - 1}},\ \omega_{m,u}^t = \omega_u^t \sqrt{1 + 2\zeta_e\sqrt{r_u^2 - 1}}, \tag{4.24}$$

where ζ_e is an expected damping level. See the Appendix for more information on the derivation of Eqn. (4.24). Any mode with a natural frequency in the range $[\omega_l^t, \omega_u^t]$ potentially participates significantly in the responses in the measurement window.

If no measurements are present inside the measurement window due to missing data or due to measurement filtering, then the damping of the target mode is flagged as not possible to identify. Also, when measurements were not taken or were removed by data filters [56] outside of the lower (or upper) measurement window, it is not possible to define X_{out}^l (or X_{out}^u). In these cases, one mode is added at a time to the modes already in the measurement window $[\omega_l^t, \omega_u^t]$ until the truncated modal matrix

$\mathbf{R\Phi}$ loses rank or $m = n$. Also, if the measurement window includes all the available measurement frequencies (then there are no measurements outside the lower or upper measurement window bounds and) the modes are added by their proximity to ω_l^t or ω_u^t. The mode closest in frequency to one of the limits is added first.

Using these definitions the new damping identification is

$$\mathbf{h}\left(\bar{\omega}\right)_t = \frac{1}{\bar{\omega}} Im \left\{ \left(\mathbf{G}_{meas}\mathbf{\Phi}_{mode}\mathbf{\Psi}_{mode}\right)^T \left(\mathbf{R}_{meas}\mathbf{x}_{meas}\mathbf{F}_{meas}^{-1}\right)^{-*} \mathbf{R}_{meas}\mathbf{\Phi}_{mode}\mathbf{\Psi}_{mode} \right\} \text{ and} \tag{4.25}$$

$$\mathbf{e}\left(\bar{\omega}\right)_t = \frac{1}{\bar{\omega}} \left(\bar{\omega}^2\mathbf{I} - \mathbf{\Lambda}_{mode}\right) \tag{4.26}$$

where subscript *meas* denotes responses inside the measurement window, subscript *mode* refers to modes with mistuned natural frequencies inside the mode window, and $\bar{\omega}$ is the excitation frequency inside of the measurement window t such that the magnitude of the target mode modal coordinate is the largest. For a given frequency window, only the identified value of the target mode t ($h\left(\bar{\omega}\right)_{tt}$ and $e\left(\bar{\omega}\right)_{tt}$) are retained from $\mathbf{h}\left(\bar{\omega}\right)_t$ and $\mathbf{e}\left(\bar{\omega}\right)_t$; the others are ignored. Then, c^t is obtained by using only the retained information for the target mode in Eqns. (4.18), (4.19), and (4.22). Note that the effect of measurement noise on the coefficient c is further reduced by averaging the results over the frequency windows. Thus, one obtains

$$c^{avg} = \frac{1}{m}\sum_{t=1}^{m} \bar{c}^t \theta_{c,t}^{avg}, \tag{4.27}$$

where $\bar{c}^t$ and $\theta_{c,t}^{avg}$ are the magnitude and phase obtained using only the information for the target mode in its frequency window. Also, one can use Eqn. (4.19) for mode $u = t$ and for $\theta_{c,t} = \theta_{c,t}^{avg}$ to obtain an average value for the phase $\theta_{h,t}$ as

$$\theta_{h,t}^{avg} = \theta_{wp,t}^{avg} - \theta_{c,t}^{avg}. \tag{4.28}$$

Thus, the phase of $h\left(\bar{\omega}\right)_{tt}$ can be modified such that $h_t^{avg} = \left|h\left(\bar{\omega}\right)_{tt}\right| e^{j\theta_{h,t}^{avg}}$ and $\mathbf{h}^{avg} = diag\left(h_t^{avg}\right)$. The final identified damping is

$$\boldsymbol{\zeta} = \frac{1}{2} diag\left(\omega_n^t\right)^{-1} Im\left\{c^{avg}\ \mathbf{h}^{avg}\right\}. \tag{4.29}$$

As the damping identification is formulated using RFRMs, it is possible that the measurement locations do not allow all of the mistuned modes to be differentiated. That is because it is possible for the columns of $\mathbf{R}\boldsymbol{\Phi}_m$ not to be linearly independent. The independence of the columns of $\mathbf{R}\boldsymbol{\Phi}_m$ can be checked though the partial modal assurance criteria (PMAC) [57]. If the mode window contains such modes (and the target mode is not one of them), then the transformation of the physical response to modal coordinates remains accurate as the modal coordinate of the target mode still lies in the space spanned by the modes in the mode window. However, if the target mode is one of the indistinguishable modes, then the modal coordinate of the target mode is not unique. Therefore, the damping identification of this target mode is not possible (unless other measurement points are selected).

4.8 Frequency Windowing Results

As an example of the proposed frequency windowing, the results discussed in this section assume an error of $\pm 2\%$ in mistuned eigenvalues of the University of Michigan validation blisk. The validation blisk is a 141,120 DOF model, with an applied stiffness mistuning pattern with values between $\pm 1\%$ and a CME [51] of approximately 1% for each mode. The validation blisk is described in detail in [52]. The damping identification used the actual mistuning and CME to focus on the accuracy of only the damping identification (not the mistuning identification). Therefore, the resonant response of the target mode is assumed to lie within $\pm\delta\omega_n^2 = \pm 2\%$ of the mistuned eigenvalue. Note that the actual error in the identified mistuned natural frequencies

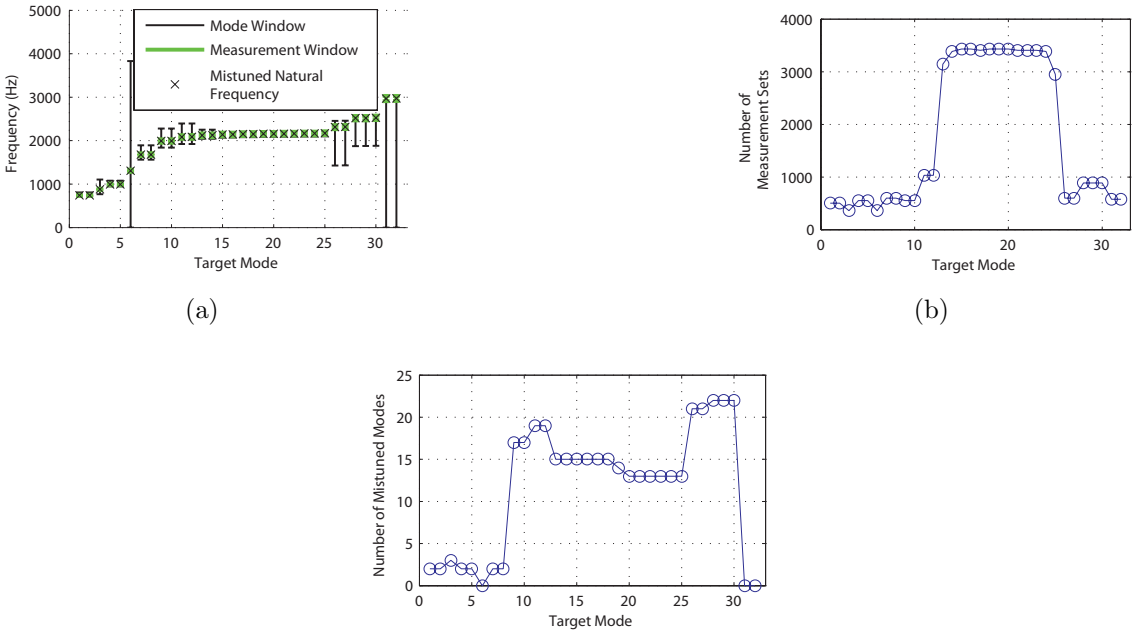

Figure 4.2: Shown are, for each target mode, the frequency of the mode, the number of measurement sets in its measurement window, and the number of modes in its mode window

is less than 0.1% for the example discussed herein. This very conservative error range was chosen to ensure that the measurement window spans the maximum potential range where mistuned modes participate and is not indicative of the mistuning identification error. Note that the more accurate the knowledge of the mistuning is, the smaller the measurement window may be, and that can have the beneficial result of fewer modes in the respective windows.

Figures 4.2(a), 4.2(b), and 4.2(c) show the effects of this windowing applied to the validation blisk. The frequency of interest is 0 to 3 kHz and covers the first mode family. The x-axis of each of the plots corresponds to the target mistuned mode ordered by increasing frequency. The y-axis of Fig. 4.2(a) is the frequency. The measurement and mode windows are between the respective bars in Fig. 4.2(a). The y-axis of Fig. 4.2(b) is the number of measurements sets inside each measurement window of each target mode. One measurement set consists of measuring the response

at various locations on the blisk at a given frequency. We considered 24 forcing cases. Thus, the number of measurements inside each measurement window for each forcing case is 1/24 of the values on the y-axis of Fig. 4.2(b). The y-axis of Fig. 4.2(c) displays the number of modes in each mode window for each target mode.

If the response is isolated (other modes are distant in frequency), then the measurement window is expected to be small and contain few measurements as only measurements close to the target mode's natural frequency contain enough information about the damping of that mode. Also, it is expected that the number of modes will also be small as only a few modes contribute to the response. Mistuned modes 1-5, 7, and 8 mistuned modes have this behavior.

If the maximum response in the measurement window of a target mode is low, then the corresponding mode window is expected to be larger as more modes may participate in the response. Target mode 6 exhibits this behavior where the mode is isolated. However, due to the low level of response of mode 6, other modes may still participate in measurements near the target mode's natural frequency. Note that regions of high modal density and large responses (modes 13 to 25) contain more measurements although their mode windows have approximately the same size. However, Fig. 4.2(c) shows that these mode windows contain many more modes than the more isolated modes.

The mistuned modes were represented using only the first cantilevered blade projection [48, 49]. Mistuned modes 26 to 32 have motions which are more similar to the second cantilevered blade. Therefore, it is expected that these modes will have larger mode windows (in an attempt to compensate for the absent second cantilevered blade projection) and less accurate damping identification values.

Recall that the goal of the frequency windowing is to reduce the number of measurements and forcing cases required for modal damping identification. Figure 4.2(c) shows that the maximum number of modes required to identify the damping of target

modes 1 to 25 is 19 instead of the 32 modes in the full frequency range of interest. Thus, the identification without windows would require 48 measurements and 32 forcing cases. In contrast, the identification with frequency windowing only requires 24 measurements (one per blade) assuming that the measurement locations are valid for each mode [56]. Also, only 19 forcing cases are required, which requires no more than one forcing location per blade. Thus, the frequency windowing reduces the experimental cost and increases the identification accuracy without significantly increasing the computational cost. Also, in general, the modal damping identification method using windowing is independent of the frequency range of interest (with the exception of the modes near the edges of the range of interest).

4.9 Damping Identification Results

This section explores the accuracy of the hybrid damping identification with respect to the measurement noise level for the University of Michigan validation blisk. To investigate the effects of measurement noise, we first used ANSYS to obtain simulated measurement data. This data is perfect in the sense that it contains no measurement noise. Next, we injected white noise in this data to simulated the presence of measurement noise. The noise was modeled using relative, absolute, and bias terms [56]. Note that the simulated measurements are computed for the full blisk model, without reduction. Thus, there are modeling differences between ANSYS and ROMs. These differences are not unlike the differences between a model and an actual blisk that is measured.

The following results were obtained using measurement filters, $R_{thresh} = 0.40$, $P_{thresh} = 0.005$, $T_l = 0.25$ for the 5% and $T_l = 0.50$ for the 10% measurement noise results [56]. It was also found that certain modes could have erroneously large modal coordinates due to noise. Therefore, surrogate data was generated and noise injected into the surrogate measured response. The surrogate data was created by solving

Eqn. (4.3) with a modal damping determined by $\zeta^{mode} = R^{mode}\zeta_e$, where R is a random number drawn from a uniform distribution between 0 and 2. Both the actual and noisy measurements were then converted to mistuned modal coordinates. If the physical to modal transformation of the noisy data for mode u at frequency i gave a modal amplitude $p_{i,u}^{noisy}$ which was much larger than the actual modal amplitude $p_{i,u}^{actual}$, then the mode is sensitive to noise. Since the reliability of the noise sensitive modes is suspect, mode u is not included in the identification equations when $p_{i,u}^{noisy} > T_b p_{i,u}^{actual}$. For the following results, $T_b = 5$. Also, modal coordinates which have low magnitudes can be inaccurate due to measurement noise. Therefore, the modal amplitude of mode u at frequency i is ignored if $|p_{i,u}| < T_p \; max_u \, |p_{i,u}|$. For the following results, $T_p = 0.75$. Also, two modes are considered to be distinguishable if the PMAC between the two corresponding columns of $\mathbf{R\Phi}_m$ is less than 0.05.

Figures 4.3 and 4.4 show the damping identification results for 5% and 10% measurement noise levels. All measurement filters were optimized for the 5% noise case. Therefore, it is expected that the 10% noise case will have larger errors than the 5% noise case. The x-axis displays the mistuned modes in the frequency range of interest for which the modal damping is to be identified. The y-axis contains identified damping values. Figure 4.3 shows the mean identified modal damping value for 1,000 measurement noise realizations. The corresponding standard deviation (denoted by Std) of the identified values is displayed in Fig. 4.4. Three measurements per blade were recorded. For these results, all modes in all of the RFRMs were distinguishable.

If measurements are in directions perpendicular to the motion of the blisk, one expects the damping identification for these modes will be inaccurate. This behavior occurs for mode 6 where the motion is perpendicular to the axis of the blisk, however all the measurements are taken in the direction of the axis of the blisk. As a result the identification is consistently and conspicuously incorrect. Also, recall that only

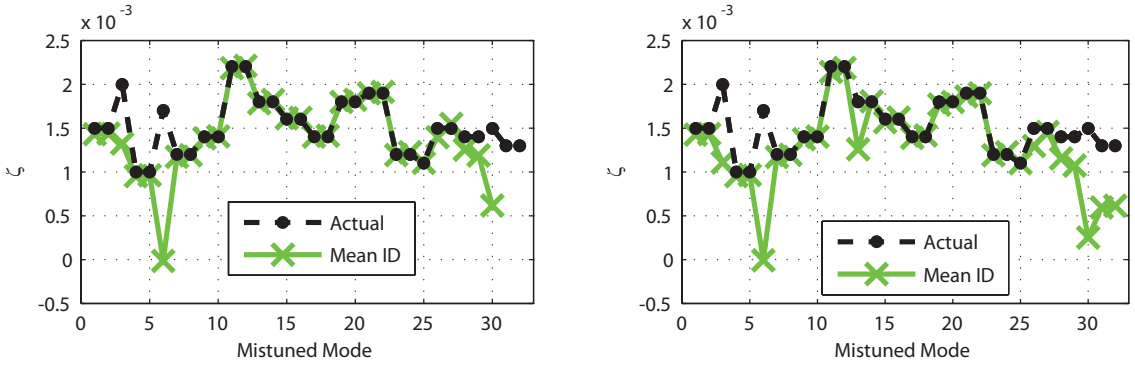

Figure 4.3: Mean identified (ID) damping for the validation blisk using data with 5% (a) and 10% (b) relative noise; mistuned modes are ordered by increasing frequency

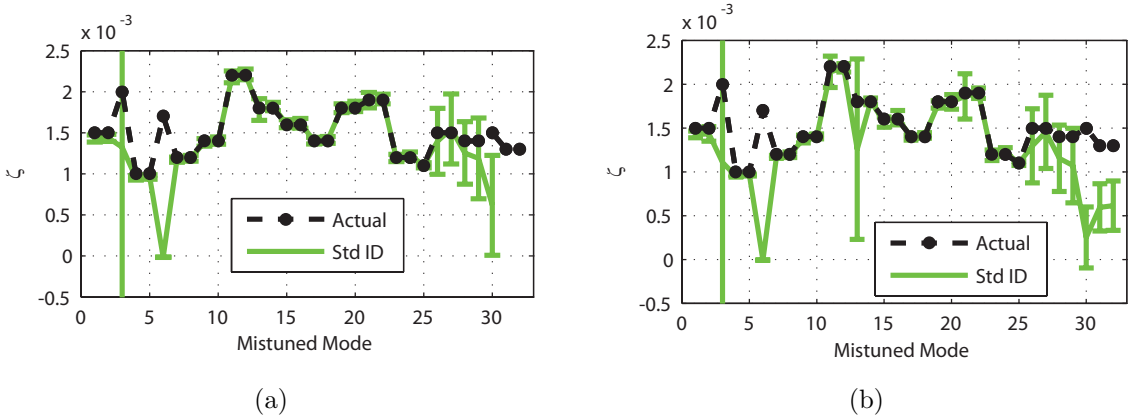

Figure 4.4: Standard deviation (Std) of identified (ID) damping for the validation blisk using data with 5% (a) and 10% (b) relative noise; mistuned modes are ordered by increasing frequency

the blade portion of the blisk is measured. Therefore, if a mode is disk dominated (i.e., most of the motion occurs in the disk and not the blades) then one could expect the damping identification of the corresponding mode to be inaccurate or sensitive to measurement noise. Mode 3 provides an example of this noise sensitivity, with a very large standard deviation (-1.5×10^{-3} to 3.8×10^{-3} in Fig. 4.4(a) and -1.6×10^{-3} to 3.9×10^{-3} in Fig. 4.4(b), which exceed the plot limits). For modes near the upper frequency limit of the ROM (modes 26 to 32), one expects the ROM to become less accurate (as modes higher in frequency and not included in the ROM

may participate in the response). Also, these modes begin to exhibit motion which resembles the second cantilevered blade instead of the first. Since only the first cantilevered blade was used to represent mistuning utilizing the CMM approach, the damping identification is expected to be less accurate for these modes.

Excluding the aforementioned modes, the results show that the damping identification is accurate for higher levels of noise. In particular, the relative error in the mean value for both noise cases shown in Fig. 4.3 is below the level of the measurement noise (with the exception of the 13^{th} mode in Fig. 4.3(b), which has a relative error of 27.3%). The standard deviation relative error in Fig. 4.4(a) is below 5% except for modes 3, 6, 13, and 26-30. Mode 13 has an error of 7.0%. The relative error for the case of 10% noise shown in Fig. 4.4(b) is below 10% except for modes 13 and 21 which have values of 58.2% and 14.6% respectively. The results indicate that the responses with a large participation of mode 13 are low causing the identification to be sensitive to the absolute and bias measurement noise. In general, the mean damping identification is accurate in the presence of measurement noise, with a relative error less than the level of the measurement noise. The standard deviation of each identified damping value is more sensitive to measurement noise than the mean identified value.

An alternative accuracy test is to compare the results of this damping identification method with the one in [56] (referred to as Multi in the figures). Figures 4.5 and 4.6 show the mean and standard deviation of the identified damping values for 5% and 10% noise levels. For comparison, the same noisy measurement data was used in both methods. Both methods use the same measurement filter values, which are optimized for the proposed method. The Multi method used a ROM consisting of 17 modes, while the hybrid method used 29 frequency windows. The results for the 5% noise level indicate that the hybrid method is less robust to measurement noise than the alternative method. However, for the 10% measurement noise case, both

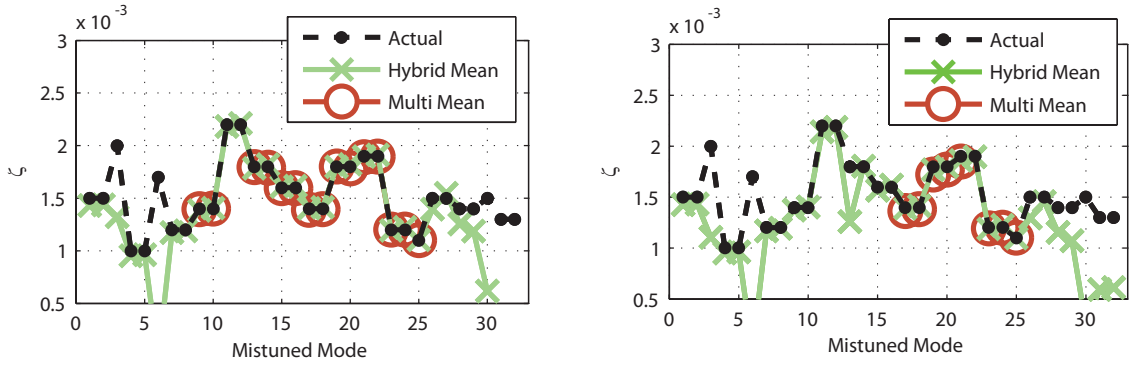

Figure 4.5: Mean identified (ID) damping for the two methods using data with 5% (a) and 10% (b) relative noise; mistuned modes are ordered by increasing frequency

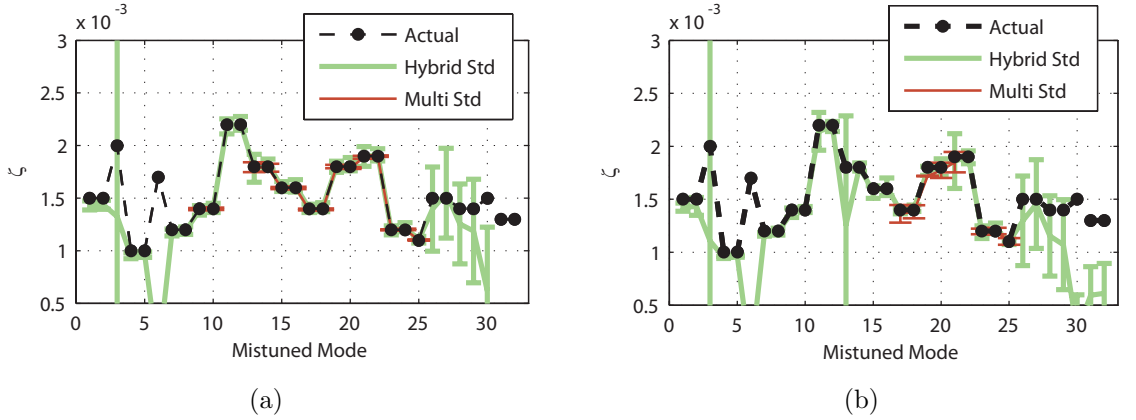

Figure 4.6: Standard deviation (Std) of identified damping (ID) for the two methods using data with 5% (a) and 10% (b) relative noise; mistuned modes are ordered by increasing frequency

method preformed with similar accuracy. In addition, note that while the hybrid method sacrifices some accuracy in the damping identification, the damping of 30 or 32 modes was identified while the Multi method only identified 15 or 8 values.

The damping identification requires that the relative forcing for a given distribution $\tilde{\mathbf{G}}_g$ be known for a given frequency range, and that the relative forcing between different distributions be known at a given frequency. One way to ensure the first requirement is to use the frequency transfer function for each speaker or magnet used for excitation, and assume that the force applied to the structure is propor-

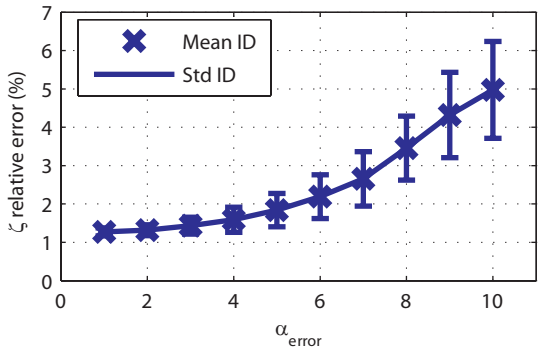

Figure 4.7: Variation in identified damping due to error in forcing

tional to the output of the speakers or magnets. The second requirement can be ensured though a forcing calibration similar to the one in [1]. To study the effects of errors in the relative forcing, the applied forcing was corrupted by using $F(\omega) = 100[1 + \alpha_{error}/100 r_1(\omega)] + j\alpha_{error} r_2(\omega)$ (measured in mN), where $r_1(\omega)$ and $r_2(\omega)$ are random numbers drawn from a uniform distribution between -1 and 1. The nominal applied force is 100 mN. 100 realizations of forcing were created and the identification was performed for each value of α_{error} between 1 and 10. Therefore, the amplitude errors considered are up to 10%. The phase angle errors are up to $\pm 6.3°$. The modes which could not be captured accurately by the damping identification due to the measurement direction, the range of validity of the ROM, and large sensitivity to measurement noise (modes 3, 6, 26-32) were excluded from this study for clarity. Figure 4.7 shows the mean relative error of the identified modal damping values for all modes for each α_{error}. Also shown is the standard deviation over the noise realizations of the standard deviation of the mean relative error of the identified modal damping values for all modes for each α_{error} (denoted Std ID). Of course, other statistical measures could be computed also. These results provide useful partial information about the average accuracy of the damping identification. The standard deviation of the identification increases with the α_{error} value. The mean relative error is approximately constant for α_{error} between 1 and 3. This trend is most likely due

to errors caused by the approach used to model mistuning. The mean relative error increases approximately linearly for α_{error} values between 4 and 10. In general, the identification error caused by variations in the relative forcing is smaller than the error due to (equivalent levels of) measurement noise.

4.10 Conclusions

This method offers several benefits as compared to current damping identification techniques. First, the proposed methodology uses a reduced frequency response matrix such that only a subset of all the DOF of the system need to be measured, with another subset being forced. The hybrid damping identification does not require knowledge of the absolute forcing, but can identify this value if the relative forcing is known (from a forcing calibration).

An important feature which allows the identification to be accurate is the introduction of the frequency windowing. The windowing can reduce the effects of measurement noise and also lower the number of required forcing cases. The proposed damping identification uses a reduced frequency response matrix, which is further reduced in size using the frequency windowing. As a result, fewer locations need to be measured and/or forced. This decrease in data acquisition has a significant impact on the computational cost of preforming the damping identification. In addition, this method can be applied to mistuned systems and uses ROMs. Therefore, the proposed method is computationally efficient also.

Results for a validation blisk show that identifying the modal damping is possible by employing the proposed approach, which uses a ROM, requires measurements at only a few locations per blade, and is effective even in the presence of relative, absolute and bias measurement noise. A comparison of this method with the alternative method of Holland et al. [56] shows that the proposed method is less accurate when using the same filter values, however more modal damping values can be identified

with the proposed approach. In general, the mean identified values for the alternative method are slightly more accurate and have lower standard deviations than the hybrid method. However, as the two methods do not use the same measurement filters (although the values are the same) the difference in the identification accuracy is from a combination of the noise sensitivity and the measurement data filtering.

Also, a study was conducted to determine the effect of forcing errors on the damping identification. The results indicate that the damping identification is more sensitive to measurement noise than to forcing errors.

CHAPTER V

Component Damping Identification Methods for Mistuned Blisks

5.1 Introduction

Wear or manufacturing processes or defects can cause slight variations in the mass or stiffness of a nominally cyclically symmetric structure such as an integrally bladed disk (blisk). These variations or mistuning can cause the vibration energy to localize at certain regions of the structure resulting in larger than expected forced responses and stresses. Therefore, these mistuned systems are susceptible to high cycle fatigue. One method to compensate for the effects of mistuning is to apply damping coatings. However, Joshi et al. [3] found that the dynamics of the system can significantly change due to variations in the thickness of the applied coating. To determine the damping characteristics of coatings, a damping identification technique is needed which can determine the damping associated with individual components of a mistuned blisk (before and after the coating is applied). Currently, damping identification relies on one of several common damping models namely, structural, viscous, and component (material) damping. In general, structural damping is defined for a full system, while viscous damping is defined for individual system modes.

Most current damping identification techniques assume that damping has a cer-

tain form at a system level. For example, the damping in complex structures is often assumed to be viscous, modal, or structural. Such assumptions provide accurate results for structures with relatively simple geometries and low modal density. However, these approximations can be cumbersome or inaccurate for structures with complex geometry and high modal density. For such systems, using a component-oriented model can be more effective. In particular, component damping corresponds to a proportional or structural damping applied to individual components of a structure (i.e., each component has an associated material damping). For instance, each blade of a blisk can be modeled as a separate component with an associated damping parameter (which is to be identified). The resulting damping is only approximately modal, and the corresponding modal damping values vary with different component damping properties. As a result, the component damping can represent the physical attributes of the structure more closely and may require less effort than identifying the modal damping for a structure with a moderate number of components and a large number of modes in the frequency range of interest.

While finite element modeling (FEM) methods incorporate component damping, most identification methods found in literature are difficult or impossible to use to identify this type of damping from experimental data [4, 6, 7, 11, 12, 14–20, 22–24, 26–29]. Statistical energy analysis (SEA) is one method for determining component (subsystem) damping loss factors. This method is useful for high frequency ranges. However, this technique is limited as the damping is assumed to be known either from the power injection method (PIM) [32,33,35,36], power modulation method [36], or a wave approach [37]. PIM and power modulation techniques require measuring energy for all the components, and that can be difficult or impossible to gather accurately. Also, wave theory only applies to periodic systems. Moreover, the SEA method can be time consuming if there are many components [36]. In addition, the accuracy of the SEA method depends on the modal density and the level of damping, as shown

by Mace [38] and Yap et al. [39].

The work herein presents a novel component damping identification technique which can be applied to mistuned blisks and use certain reduced-order models (ROMs) in regions of low and/or high modal density. In addition, a method for predicting the forced response of the system using ROMs is provided, and that can decrease design time and enable statistical analyses of component damping scenarios.

5.2 Equations of Motion

In this section, equations of motion are developed beginning with Lagrange's equation. Component-level damping is introduced to the disassembled system by including a Rayleigh damping function. Finally, the system-level structural equation of motion incorporating component damping is obtained.

The kinetic and potential energies and the Rayleigh damping function for a structure can be expressed as

$$\begin{aligned} T &= \tfrac{1}{2}\dot{\mathbf{q}}^{c_1{}^T}\boldsymbol{\mu}^{c_1}\dot{\mathbf{q}}^{c_1} + \tfrac{1}{2}\dot{\mathbf{q}}^{c_2{}^T}\boldsymbol{\mu}^{c_2}\dot{\mathbf{q}}^{c_2} + \ldots + \tfrac{1}{2}\dot{\mathbf{q}}^{c_n{}^T}\boldsymbol{\mu}^{c_n}\dot{\mathbf{q}}^{c_n}, \\ V &= \tfrac{1}{2}\mathbf{q}^{c_1{}^T}\tilde{\boldsymbol{\kappa}}^{c_1}\mathbf{q}^{c_1} + \tfrac{1}{2}\mathbf{q}^{c_2{}^T}\tilde{\boldsymbol{\kappa}}^{c_2}\mathbf{q}^{c_2} + \ldots + \tfrac{1}{2}\mathbf{q}^{c_n{}^T}\tilde{\boldsymbol{\kappa}}^{c_n}\mathbf{q}^{c_n}, \\ D &= \tfrac{1}{2}\dot{\mathbf{q}}^{c_1{}^T}\boldsymbol{\eta}^{c_1}\dot{\mathbf{q}}^{c_1} + \tfrac{1}{2}\dot{\mathbf{q}}^{c_2{}^T}\boldsymbol{\eta}^{c_2}\dot{\mathbf{q}}^{c_2} + \ldots + \tfrac{1}{2}\dot{\mathbf{q}}^{c_n{}^T}\boldsymbol{\eta}^{c_n}\dot{\mathbf{q}}^{c_n}, \end{aligned} \tag{5.1}$$

where T is the kinetic energy, V is the potential energy, D is the Rayleigh damping function, c_i denotes component i, $i \in 1, 2, \ldots, n$, and the component mass, stiffness, and damping matrices are $\boldsymbol{\mu}^{c_i}$, $\tilde{\boldsymbol{\kappa}}^{c_i}$, and $\boldsymbol{\eta}^{c_i}$ respectively. The generalized coordinates $\mathbf{q}^{c_i}$ for all components are, in general, not independent because the components are coupled. The coupling can be modeled as constraints. Expressing the geometric constraint equations in terms of all generalized coordinates grouped in a vector $\mathbf{q}$, one obtains

$$\mathbf{E}\mathbf{q} = \mathbf{0}, \tag{5.2}$$

where the size of the vector $\mathbf{q}$ is $N \times 1$ and the size of the matrix $\mathbf{E}$ is $(N-a) \times N$ with N being the number of disassembled degrees of freedom (DOFS) and a being the number of independent DOFs.

Lagrange's equation with Rayleigh damping is

$$\frac{\partial}{\partial t}\left(\frac{\partial L}{\partial \dot{\mathbf{q}}}\right) - \frac{\partial L}{\partial \mathbf{q}} + \frac{\partial D}{\partial \dot{\mathbf{q}}} = \mathbf{F}, \tag{5.3}$$

where $L = T - V + \boldsymbol{\sigma}^T \mathbf{E}\mathbf{q}$, the vector $\mathbf{F}$ has a size of $N \times 1$ and contains all the non-conservative generalized forces, and the vector $\boldsymbol{\sigma}$ of size $(N-a) \times 1$ contains Lagrange multipliers.

Substituting Eqns. (5.1) and (5.2) into (5.3), one obtains

$$\boldsymbol{\mu}\ddot{\mathbf{q}} + \bar{\boldsymbol{\eta}}\dot{\mathbf{q}} + \boldsymbol{\kappa}\mathbf{q} = \mathbf{E}^T\boldsymbol{\sigma} + \mathbf{F}, \tag{5.4}$$

where matrices $\boldsymbol{\mu}$, $\boldsymbol{\kappa}$, and $\bar{\boldsymbol{\eta}}$ are of size $N \times N$ and are given by

$$\boldsymbol{\mu} = \begin{bmatrix} \boldsymbol{\mu}^{c_1} & \mathbf{0} & \cdots & \mathbf{0} \\ \mathbf{0} & \boldsymbol{\mu}^{c_2} & \ddots & \vdots \\ \vdots & \ddots & \ddots & \mathbf{0} \\ \mathbf{0} & \cdots & \mathbf{0} & \boldsymbol{\mu}^{c_n} \end{bmatrix} = Bdiag\left[\boldsymbol{\mu}^{c_i}\right], \boldsymbol{\kappa} = Bdiag\left[\tilde{\boldsymbol{\kappa}}^{c_i}\right], \text{ and } \bar{\boldsymbol{\eta}} = Bdiag\left[\boldsymbol{\eta}^{c_i}\right].$$

The vector of generalized coordinates which are independent at a system level is denoted by $\mathbf{X}$. Vector $\mathbf{X}$ is of size $a \times 1$. The relation between $\mathbf{q}$ and $\mathbf{X}$ can be expressed by using a matrix $\mathbf{S}$ os size $N \times a$. One obtains

$$\mathbf{q} = \mathbf{S}\mathbf{X}, \ \dot{\mathbf{q}} = \mathbf{S}\dot{\mathbf{X}}, \text{ and } \ddot{\mathbf{q}} = \mathbf{S}\ddot{\mathbf{X}}. \tag{5.5}$$

Pre-multiplying both sides by $\mathbf{E}$ and noting that $\mathbf{X}$ is a vector of independent co-ordinates, one can conclude that $\mathbf{E}\mathbf{q} = \mathbf{E}\mathbf{S}\mathbf{X} = \mathbf{0}$ for any $\mathbf{X}$. For most systems of

practical interest the number $(N-a)$ of constraints is much larger than the number of independent coordinates. Thus, $N-a >> a$. Since $\mathbf{ES}$ is of size $(N-a)\times a$ and $\mathbf{ESX}=\mathbf{0}$ for any $\mathbf{X}$, one may conclude that

$$\mathbf{ES}=\mathbf{0}. \tag{5.6}$$

Pre-multiplying Eqn. (5.4) by $\mathbf{S}^T$ and using Eqn. (5.5), one obtains

$$\mathbf{S}^T\boldsymbol{\mu}\mathbf{S}\ddot{\mathbf{X}}+\mathbf{S}^T\bar{\boldsymbol{\eta}}\mathbf{S}\dot{\mathbf{X}}+\mathbf{S}^T\boldsymbol{\kappa}\mathbf{S}\mathbf{X}=\left(\mathbf{ES}\right)^T\boldsymbol{\sigma}+\mathbf{S}^T\mathbf{F}=\mathbf{S}^T\mathbf{F}.$$

Defining $\mathbf{M}=\mathbf{S}^T\boldsymbol{\mu}\mathbf{S}$, $\mathbf{C}=\mathbf{S}^T\bar{\boldsymbol{\eta}}\mathbf{S}$, and $\mathbf{K}=\mathbf{S}^T\boldsymbol{\kappa}\mathbf{S}$ produces

$$\mathbf{M}\ddot{\mathbf{X}}+\mathbf{C}\dot{\mathbf{X}}+\mathbf{K}\mathbf{X}=\mathbf{S}^T\mathbf{F}. \tag{5.7}$$

5.3 Component Damping Response

Next, we focus on both damping and stiffness mistuning in blisks. The equation of motion in Eqn. (5.7) is transformed to mistuned modal coordinates. The resulting equations are decoupled in mass and stiffness, but remain coupled though damping. Finally, forced response equations for ROMs are developed to facilitate the design of systems with component damping.

First, assume $\mathbf{F}$ is a harmonic forcing with (complex) magnitude $\mathbf{f}$ at frequency ω. Using Eqn. (5.7), one obtains

$$-\omega^2\mathbf{M}\mathbf{x}+j\omega\mathbf{S}^T Bdiag\left[\bar{\boldsymbol{\eta}}^{c_i}\right]\mathbf{S}\mathbf{x}+\mathbf{K}\mathbf{x}=\mathbf{S}^T\mathbf{f},$$

where $\mathbf{x}$ is a vector of size $a\times 1$ containing the (complex) magnitude of the harmonic response. Let the damping be represented using a mean term and a variation from the mean, so that $\bar{\boldsymbol{\eta}}^{c_i}=\Gamma^m\tilde{\boldsymbol{\kappa}}^{c_i}+\delta\Gamma^{c_i}\tilde{\boldsymbol{\kappa}}^{c_i}$, where Γ^m is a single damping value (which

is the same for all components) and $\delta\Gamma^{c_i}$ is the damping mistuning associated with component i. Thus, the damping in component i is given by $\Gamma^{c_i} = \Gamma^m + \delta\Gamma^{c_i}$. Combining the $\tilde{\boldsymbol{\kappa}}^{c_i}$ matrices from the damping and stiffness terms, one obtains

$$\left(-\omega^2\mathbf{M} + \mathbf{S}^T Bdiag\left[\left(1 + j\omega\Gamma^m\right)\tilde{\boldsymbol{\kappa}}^{c_i} + j\omega\delta\Gamma^{c_i}\tilde{\boldsymbol{\kappa}}^{c_i}\right]\mathbf{S}\right)\mathbf{x} = \mathbf{S}^T\mathbf{f}. \tag{5.8}$$

For a blisk with stiffness mistuning, $\tilde{\boldsymbol{\kappa}}^{c_i} = (\boldsymbol{\kappa}^{c_i} + \delta\boldsymbol{\kappa}^{c_i})$, where $\boldsymbol{\kappa}^{c_i}$ is the stiffness matrix (from a tuned analysis) for component c_i, and δ denotes a mistuned matrix. Then,

$$\left(1 + j\omega\Gamma^m\right)\tilde{\boldsymbol{\kappa}}^{c_i} + j\omega\delta\Gamma^{c_i}\tilde{\boldsymbol{\kappa}}^{c_i} = \left(1 + j\omega\Gamma^m\right)\left(\boldsymbol{\kappa}^{c_i} + \delta\boldsymbol{\kappa}^{c_i}\right) + j\omega\delta\Gamma^{c_i}\left(\boldsymbol{\kappa}^{c_i} + \delta\boldsymbol{\kappa}^{c_i}\right). \tag{5.9}$$

Next, we convert to (mass normalized) mistuned modal coordinates by using $\mathbf{x} = \bar{\boldsymbol{\Phi}}\bar{\mathbf{p}}$, where $\bar{\boldsymbol{\Phi}}$ is a matrix of size $a \times a$ containing all mistuned modes, and $\bar{\mathbf{p}}$ is a vector of size $a \times 1$ containing all the mistuned modal amplitudes. Pre-multiplying Eqn. (5.8) by $\bar{\boldsymbol{\Phi}}^T$, letting $\bar{\boldsymbol{\Psi}} = \mathbf{S}\bar{\boldsymbol{\Phi}}$, and using Eqn. (5.9), one obtains

$$-\omega^2\bar{\mathbf{p}} + \left(1 + j\omega\Gamma^m\right)\bar{\boldsymbol{\Lambda}}_{mist}\bar{\mathbf{p}} + j\omega\bar{\boldsymbol{\Psi}}^T Bdiag\left[\delta\Gamma^{c_i}\left(\boldsymbol{\kappa}^{c_i} + \delta\boldsymbol{\kappa}^{c_i}\right)\right]\bar{\boldsymbol{\Psi}}\bar{\mathbf{p}} = \bar{\boldsymbol{\Psi}}^T\mathbf{f}, \tag{5.10}$$

where the diagonal matrix of mistuned eigenvalues is $\bar{\boldsymbol{\Lambda}}_{mist} = \bar{\boldsymbol{\Psi}}^T Bdiag\left[\boldsymbol{\kappa}^{c_i} + \delta\boldsymbol{\kappa}^{c_i}\right]\bar{\boldsymbol{\Psi}}$. Note that $\bar{\boldsymbol{\Psi}}$ is a matrix which contains the disassembled mistuned system modes (where the interface is duplicated). Thus, $\bar{\boldsymbol{\Psi}}$ is of size $N \times a$, where N is the number of disassembled DOFs.

Next, we use ROMs to efficiently and accurately generate the forced response of a mistuned system with component damping variability. First, we assume that outside a given frequency range of interest, $\bar{p}_t \approx 0$ for modes t. Therefore, $\bar{\mathbf{p}}$ can be reduced from size $a \times 1$ to $\mathbf{p}$ of size $m \times 1$, where $m = a - t$. Also, the columns of $\bar{\boldsymbol{\Phi}}$ corresponding to these modes can be ignored reducing $\bar{\boldsymbol{\Phi}}$ from size $a \times a$ to $\boldsymbol{\Phi}$ of size

$a \times m$. A similar change occurs for $\bar{\mathbf{\Psi}}$, which is reduced from size $N \times a$ to $\mathbf{\Psi}$ of size $N \times m$. In addition, $\bar{\mathbf{\Lambda}}_{mist}$ is reduced from size $a \times a$ to $\mathbf{\Lambda}_{mist}$ of size $m \times m$. As the left side of Eqn. (5.10) contains near-zero values for modes t, these equations can be ignored.

The use of $\mathbf{\Lambda}_{mist}$ indicates that only the m modes participating in the response for a given frequency range of interest are needed to complete the identification. For blisks with small mistuning, Griffin et al. [40] also found that the mistuned modes can be represented as a linear combination of tuned system modes. Therefore, $\mathbf{\Phi} = \boldsymbol{\phi}\mathbf{\Theta}$, where $\boldsymbol{\phi}$ is a $a \times \theta$ matrix which contains θ tuned system modes in the frequency range of interest. $\mathbf{\Theta}$ is a $\theta \times m$ matrix of participation factors for the mistuned modes. Therefore, the forced response can also be accurately calculated using the subset of θ tuned modes in matrix $\boldsymbol{\phi}$.

Using a ROM, solving Eqn. (5.10) for $\mathbf{p}$, and pre-multiplying by $\mathbf{\Phi}$, one obtains

$$\begin{aligned} &\mathbf{x} = \mathbf{\Phi}\mathbf{p} = \\ &\mathbf{\Phi}\left\{-\omega^2\mathbf{I} + (1 + j\omega\Gamma^m)\,\mathbf{\Lambda}_{mist} + \mathbf{\Psi}^T j\omega B diag\left[\delta\Gamma^{c_i}\left(\boldsymbol{\kappa}^{c_i} + \delta\boldsymbol{\kappa}^{c_i}\right)\right]\mathbf{\Psi}\right\}^{-1}\mathbf{\Psi}^T\mathbf{f}. \end{aligned} \tag{5.11}$$

Using a given stiffness mistuning and component damping, the forced response of the system can be calculated using Eqn. (5.11). An equivalent form of Eqn. (5.11) can be found for a system with mass mistuning (omitted here for the sake of brevity).

Consider that the forced response has to be predicted at only r DOFs. Retaining only these DOFs, $\boldsymbol{\phi}$ can be reduced from size $a \times \theta$ to $\tilde{\boldsymbol{\phi}}$ of size $r \times \theta$ so that $\tilde{\mathbf{x}} = \tilde{\boldsymbol{\phi}}\mathbf{\Theta}\mathbf{p}$, where $\tilde{\mathbf{x}}$ is a vector of size $r \times 1$ containing the measured DOFs. This reduction leads to more computationally efficient forced response predictions.

5.4 Component Damping Identification

This section presents a component damping identification method. A least squares solution is detailed. After the initial damping identification formulation, issues specific to blisks are highlighted.

Partitioning $\boldsymbol{\Psi}$ according to the corresponding components, one obtains $\boldsymbol{\Psi} = \left[\boldsymbol{\Psi}_{c_1}^T \boldsymbol{\Psi}_{c_2}^T \cdots \boldsymbol{\Psi}_{c_n}^T\right]^T$. Next, Eqn. (5.10) can be transformed by using a ROM and carrying out the multiplication. One obtains

$$\begin{aligned}
\boldsymbol{\Psi}^T Bdiag\left[\delta\Gamma^{c_i}\left(\boldsymbol{\kappa}^{c_i}+\delta\boldsymbol{\kappa}^{c_i}\right)\right]\boldsymbol{\Psi}\mathbf{p} &= \boldsymbol{\Psi}^T \begin{bmatrix} \delta\Gamma^{c_1}\left(\boldsymbol{\kappa}^{c_1}+\delta\boldsymbol{\kappa}^{c_1}\right)\boldsymbol{\Psi}_{c_1} \\ \delta\Gamma^{c_2}\left(\boldsymbol{\kappa}^{c_2}+\delta\boldsymbol{\kappa}^{c_2}\right)\boldsymbol{\Psi}_{c_2} \\ \vdots \\ \delta\Gamma^{c_n}\left(\boldsymbol{\kappa}^{c_n}+\delta\boldsymbol{\kappa}^{c_n}\right)\boldsymbol{\Psi}_{c_n} \end{bmatrix}_{N\times m} \mathbf{p} \\
&= \boldsymbol{\Psi}^T Bdiag\left[\boldsymbol{\kappa}^{c_i}+\delta\boldsymbol{\kappa}^{c_i}\right]_{N\times N} Bdiag\left[\boldsymbol{\Psi}_{c_i}\right]_{N\times nm}\left(\mathbf{I}_{n\times n}\otimes\mathbf{p}\right)\begin{Bmatrix} \delta\Gamma^{c_1} \\ \vdots \\ \delta\Gamma^{c_n} \end{Bmatrix} \\
&= \boldsymbol{\Psi}^T\tilde{\mathbf{K}}\left(\mathbf{I}_{n\times n}\otimes\mathbf{p}\right)\begin{Bmatrix} \delta\Gamma^{c_1} \\ \vdots \\ \delta\Gamma^{c_n} \end{Bmatrix}, \qquad (5.12)
\end{aligned}$$

where the subscripts on matrices $[\,]_{.\times.}$ indicate the size of the matrix, $\tilde{\mathbf{K}} = Bdiag\left[\left(\boldsymbol{\kappa}^{c_i}+\delta\boldsymbol{\kappa}^{c_i}\right)\boldsymbol{\Psi}_{c_i}\right]$, $\mathbf{I}$ is the identity matrix, $\otimes$ denotes the Kronecker product, and n is the number of components.

Substituting Eqn. (5.12) into Eqn. (5.10) and using a ROM, one obtains

$$j\omega\boldsymbol{\Psi}^T\tilde{\mathbf{K}}\left(\mathbf{I}_{n\times n}\otimes\mathbf{p}\right)\begin{Bmatrix} \delta\Gamma^{c_1} \\ \vdots \\ \delta\Gamma^{c_n} \end{Bmatrix} = \boldsymbol{\Psi}^T\mathbf{f}+\omega^2\mathbf{p}-\left(1+j\omega\Gamma^m\right)\boldsymbol{\Lambda}_{mist}\mathbf{p}. \qquad (5.13)$$

For two frequencies, ω_u and ω_v denoted by subscripts u and v, one obtains

$$j\omega_u \boldsymbol{\Psi}^T \tilde{\mathbf{K}} \left(\mathbf{I}_{n\times n} \otimes \mathbf{p}_u\right) \left\{ \begin{array}{c} \delta\Gamma^{c_1} \\ \vdots \\ \delta\Gamma^{c_n} \end{array} \right\} = \boldsymbol{\Psi}^T \mathbf{f}_u + \omega_u^2 \mathbf{p}_u - \left(1 + j\omega_u \Gamma^m\right) \boldsymbol{\Lambda}_{mist} \mathbf{p}_u, \tag{5.14}$$

and

$$\boldsymbol{\Psi}^T \mathbf{f}_v = j\omega_v \boldsymbol{\Psi}^T \tilde{\mathbf{K}} \left(\mathbf{I}_{n\times n} \otimes \mathbf{p}_v\right) \left\{ \begin{array}{c} \delta\Gamma^{c_1} \\ \vdots \\ \delta\Gamma^{c_n} \end{array} \right\} - \omega_v^2 \mathbf{p}_v + \left(1 + j\omega_v \Gamma^m\right) \boldsymbol{\Lambda}_{mist} \mathbf{p}_v. \tag{5.15}$$

Next, assume that the spatial distribution of the excitation forces $\mathbf{f}_u$ and $\mathbf{f}_v$ applied to the system at frequencies u and v is known. Assume also that the magnitude and phase of these excitations are known up to a multiplicative constant α_{uv}, where $\alpha_{uv} \in \mathbb{C}$ so that $\mathbf{f}_u = \alpha_{uv} \mathbf{f}_v$. Note that one way to extract α_{uv} is to use the frequency transfer function of the speakers or magnets used for excitation, and assume that the force applied to the structure in a given frequency band is proportional to the signal applied to the speakers or magnets in that frequency band. Multiplying Eqn. (5.15) by α_{uv}, one obtains

$$\begin{aligned} \boldsymbol{\Psi}^T \alpha_{uv} \mathbf{f}_v = & j\omega_v \boldsymbol{\Psi}^T \tilde{\mathbf{K}} \left(\mathbf{I}_{n\times n} \otimes \alpha_{uv} \mathbf{p}_v\right) \left\{ \begin{array}{c} \delta\Gamma^{c_1} \\ \vdots \\ \delta\Gamma^{c_n} \end{array} \right\} \\ & - \alpha\omega_v^2 \mathbf{p}_v + \left(1 + j\omega_v \Gamma^m\right) \boldsymbol{\Lambda}_{mist} \alpha_{uv} \mathbf{p}_v, \end{aligned} \tag{5.16}$$

Considering the forces to be calibrated over the frequency range of interest ($\alpha_{uv} = 1$),

combining Eqns. (5.14) and (5.16), and grouping like-terms, one obtains

$$j\boldsymbol{\Psi}^T\tilde{\mathbf{K}}\left(\mathbf{I}_{n\times n}\otimes\left[\omega_u\mathbf{p}_u-\omega_v\mathbf{p}_v\right]\right)\left\{\begin{array}{c}\delta\Gamma^{c_1}\\ \vdots\\ \delta\Gamma^{c_n}\end{array}\right\}=\omega_u^2\mathbf{p}_u-\omega_v^2\mathbf{p}_v-\boldsymbol{\Lambda}_{mist}\left(\mathbf{p}_u-\mathbf{p}_v\right) - j\Gamma^m\boldsymbol{\Lambda}_{mist}\left(\omega_u\mathbf{p}_u-\omega_v\mathbf{p}_v\right). \tag{5.17}$$

Notice that the right side of the equation contains terms similar to those used for mistuning identification [49] where the response is at two different frequencies. Solving the least squares problem given by Eqn. (5.17) using the Moore-Penrose pseudo-inverse, one obtains

$$\left\{\begin{array}{c}\delta\Gamma^{c_1}\\ \vdots\\ \delta\Gamma^{c_n}\end{array}\right\}=Im\left(\left[\mathbf{A}_{uv}^T\mathbf{A}_{uv}\right]^{-1}\mathbf{A}_{uv}^T\left\{\omega_u^2\mathbf{p}_u-\omega_v^2\mathbf{p}_v -\boldsymbol{\Lambda}_{mist}\left(\mathbf{p}_u-\mathbf{p}_v\right)-j\Gamma^m\boldsymbol{\Lambda}_{mist}\left(\omega_u\mathbf{p}_u-\omega_v\mathbf{p}_v\right)\right\}\right), \tag{5.18}$$

where $\mathbf{A}_{uv}=\boldsymbol{\Psi}^T\tilde{\mathbf{K}}\left(\mathbf{I}_{n\times n}\otimes\left[\omega_u\mathbf{p}_u-\omega_v\mathbf{p}_v\right]\right)$ is a matrix of size $m\times n$ with m being the number of modes and n being the total number of components. For the solution in Eqn. (5.18) to be unique, m must be larger than or equal to n. In that case Eqn. (5.18) provides the individual damping values (identified) for all the components of a structure.

Note that if the damping in each component is structural, then $\delta\Gamma^{c_i}=\delta\tilde{\Gamma}^{c_i}/\omega$ with $\delta\tilde{\Gamma}^{c_i}$ being constant for all i, and $\delta\Gamma^m=\delta\tilde{\Gamma}^m/\omega$ with $\delta\tilde{\Gamma}^m$ being a constant.

Substituting into Eqn. (5.13) and following similar steps, one obtains

$$\left\{ \begin{array}{c} \delta\tilde{\Gamma}^{c_1} \\ \vdots \\ \delta\tilde{\Gamma}^{c_n} \end{array} \right\} = Im \left(\left[\tilde{\mathbf{A}}_{uv}^{T} \tilde{\mathbf{A}}_{uv} \right]^{-1} \tilde{\mathbf{A}}_{uv}^{T} \left\{ \omega_u^2 \mathbf{p}_u - \omega_v^2 \mathbf{p}_v - \left(1 + j\tilde{\Gamma}^m \right) \mathbf{\Lambda}_{mist} \left(\mathbf{p}_u - \mathbf{p}_v \right) \right\} \right), \tag{5.19}$$

where $\tilde{\mathbf{A}}_{uv} = \mathbf{\Psi}^T \tilde{\mathbf{K}} \left(\mathbf{I}_{n \times n} \otimes [\mathbf{p}_u - \mathbf{p}_v] \right)$. Equation (5.19) is the structural damping version of Eqn. (5.18), where the components have individual structural damping coefficients.

Note also that if the system consists of uniform proportional damping (i.e., the damping is the same for all components), then $\delta\Gamma^{c_i} = 0$ for all components. Substituting into Eqn. (5.17), one obtains

$$\mathbf{0} = \omega_u^2 \mathbf{p}_u - \omega_v^2 \mathbf{p}_v - \mathbf{\Lambda}_{mist} \left(\mathbf{p}_u - \mathbf{p}_v \right) - j\Gamma^m \mathbf{\Lambda}_{mist} \left(\omega_u \mathbf{p}_u - \omega_v \mathbf{p}_v \right).$$

Letting $\mathbf{d}_{uv}^{\omega} = (\omega_u \mathbf{p}_u - \omega_v \mathbf{p}_v)$, taking the inverse of $\mathbf{\Lambda}_{mist}$, and solving in a least squares sense, one obtains

$$\Gamma^m = Im \left(\left[\mathbf{d}_{uv}^{\omega\ T} \mathbf{d}_{uv}^{\omega} \right]^{-1} \mathbf{d}_{uv}^{\omega T} \left[\mathbf{\Lambda}_{mist}^{-1} \left\{ \omega_u^2 \mathbf{p}_u - \omega_v^2 \mathbf{p}_v \right\} - \left(\mathbf{p}_u - \mathbf{p}_v \right) \right] \right). \tag{5.20}$$

Equation (5.20) can be used to identify the proportional damping in a system without damping variability. Similarly, for a uniformly structurally damped system, damping can be identified as

$$\tilde{\Gamma}^m = Im \left(\left[\mathbf{d}_{uv}^T \mathbf{d}_{uv} \right]^{-1} \mathbf{d}_{uv}^T \mathbf{\Lambda}_{mist}^{-1} \left\{ \omega_u^2 \mathbf{p}_u - \omega_v^2 \mathbf{p}_v \right\} \right), \tag{5.21}$$

where $\mathbf{d}_{uv} = (\mathbf{p}_u - \mathbf{p}_v)$. Equation (5.21) shows that for the special case of a system

with uniform structural damping the proposed method reduces to the technique by Holland et al. [53].

5.5 Refinements for Cyclically Symmetric Structures

The identification approach presented in the previous section can utilize special properties of cyclically symmetric structures (i.e., structures consisting of one sector duplicated about a central axis) to decrease the computational cost. Representing a cyclically symmetric structure using only one sector is desirable as the number of DOFs in a sector is $\tilde{N}$, approximately s times smaller than the total number N of DOFs in the entire blisk ($\tilde{N} \approx N/s$), where s is the number of sectors. In particular, matrices $\boldsymbol{\kappa}$ and $\boldsymbol{\Psi}$ for a single sector are of size $\tilde{N} \times \tilde{N}$ and $\tilde{N} \times m$. To represent a cyclically symmetric system using only sector level calculations, each sector corresponds to two components, a blade portion (denoted using β) and a disk portion (denoted using Δ). Cyclic coordinates are chosen so that $\boldsymbol{\kappa}_\beta = \boldsymbol{\kappa}_\beta^1 = \cdots = \boldsymbol{\kappa}_\beta^s$ and $\boldsymbol{\kappa}_\Delta = \boldsymbol{\kappa}_\Delta^1 = \cdots = \boldsymbol{\kappa}_\Delta^s$. As a result, one obtains

$$\begin{aligned}
&\boldsymbol{\Psi}^T \tilde{\mathbf{K}} \left(\mathbf{I}_{s+1 \times s+1} \otimes \mathbf{d}_{uv} \right) = \\
&\quad \Big[\boldsymbol{\Psi}_{c_1,\beta}^T \left(\boldsymbol{\kappa}_\beta + \delta \boldsymbol{\kappa}_\beta^{c_1} \right) \boldsymbol{\Psi}_{c_1,\beta} \mathbf{d}_{uv} \;\; \cdots \;\; \boldsymbol{\Psi}_{c_s,\beta}^T \left(\boldsymbol{\kappa}_\beta + \delta \boldsymbol{\kappa}_\beta^{c_s} \right) \boldsymbol{\Psi}_{c_s,\beta} \mathbf{d}_{uv} \\
&\quad \sum_{i=1}^{s} \boldsymbol{\Psi}_{c_i,\Delta}^T \left(\boldsymbol{\kappa}_\Delta + \delta \boldsymbol{\kappa}_\Delta^{c_i} \right) \boldsymbol{\Psi}_{c_i,\Delta} \mathbf{d}_{uv} \Big],
\end{aligned} \tag{5.22}$$

where $\boldsymbol{\kappa}_\beta + \delta \boldsymbol{\kappa}_\beta^{c_i}$ and $\boldsymbol{\kappa}_\Delta + \delta \boldsymbol{\kappa}_\Delta^{c_i}$ are the mistuned stiffness matrices of the blade and disk portions of sector i, $\boldsymbol{\Psi}_{c_i,\beta}$ and $\boldsymbol{\Psi}_{c_i,\Delta}$ are the blade and disk portions of the modal matrices. Note that the tuned mode shapes for all sectors can be related to those of a single sector with cyclically symmetric boundary conditions using the real Fourier matrix [52, 58]. Also, note that $\mathbf{d}_{uv}^\omega$ is replaced with $\mathbf{d}_{uv}$ when the damping is structural.

System level characteristics such as cyclic modeling error [51] are more difficult to

represent as changes in the component stiffness matrices in comparison to blade to blade variability. Using the component mode mistuning method [48,49] and assuming that there is no mistuning in the disk, one obtains

$$\begin{aligned}
&\boldsymbol{\Psi}^T\tilde{\mathbf{K}}\left(\mathbf{I}_{s+1\times s+1}\otimes\tilde{\mathbf{p}}_{uv}\right)= \\
&\Big[\left(\boldsymbol{\Psi}_{c_1,\beta}^T\boldsymbol{\kappa}_\beta\boldsymbol{\Psi}_{c_1}+\boldsymbol{\phi}_{c_1}^T\mathbf{q}_{c_1}^T\boldsymbol{\Lambda}_{CB}^1\mathbf{q}_{c_1}\boldsymbol{\phi}_{c_1}\right)\tilde{\mathbf{p}}_{uv}\ \cdots\ \left(\boldsymbol{\Psi}_{c_s,\beta}^T\boldsymbol{\kappa}_\beta\boldsymbol{\Psi}_{c_s}+\boldsymbol{\phi}_{c_s}^T\mathbf{q}_{c_s}^T\boldsymbol{\Lambda}_{CB}^s\mathbf{q}_{c_s}\boldsymbol{\phi}_{c_s}\right)\tilde{\mathbf{p}}_{uv} \\
&\sum_{i=1}^{s}\boldsymbol{\Psi}_{c_1,\Delta}^T\boldsymbol{\kappa}_\Delta\boldsymbol{\Psi}_{c_1,\Delta}\ \tilde{\mathbf{p}}_{uv}\Big],
\end{aligned}\tag{5.23}$$

where $\boldsymbol{\Lambda}_{CB}^i$ is a diagonal matrix of the mistuned cantilevered blade eigenvalues for blade i [48, 49], and $\mathbf{q}_{c_i}$ contains the participation factors of mistuned cantilevered blade i onto the tuned system modes (in a ROM). Note that the vectors $\mathbf{q}_{c_i}$ are not to be confused with the matrix of participations $\boldsymbol{\Theta}$ (that relate tuned and mistuned mode shapes) or to the vector of generalized coordinates $\mathbf{q}$. Equations (5.23) and (5.18) or (5.19) are used to identify damping in sector level components for a blisk.

5.6 Damping Solution

To avoid numerical errors, there are some conditions which must be met by the damping identification. First, the number of modes used during the identification m must be greater than the number of unknown damping values, so $m \geq n$. Otherwise, matrix $\mathbf{A}$ has a rank less than n. This condition is satisfied by using an appropriate ROM. Second, as some of the modal amplitudes in $\mathbf{p}$ may be low or sensitive to measurement noise, it is necessary to retain enough data to determine all n damping values.

Recall that the damping identification is valid for all frequency pairs u, v in Eqn. (5.18) (or Eqn. (5.19) for structural damping. Therefore, it is possible to combine these equations by concatenating the column of $\mathbf{d}_{uv}$ for one frequency pair uv

with all other frequency pairs. The resulting vector $\mathbf{d}_{uv}^{aug}$ of size $b \times 1$, where b is the number of frequency pairs. Likewise, $\mathbf{d}_{uv}^{\omega} = \omega_u \mathbf{p}_u - \omega_v \mathbf{p}_v$ and $\mathbf{d}_{uv}^{\lambda} = \omega_u^2 \mathbf{p}_u - \omega_v^2 \mathbf{p}_v$ can be augmented into vectors $\mathbf{d}_{uv}^{\omega,aug}$ and $\mathbf{d}_{uv}^{\lambda,aug}$ of sizes $b \times 1$. For simplicity, $\mathbf{d}_{uv}$, $\mathbf{d}_{uv}^{\omega}$, and $\mathbf{d}_{uv}^{\lambda}$ will be referred to as the non-augmented vectors and $\mathbf{d}_{uv}$, $\mathbf{d}_{uv}^{\omega}$, and $\mathbf{d}_{uv}^{\lambda}$ will be referred to as the augmented vectors. Using the non-augmented vectors in Eqn. (5.17), one obtains

$$j\boldsymbol{\Psi}^T \tilde{\mathbf{K}} \left(\mathbf{I}_{n \times n} \otimes \mathbf{d}_{uv}^{\omega} \right) \left\{ \begin{array}{c} \delta\Gamma^{c_1} \\ \vdots \\ \delta\Gamma^{c_n} \end{array} \right\} = \mathbf{d}_{uv}^{\lambda} - \boldsymbol{\Lambda}_{mist} \mathbf{d}_{uv} - j\Gamma^m \boldsymbol{\Lambda}_{mist} \mathbf{d}_{uv}^{\omega}.$$

When there are many frequency pairs, the size of these augmented matrices may become prohibitively large. Thus, it is desired to reduce the number of frequency pairs to $\bar{b}$. The partial modal assurance criteria (PMAC) [57] is used to determine which non-augmented vectors to average, thus decreasing the number of frequency pairs and reducing zero-mean noise. The augmentation process is summarized in Fig. 5.1. The dashed lines indicate paths which only occur one time, while the solid lines indicates repeated processes.

The augmented vectors starts as void vectors. The first frequency pair u, v is used to form the non-augmented vectors which are used to augment $\mathbf{d}_{uv}^{aug}$, $\mathbf{d}_{uv}^{\omega,aug}$, and $\mathbf{d}_{uv}^{\lambda,aug}$. Thus, the first vector set in the augmented matrices is $\mathbf{d}_{uv}^{aug} = \mathbf{d}_{uv}$, $\mathbf{d}_{uv}^{\omega,aug} = \mathbf{d}_{uv}^{\omega}$, and $\mathbf{d}_{uv}^{\lambda,aug} = \mathbf{d}_{uv}^{\lambda}$, where the set only consists of one vector. Thus, the augmented matrices contain one set and are of size $m \times 1$

Then, all non-augmented vectors are calculated for all v frequency pairs, while using the same frequency u. These additional non-augmented vectors will be referred to as the candidate vectors. Let h be the number of candidate vectors.

To compare the information contained in the candidate vectors with the information in the augmented matrices, the PMAC is calculated between the candidate

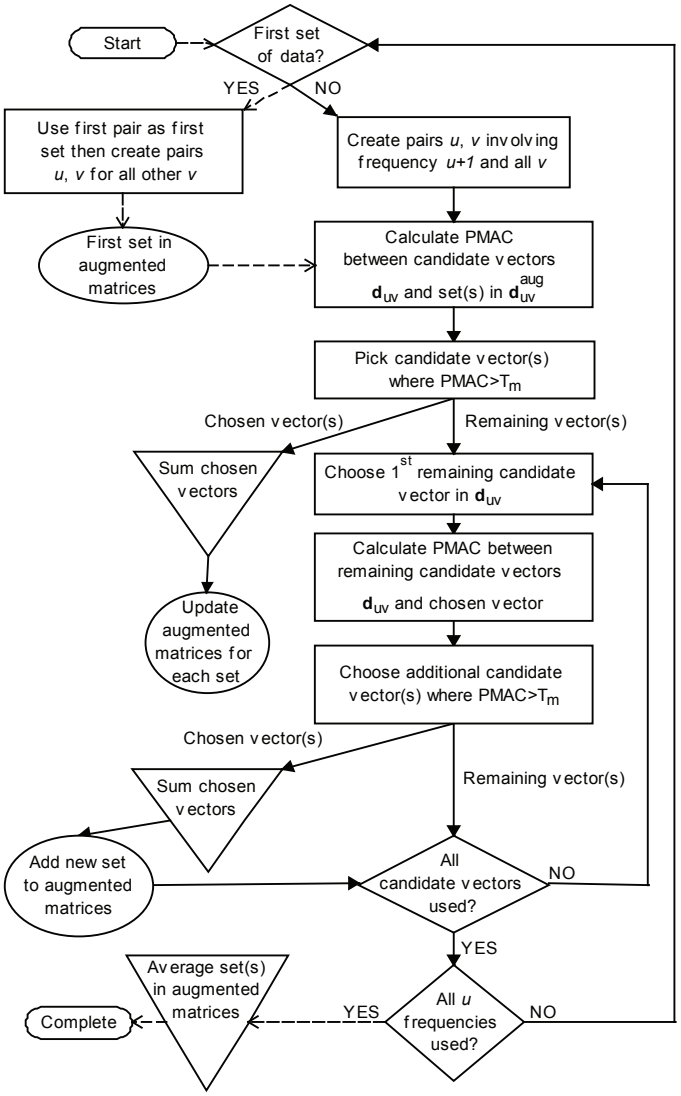

Figure 5.1: Algorithm for augmenting damping identification matrices

vectors formed from the non-augmented matrix $\mathbf{d}_{uv}$ and each set in $\mathbf{d}_{uv}^{aug}$ (which consists of only one set initially). The d candidate vectors which have a PMAC (for a given set in $\mathbf{d}_{uv}^{aug}$) above T_m are considered to be dependent.

To reduce the zero-mean noise and decrease the size of the augmented matrices, these corresponding candidate vectors are summed with the corresponding set in the augmented matrices. Then, these vectors are removed from the candidate vectors. Thus, the augmented matrices remain of size $m \times 1$, however the set now contains the sum of $d+1$ vectors (including the initial vector). For the remaining $h-d$ candidate

vectors, the first of the remaining vectors is added as a new set to the augmented matrices. Then, the first candidate vector is removed from the candidate vectors resulting in $h-d-1$ candidate vectors. The augmented matrices are of size $2m \times 1$.

The PMAC is calculated between the remaining $h-d-1$ candidate vectors for $\mathbf{d}_{uv}$ and the newly added set in $\mathbf{d}_{uv}^{aug}$. The candidate vectors corresponding to a PMAC (based on $\mathbf{d}_{uv}$ and the sets in $\mathbf{d}_{uv}^{aug}$) above T_m are summed with the new set in the augmented matrices and then they are removed from the candidate vectors. The process repeats with new sets added and summed until no more candidate vectors remain.

Then, new candidate vectors are creating from the next u frequency. The algorithm repeats until all frequency pairs are either summed with a set already in the augmented matrices or are added as a new set in those matrices. The final step involves averaging the $\bar{b}$ sets by dividing each set in the augmented matrices by the number of vectors which were summed in the set. To formulate the augmented equations, matrices $\mathbf{\Psi}$, $\tilde{\mathbf{K}}$, $\mathbf{I}_{n\times n}$, and $\mathbf{\Lambda}_{mist}$ are duplicated $\bar{b}$ times such that $\mathbf{\Psi}^{aug} = Bdiag\left[\mathbf{\Psi}\right]$, $\tilde{\mathbf{K}}^{aug} = Bdiag\left[\tilde{\mathbf{K}}\right]$, $\mathbf{I}^{aug} = Bdiag\left[\mathbf{I}_{n\times n}\right]$, and $\mathbf{\Lambda}_{mist}^{aug} = Bdiag\left[\mathbf{\Lambda}_{mist}\right]$. Using the augmented matrices, one obtains

$$\begin{aligned} j\mathbf{\Psi}^{augT}\tilde{\mathbf{K}}^{aug}\left(\mathbf{I}_{\bar{b}n\times\bar{b}n}\otimes\mathbf{d}_{uv}^{aug,\omega}\right)\left\{\begin{array}{c}\delta\Gamma^{c_1}\\ \vdots \\ \delta\Gamma^{c_n}\end{array}\right\} =& \mathbf{d}_{uv}^{aug,\lambda} - \mathbf{\Lambda}_{mist}^{aug}\mathbf{d}_{uv}^{aug} \\ & - j\Gamma^{m}\mathbf{\Lambda}_{mist}^{aug}\mathbf{d}_{uv}^{aug,\omega}. \end{aligned} \tag{5.24}$$

Note that while Eqn. (5.24) is for the case of proportional damping, structural damping has terms $\mathbf{d}_{uv}$ and $\mathbf{d}_{uv}^{\lambda}$ and so this algorithm remains the same with the exceptions that there are no $\mathbf{d}_{uv}^{\omega}$ or $\mathbf{d}_{uv}^{\omega,aug}$ matrices involved.

This augmentation includes utilizing the frequency windowing introduced by Holland et al. [59] when selecting the frequency pairs. Therefore, the augmentation al-

gorithm is applied to each frequency window. This frequency windowing uses smaller ROMs which are valid around each individual mistuned mode. As the response of each component has the potential to be localized for a given mistuned mode, it is imperative to capture the motion of as many modes as possible. For regions of high modal density, there may be many components responding each in a localized mode. Therefore, there are many modes and measurements inside a frequency window for this region. Conversely, for an isolated mistuned mode (i.e., a mode which responds alone to excitations near or at its natural frequency), the ROM would include only the predominant mistuned mode. As a result, the physical to modal coordinate transformation $\mathbf{x} = \mathbf{\Phi p} = \boldsymbol{\phi}\boldsymbol{\Theta}\mathbf{p}$, and thus the damping identification is more accurate, while effectively capturing the dynamics of a larger frequency range.

5.7 Modal Sensitivity to Component Damping

Mistuned systems exhibit localization. As a result, it is possible that only a few blades participate in a given mistuned mode. Therefore, the damped responses near the frequency of that mistuned mode are sensitive to the (component) damping in those few localized blades. To obtain an accurate component damping identification, one must incorporate information for mistuned modes which are sensitive to each component so that information about the damping of each component can be obtained. This section introduces a method for determining the sensitivity of a mistuned mode inside of a frequency window to the damping of a given component. The frequency windows can then be selected for an accurate damping identification.

Note that the energy loss for the structure due to the damping mistuning is modeled using $j\omega\delta\Gamma^{c_i}\left(\boldsymbol{\kappa}^{c_i} + \delta\boldsymbol{\kappa}^{c_i}\right)$ in Eqn. (5.9). In mistuned modal coordinates this can be expressed as $j\omega\delta\Gamma^{c_i}\mathbf{\Phi}_{c_i}^T\left(\boldsymbol{\kappa}^{c_i} + \delta\boldsymbol{\kappa}^{c_i}\right)\mathbf{\Phi}_{c_i}$, where $\mathbf{\Phi}_{c_i}$ represents the portion of the mistuned mode shapes corresponding to component c_i. The term $\mathbf{\Phi}_{c_i}^T\left(\boldsymbol{\kappa}^{c_i} + \delta\boldsymbol{\kappa}^{c_i}\right)\mathbf{\Phi}_{c_i}$ is a strain energy-like term for the energy loss in a given component c_i. Now for a given

frequency window consisting of target mode u and non-target mode v, the normalized energy loss (or sensitivity of the target mistuned mode) can be expressed using

$$\bar{S}_{uv}^{c_i} = \frac{1}{\omega^{n,u}\omega^{n,v}} \mathbf{\Phi}_{c_i,u}^T \left(\boldsymbol{\kappa}^{c_i} + \delta\boldsymbol{\kappa}^{c_i}\right) \mathbf{\Phi}_{c_i,v}, \tag{5.25}$$

where $\omega^{n,u}$ and $\omega^{n,v}$ are the mistuned natural frequencies of modes u and v, and $\mathbf{\Phi}_{c_i,u}$ and $\mathbf{\Phi}_{c_i,v}$ are vectors containing the portion of the u^{th} and v^{th} mistuned mode shapes corresponding to component c_i. For a given frequency window, only the chosen mode v varies.

To effectively use the sensitivity $\bar{S}_{uv}^{c_i}$, a process to order the frequency windows is introduced. First, calculate the sensitivity for all components for all target modes u paired with non-target modes v in each frequency window. Then, for each frequency window choose the largest sensitivity value $\bar{S}^{c_i} = \max_{u,v} \left\{\bar{S}_{uv}^{c_i}\right\}$ for any mode pair u and v. As a result, the maximum sensitivity for each component c_i in each frequency window is obtained. Then, choose the first set of frequency windows to be used for the component damping identification to be the frequency windows that give the maximum sensitivity $\bar{S}^{c_i}$, i.e., for each component (one window per component). Now, the damping identification should be less accurate for the component with the lowest sensitivity in the set. Therefore, add to the set of windows the next frequency window (ordered by decreasing sensitivity) corresponding to the component with the lowest sensitivity in the previous set. Continue until each component has two frequency windows. Repeat the process for the 3^{rd} most sensitive frequency windows until all mode windows have been chosen, or no sensitivity values are left to compare. Consider any frequency windows which remain unchosen as equally insensitive to component damping and add them as the final set. Once, the frequency window order has been determined, the surrogate process introduced by Holland et al. [59] can be used to statistically optimize the number of frequency windows in the component damping

identification.

5.8 Damping Identification Results and Discussion

This section explores the accuracy of the proposed damping identification method with respect to the measurement noise level for the 141,120 DOF University of Michigan validation blisk. This validation blisk is described in detail in [52]. To investigate the effects of measurement noise, we first used Eqn. (5.11) to obtain simulated measurement data. This data is perfect in the sense that it contains no measurement noise. Next, we inject relative white noise in this data to simulated the presence of measurement noise [55]. Note that the simulated measurements use an accurate model which incorporates all tuned modes in a frequency range from 0 to 10 kHz. To simulate a practical case, the damping identification method was applied by using modes and measurements only in the frequency range 0 to 3 kHz.

The University of Michigan validation blisk has an applied blade stiffness mistuning pattern with values between $\pm 2\%$ (in eigenvalue). The damping identification uses the structural damping formulation in Eqn. (5.19) with the definition of $\tilde{\mathbf{K}}$ provided in Eqn. (5.23). These results also utilize the surrogate data method to determine the optimal number of modes to achieve an accurate physical to modal transformation [59]. The results were obtained using the actual stiffness mistuning values to focus on the accuracy of only the damping identification (instead of the mistuning identification).

The following results were obtained using previous measurement and residual filters with values $R_{thresh} = 0.1$ and $T_l = 0.05$ [56]. Also, two additional measurement filters are proposed. The first measurement filter removes data which is sensitive to measurement noise. This filter duplicates the measurement data and then corrupts this data with measurement noise. The modal amplitudes of the noisy measurement data is compared to the modal amplitudes of the uncorrupted measurement data.

If the magnitude of any of the modal amplitudes differ by a factor of T_b, then the measurement data is removed from the identification. Therefore, data is removed for which one modal amplitude satisfies

$$|p_{u,i}^{noisy}| > T_b N_l |p_{u,i}^{actual}|, \tag{5.26}$$

where $|\cdot|$ denotes the magnitude, $p_{u,i}^{noisy}$ and $p_{u,i}^{actual}$ are the noisy and actual modal amplitudes at frequency u for mistuned mode i, T_b is the noise sensitivity threshold, and N_l is the noise level. The second measurement filter removes measurement pairs which are too close in frequency. If $\mathbf{p}_u \approx \mathbf{p}_v$ and $\omega_u \approx \omega_v$, then the identification equation of frequency pair u, v become strongly dependent on the measurement noise. Therefore, measurement pair u, v is removed from the identification if

$$max_{i=1\ldots m}(|p_{u,i} - p_{v,i}|) \leq T_p. \tag{5.27}$$

In the following results, $T_p = 1 \times 10^{-5}$, $T_b = 5$, and the PMAC threshold is $T_m = 0.75$.

The following figures display the damping coefficient on the y-axis. The x-axis is the component number. Components 1 to 24 correspond to blades 1 to 24 of the blisk, while component 25 is the disk portion. Both the identified and the actual structural damping coefficients are provided. Five measurement locations per blade were used to obtain the results.

Figure 5.2 shows the mean values and the standard deviation of the identified damping for 1,000 noise realizations. The mean values are extremely accurate with a maximum relative error of 0.83% for the case of 1% relative measurement noise (Fig. 5.2(a)), and 1.1% for the case of 5% relative measurement noise (Fig. 5.2(b)). Figure 5.2 shows that all blades are identified with similar accuracy. The maximum standard deviations are 2.6% and 7.4% for the two cases of 1% and 5% measurement noise. The mean standard deviations are 2.0% and 5.3% respectively. In general, the

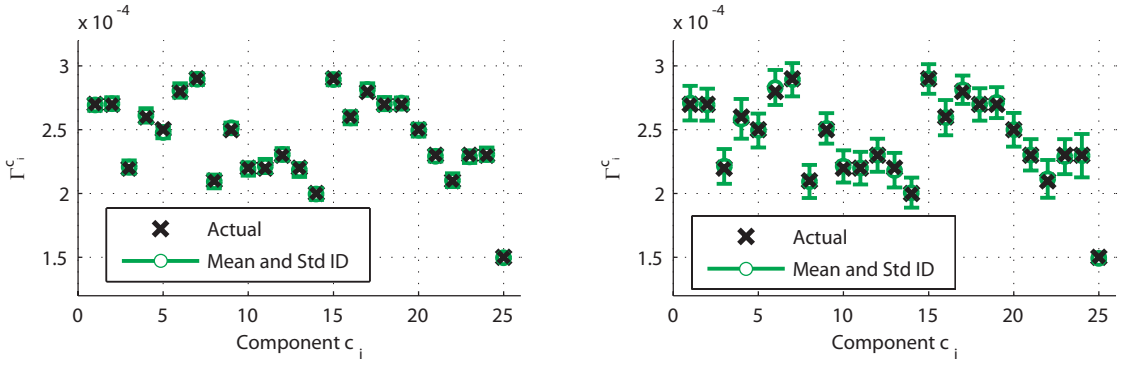

(a) (b)

Figure 5.2: Mean values and standard deviations of the identified damping for the case of (a) 1% relative measurement noise and (b) 5% relative measurement noise

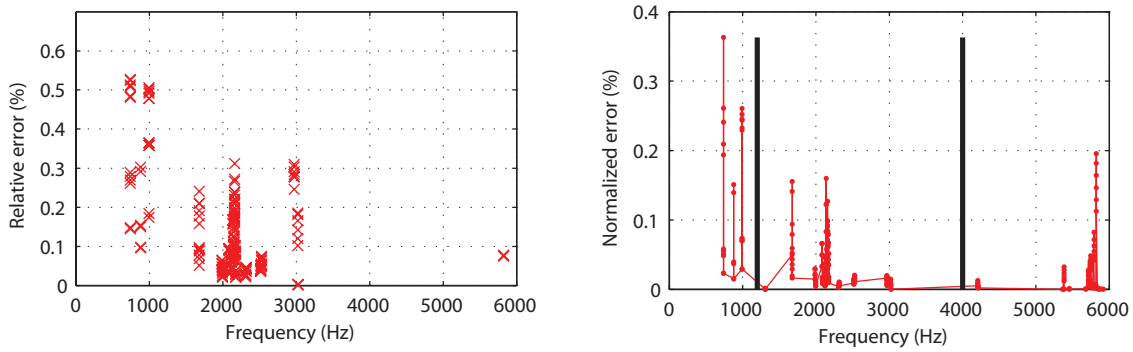

(a) (b)

Figure 5.3: Relative (a) and normalized (b) error in the forced response predicted by using the identified damping for the case of 5% measurement noise

damping identification error is of a similar level as the measurement noise level.

As the ROM used only 30 frequency windows, it is important that the blade damping is identified such that the forced response is obtained accurately. Therefore, to assess the accuracy of the damping identification, the forced response of the blisk using the (mean) identified damping values should be compared with the forced response using the actual component damping. Figure 5.3(a) shows the relative error between the two forced response predications for a frequency range 0 to 6 kHz which were generated using Eqn. (5.11) and modes in the frequency range of 0 to 10 kHz. Only the relative error for responses above 4% of the maximum response are plotted.

The y-axis of Fig. 5.3 displays the maximum relative error obtained for all measured DOFs and single blade excitations for all blades. The x-axis is the frequency of the excitation. Figure 5.3(b) shows the identification error which has been normalized by the maximum response in the corresponding frequency range 0 to 1.2 kHz, 1.2 to 4 kHz, or 4 to 6 kHz. The separation of the frequency ranges is denoted by the two vertical black lines. Notice that the 0 to 10 kHz frequency range contains 95 modes as compared to the 30 frequency windows used in the damping identification. As the resonant responses are of primary interest, responses near the mistuned natural frequencies are shown. The maximum relative error in Fig. 5.3(a) is 0.53%. The maximum normalized error in Fig. 5.3(b) is 0.36%, which is comparable to the corresponding maximum error of 0.31% in the identified damping values. This indicates that that the identified damping values can represent the dynamics of the blisk for a frequency range (of 0 to 6 kHz) larger than the identification frequency range (of 0 to 3 kHz).

In general, it was found that the maximum relative error in the damping identification is greater than or equal to the maximum relative error in the forced response. Therefore, the error in the damping identification is not a suitable indicator of how well the structural dynamics are captured. Similar forced response results were obtained for the forced response using the mean identified values with 1% measurement noise, but are omitted here for brevity.

Figure 5.4 shows the standard deviation of the identified damping for 1,000 noise realizations where the measurement noise is modeled with 1% relative, absolute, and bias terms [56]. Note that the absolute and bias terms contribute more than 1% noise to low responding data. For the frequency range 0 to 3 kHz, the disk dominated responses are larger than the blade dominated regions. Thus, the identified blade damping is expected to be less accurate than the identified disk damping as absolute and bias noise affect the blade dominated data more. This behavior can be seen

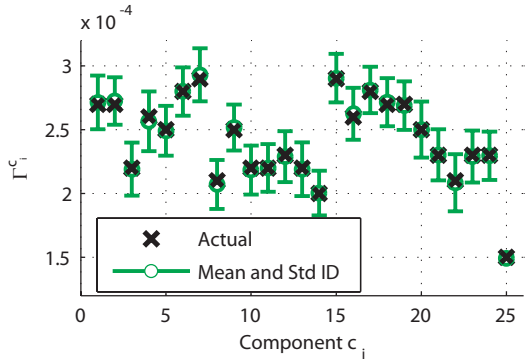

Figure 5.4: Mean values and standard deviations of the identified damping for the case of 1% relative, bias and absolute measurement noise

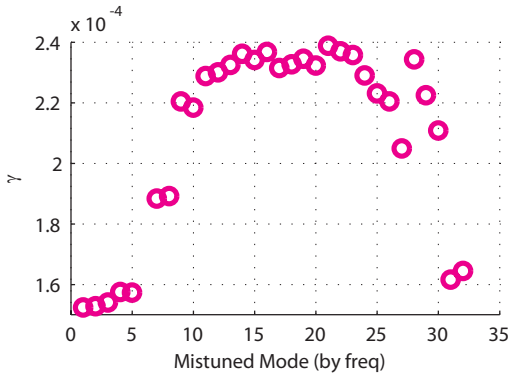

Figure 5.5: Modal damping identification of blisk with component damping

in Fig. 5.4. The mean values are accurate with a maximum relative error of 1.4%. However, the standard deviation of the damping identification becomes larger than the measurement noise level with a maximum value of 10.7%. Thus, the damping identification is more sensitive to absolute and bias measurement noise than relative measurement noise.

It is possible that the component damping identification will represent the damping of the system with fewer parameters than other methods such as modal damping identification. Figure 5.5 demonstrates this feature. The y-axis of Fig. 5.5 displays the identified modal damping obtained for this blisk (which actually contains component damping) obtained using the method of Holland et al. [59]. The x-axis corresponds to the the mistuned modes in the identification frequency range of 0 to 3 kHz organized

by increasing natural frequency. Note that the damping of mode 6 was not identified. The disk dominated modes 1-5, 31, and 32 have values similar to the actual disk component damping. Also, modes 11 to 24 corresponding to blade dominated motion have values similar to the level of the component damping in the blades. Modes 7 to 11 which are in a veering region have an equivalent modal damping between the disk and blade component damping values. This modal damping identification method required 31 parameters to describe the system dynamics in the frequency range of interest. The component damping identification only required 25 values.

5.9 Conclusions

In contrast to current damping identification methods, the novel method herein can identify the component damping. This feat allows the damping to have a more meaningful physical interpretation especially for structures with complex geometry. In particular, this type of damping identification enables a more accurate analysis of damping coatings. Also, the presented formulation can be used to generate the forced response of a mistuned structure with a prescribed component damping for a given harmonic excitation and ranges larger than the identification frequency range.

Results for a validation blisk show that the identification is possible when using reduced-order models (ROMs), in the presence of measurement noise, and when both low and high modal density is present. In addition, the dynamics of the structure are captured by the identified component damping. However, the component damping method can be more sensitive to absolute and bias measurement noise than other damping identification methods.

As the forced response method uses ROMs, it is computationally efficient. In addition, the complex interaction between mass or stiffness mistuning and component damping variability can be studied. Also, it is possible for the component damping identification to accurately represent the damping of the system with fewer parameters

than other methods.

CHAPTER VI

Proportional Component Damping Hybrid Identification

6.1 Introduction

Wear or manufacturing processes or defects can cause slight variations in the mass or stiffness of a nominally cyclically symmetric structure such as an integrally bladed disk (blisk). These variations or mistuning can cause the vibration energy to localize at certain regions of the structure resulting in larger than expected forced responses and stresses. Therefore, these mistuned systems are susceptible to high cycle fatigue. One method to compensate for the effects of mistuning is to apply damping coatings. However, Joshi et al. [3] found that the dynamics of the system can significantly change due to variations in the thickness of the applied coating. To determine the damping characteristics of coatings, a damping identification technique is needed which can determine the damping associated with individual components of a mistuned blisk (before and after the coating is applied). Currently, damping identification relies on one of several common damping models namely, structural, viscous, and component (material) damping. In general, structural damping is defined for a full system, while viscous damping is defined for individual system modes.

Most current damping identification techniques assume that damping has a cer-

tain form at a system level. For example, the damping in complex structures is often assumed to be viscous, modal, or structural. Such assumptions provide accurate results for structures with relatively simple geometries and low modal density. However, these approximations can be cumbersome or inaccurate for structures with complex geometry and high modal density. For such systems, using a component-oriented model can be more effective. In particular, component damping corresponds to a proportional or structural damping applied to individual components of a structure (i.e., each component has an associated material damping). For instance, each blade of a blisk can be modeled as a separate component with an associated damping parameter (which is to be identified). The resulting damping is only approximately modal, and the corresponding modal damping values vary with different component damping properties. As a result, the component damping can represent the physical attributes of the structure more closely and may require less effort than identifying the modal damping for a structure with a moderate number of components and a large number of modes in the frequency range of interest.

While finite element modeling (FEM) methods incorporate component damping, most identification methods found in literature are difficult or impossible to use to identify this type of damping from experimental data [4, 6, 7, 14–20, 22, 26–29]. Statistical energy analysis (SEA) is one method for determining component (subsystem) damping loss factors. This method is useful for high frequency ranges. However, this technique is limited as the damping is assumed to be known either from the power injection method (PIM) [32, 33, 35, 36], power modulation method [36], or a wave approach [37]. PIM and power modulation techniques require measuring energy for all the components, and that can be difficult or impossible to gather accurately. Also, wave theory only applies to periodic systems. Moreover, the SEA method can be time consuming if there are many components [36]. In addition, the accuracy of the SEA method depends on the modal density and the level of damping, as shown by

Mace [38] and Yap et al. [39].

The work herein presents a novel component damping identification technique which can be applied to mistuned blisks and use certain reduced-order models (ROMs) in regions of low and/or high modal density.

6.2 Proportional Component Damping Hybrid Identification

An alternative to the damping identification method in Ch. 5.1 is presented herein. This alternative approach makes use of a frequency response matrix to identify the damping. First, the identification is described assuming that the forcing is known. Then, a version of the damping identification method in Sec. 5.4 is used to recast this identification using a relative forcing by solving for a relative forcing constant. First, assume that the relative magnitudes and phases of the excitation have been determined from a calibration procedure such as the one by Holland et al. [1]. Consider that $\tilde{\mathbf{F}}$ contains many forcing cases at a given frequency. At a given frequency, a forcing case is a spatially unique forcing which is applied to the structure such that each forcing case is independent from each other. Applying forcing to different blades (single blade excitation) or of different nodal diameters (traveling wave excitation) are examples of forcing cases. Thus, each column of $\tilde{\mathbf{F}}$ represents the forcing vector (of size $a \times 1$) for one forcing case. Therefore, $\tilde{\mathbf{F}}$ is of size $c \times a$. Then, one may relate the actual forcing values, grouped in a matrix $\bar{\mathbf{F}}$ to the relative forcing values in the matrix $\tilde{\mathbf{F}}$ as $\bar{\mathbf{F}} = e\tilde{\mathbf{F}}$, where $e \in \mathbb{C}$ is a scalar. Also, the responses to these forcing cases can be grouped into a matrix $\bar{\mathbf{X}}$ which is of size $a \times c$ From the hybrid damping identification method introduced by Holland et al. [59],

$$e\mathbf{G}^T \left(\mathbf{R}\bar{\mathbf{X}}\tilde{\mathbf{F}}^{-1} \right)^{-*} \mathbf{R}\bar{\mathbf{X}} = \left(-\omega^2 \mathbf{M} + j\omega \mathbf{C} + \mathbf{K} \right) \bar{\mathbf{X}}, \tag{6.1}$$

where $\bullet^{-*}$ denotes the Moore-Penrose pseudo-inverse, $\mathbf{G}$ is a matrix representing the applied forcing distribution, and $\mathbf{R}$ is a matrix which selects only the measured DOF. Note that Eqn. (6.1) is in the form $\mathbf{Y}\bar{\mathbf{X}} = \mathbf{Z}\bar{\mathbf{X}}$ for all $\bar{\mathbf{X}}$, where $\mathbf{Y}$ and $\mathbf{Z}$ are of size $a \times a$ and therefore, $\mathbf{Y} = \mathbf{Z}$. Thus,

$$e\mathbf{G}^T \left(\mathbf{R}\bar{\mathbf{X}}\tilde{\mathbf{F}}^{-1}\right)^{-*} \mathbf{R} = \left(-\omega^2\mathbf{M} + j\omega\mathbf{C} + \mathbf{K}\right), \tag{6.2}$$

Converting to mass normalized mistuned modal coordinates, pre-multiplying by $\mathbf{\Phi}^T$, and using the damping expression in Eqn. (5.10) and a ROM, one obtains

$$\begin{aligned} e\mathbf{\Phi}^T\mathbf{G}^T \left(\mathbf{R}\bar{\mathbf{X}}\tilde{\mathbf{F}}^{-1}\right)^{-*} \mathbf{R}\mathbf{\Phi} = &-\omega^2\mathbf{I} + (1 + j\omega\Gamma^m)\,\mathbf{\Lambda}_{mist} \\ &+ j\omega\mathbf{\Psi}^T Bdiag\left[\delta\Gamma^{c_i}\left(\boldsymbol{\kappa}^{c_i} + \delta\boldsymbol{\kappa}^{c_i}\right)\right]\mathbf{\Psi}. \end{aligned} \tag{6.3}$$

Also,

$$\mathbf{\Psi}^T Bdiag\left[\delta\Gamma^{c_i}\left(\boldsymbol{\kappa}^{c_i} + \delta\boldsymbol{\kappa}^{c_i}\right)\right]\mathbf{\Psi} = \mathbf{\Psi}^T\tilde{\mathbf{K}} \begin{Bmatrix} \delta\Gamma^{c_1}\mathbf{I}_{m\times m} \\ \vdots \\ \delta\Gamma^{c_n}\mathbf{I}_{m\times m} \end{Bmatrix}. \tag{6.4}$$

Substituting Eqn.(6.4) into Eqn. (6.3) and taking the imaginary part, one obtains

$$Im\left\{e\mathbf{\Phi}^T\mathbf{G}^T \left(\mathbf{R}\bar{\mathbf{X}}\tilde{\mathbf{F}}^{-1}\right)^{-*} \mathbf{R}\mathbf{\Phi}\right\} - \omega\Gamma^m\mathbf{\Lambda}_{mist} = \omega\mathbf{\Psi}^T\tilde{\mathbf{K}} \begin{Bmatrix} \delta\Gamma^{c_1}\mathbf{I}_{m\times m} \\ \vdots \\ \delta\Gamma^{c_n}\mathbf{I}_{m\times m} \end{Bmatrix}. \tag{6.5}$$

Letting $\bar{\mathbf{A}}$ be the left side of Eqn. (6.5) and $\bar{\mathbf{B}} = \omega\mathbf{\Psi}^T\tilde{\mathbf{K}}$, one obtains

$$\bar{\mathbf{A}} = \bar{\mathbf{B}} \begin{Bmatrix} \delta\Gamma^{c_1}\mathbf{I}_{m\times m} \\ \vdots \\ \delta\Gamma^{c_n}\mathbf{I}_{m\times m} \end{Bmatrix}.$$

Note that $\bar{A}_{pq} = \sum_{i=1}^{n} \bar{B}_{p\ m(i-1)+q} \delta\Gamma^i$. Reshaping $\bar{\mathbf{A}}$ by concatenating the columns, one obtains

$$\begin{Bmatrix} \bar{A}_{11} \\ \vdots \\ \bar{A}_{1m} \\ \bar{A}_{21} \\ \vdots \\ \bar{A}_{m1} \\ \vdots \\ \bar{A}_{mm} \end{Bmatrix} = \begin{bmatrix} \bar{B}_{11} & \bar{B}_{1\ m+1} & \cdots & \bar{B}_{1\ m(n-1)+1} \\ \vdots & \vdots & & \vdots \\ \bar{B}_{1m} & \bar{B}_{1\ 2m} & \cdots & \bar{B}_{1\ mn} \\ \bar{B}_{21} & \bar{B}_{2\ m+1} & \cdots & \bar{B}_{2\ m(n-1)+1} \\ \vdots & \vdots & & \vdots \\ \bar{B}_{m1} & \bar{B}_{m\ m+1} & \cdots & \bar{B}_{m\ m(n-1)+1} \\ \vdots & \vdots & & \vdots \\ \bar{B}_{mm} & \bar{B}_{m\ 2m} & \cdots & \bar{B}_{m\ mn} \end{bmatrix} \begin{Bmatrix} \delta\Gamma^{c_1} \\ \delta\Gamma^{c_2} \\ \vdots \\ \delta\Gamma^{c_n} \end{Bmatrix} \Rightarrow \tilde{\mathbf{a}} = \tilde{\mathbf{B}}\boldsymbol{\Gamma}. \quad (6.6)$$

If $m \geq n$, pre-multiplying by the Moore-Penrose pseudo-inverse $\mathbf{B}^{-*}$, one obtains

$$\begin{Bmatrix} \delta\Gamma^{c_1} \\ \delta\Gamma^{c_2} \\ \vdots \\ \delta\Gamma^{c_n} \end{Bmatrix} = \tilde{\mathbf{B}}^{-*}\tilde{\mathbf{a}}. \quad (6.7)$$

Equation (6.7) is used for proportional damping identification where the forcing distribution, magnitude, and phase are known. Note that it can be difficult to know the absolute applied force. However, Holland et al. [1] introduced a forcing calibration method which can provide the magnitude and phase of the *relative* applied force.

6.3 Relative Structural Damping Identification using Calibration

In this section, assume that e is unknown, i.e. the applied forcing is known up to a multiplicative constant. Then, multiplying Eqn. (6.3) by $-j$, letting $\mathbf{U} =$

$-j\mathbf{\Phi}^T\mathbf{G}^T\left(\mathbf{R}\bar{\mathbf{X}}\tilde{\mathbf{F}}^{-1}\right)^{-*}\mathbf{R}\mathbf{\Phi}$, and $\mathbf{W} = j\omega^2\mathbf{I} + (-j + \omega\Gamma^m)\,\mathbf{\Lambda}_{mist}$, one obtains

$$e\ \mathbf{U} - \mathbf{W} = \bar{\mathbf{B}} \left\{ \begin{array}{c} \delta\Gamma^{c_1}\mathbf{I}_{m\times m} \\ \vdots \\ \delta\Gamma^{c_n}\mathbf{I}_{m\times m} \end{array} \right\}. \tag{6.8}$$

Note that $e\ U_{pq} - W_{pq} = \sum_{i=1}^{n} \bar{B}_{p\ m(i-1)+q}\delta\Gamma^{c_i}$. Reshaping $(e\ \mathbf{U} - \mathbf{W})$ by concatenating the columns, one obtains

$$e \left\{ \begin{array}{c} U_{11} \\ \vdots \\ U_{1m} \\ U_{21} \\ \vdots \\ U_{m1} \\ \vdots \\ U_{mm} \end{array} \right\} - \left\{ \begin{array}{c} W_{11} \\ \vdots \\ W_{1m} \\ W_{21} \\ \vdots \\ W_{m1} \\ \vdots \\ W_{mm} \end{array} \right\} = \tilde{\mathbf{B}}\mathbf{\Gamma} \Rightarrow e\ \tilde{\mathbf{U}} - \tilde{\mathbf{W}} = \tilde{\mathbf{B}}\mathbf{\Gamma}, \tag{6.9}$$

where $\tilde{\mathbf{U}}$ contains information about the modal response and forcing distribution, and $\tilde{\mathbf{W}}$ is a vector pertaining to a reference average proportional damping.

6.4 Component Damping Constant

After applying the approach in the previous section, only the relative structural damping is known. Thus, the value of e must be found by an alternate technique. As two methods are required, the approach proposed herein is referred to as the component hybrid damping identification method. Thus, the method proposed in Sec. 5.4 is adapted for finding e. Pre-multiplying Eqn. (6.9) by $\tilde{\mathbf{B}}^{-*}$ (and assuming

$m \geq n$) and substituting into Eqn. (5.17), one obtains

$$\begin{aligned} j\boldsymbol{\Psi}^T\tilde{\mathbf{K}}\left(\mathbf{I}_{n\times n}\otimes[\omega_u\mathbf{p}_u-\omega_v\mathbf{p}_v]\right)\left(e\tilde{\mathbf{B}}^{-*}\mathbf{U}-\tilde{\mathbf{B}}^{-*}\tilde{\mathbf{W}}\right)= \\ \omega_u^2\mathbf{p}_u-\omega_v^2\mathbf{p}_v-\boldsymbol{\Lambda}_{mist}\left(\mathbf{p}_u-\mathbf{p}_v\right)-j\Gamma^m\boldsymbol{\Lambda}_{mist}\left(\omega_u\mathbf{p}_u-\omega_v\mathbf{p}_v\right). \end{aligned} \tag{6.10}$$

Letting $\mathbf{Y}=j\boldsymbol{\Psi}^T\tilde{\mathbf{K}}\left(\mathbf{I}_{n\times n}\otimes[\omega_u\mathbf{p}_u-\omega_v\mathbf{p}_v]\right)$ and $\mathbf{Z}$ be the right side of Eqn. (6.10), one obtains

$$\mathbf{Y}\tilde{\mathbf{B}}^{-*}\mathbf{U}e=\mathbf{Z}+\mathbf{Y}\tilde{\mathbf{B}}^{-*}\tilde{\mathbf{W}}\Rightarrow\bar{\mathbf{Y}}e=\bar{\mathbf{Z}},$$

where $\bar{\mathbf{Y}}$ and $\bar{\mathbf{Z}}$ are vectors of size $m\times 1$. Note that this equation is valid for all frequency pairs. Therefore, letting $\tilde{\mathbf{y}}_r=\bar{\mathbf{Y}}\left(\omega\right)$ and $\tilde{\mathbf{z}}_r=\bar{\mathbf{Z}}\left(\omega\right)$ for the r^{th} (frequency) pair and concatenating the vectors, one obtains

$$\left\{\begin{array}{c}\tilde{\mathbf{y}}_1\\ \vdots\\ \tilde{\mathbf{y}}_p\end{array}\right\}e=\left\{\begin{array}{c}\tilde{\mathbf{z}}_1\\ \vdots\\ \tilde{\mathbf{z}}_p\end{array}\right\}\Rightarrow\tilde{\mathbf{Y}}e=\tilde{\mathbf{Z}}$$

where p is the total number of frequency pairs. Pre-multiplying by $\tilde{\mathbf{Y}}^T$, one obtains

$$e=\frac{\tilde{\mathbf{Y}}^T\tilde{\mathbf{Z}}}{\tilde{\mathbf{Y}}^T\tilde{\mathbf{Y}}} \tag{6.11}$$

If the forcing distribution is known, the forcing can be identified using $\mathbf{F}=e\mathbf{G}^T\tilde{\mathbf{F}}$. In addition, pre-multiplying Eqn. (6.9) by $\tilde{\mathbf{B}}^{-*}$ and using e from Eqn. (6.11), one obtains

$$\boldsymbol{\Gamma}=\tilde{\mathbf{B}}^{-*}\left(\frac{\tilde{\mathbf{Y}}^T\tilde{\mathbf{Z}}}{\tilde{\mathbf{Y}}^T\tilde{\mathbf{Y}}}\tilde{\mathbf{U}}-\tilde{\mathbf{W}}\right). \tag{6.12}$$

Using Eqn. (6.12) the component damping can be identified. This method is applicable to mistuned systems, may use ROMs, and only requires the forcing to be known up to a multiplicative constant.

CHAPTER VII

Conclusions and Future Work

7.1 Contributions

Chapter II included a novel, general structural damping identification procedure, which only requires knowledge of the undamped system modes, mistuning, relative forcing, and damped forced responses. The proposed method was shown to identify the damping without requiring measurements precisely at resonance. Surely, large responses are preferable (because of their favorable signal to noise ratio), but they are not required to be precisely at resonant conditions. Furthermore, the proposed method was noted to be equally effective for both low and high modal density cases. In fact, the proposed method was shown to reduce to the half-power method for isolated modes. In contrast, the blisk example provided is a very difficult case for other methodologies because most current techniques do not apply to systems with high modal density. The results indicated that the proposed approach is robust with respect to measurement noise and can make use of highly effective reduced order models (ROMs). Also, two measurement filters were shown to allow an accurate damping identification by reducing the impact of measurement noise. In addition, forcing errors were found to affect the damping identification less than measurement noise. Hence, using the proposed method to identify structural damping allows for more accurate forced response and high-cycle fatigue predictions, especially when

mistuning is present. The proposed method allows multiple time scales, in contrast to other techniques that also identify one damping value per system.

Chapter III presented an extended measurement point selection (MPS) method which is shown to be equivalent to the full system EIDV method, but it decreases the computational cost, increases the robustness of the identification, and minimizes the measurement time. This method addresses the lack of information in current damping identification methods regarding the crucial step of deciding which locations to measure on a structure. In addition, a modal damping identification method is introduced which avoids the complications of current damping identification methods while offering a more realistic type of damping than in Chapter II. The validation blisk results indicate that using the optimized MPS technique increases the accuracy of the identification for modes which are sensitive to measurement noise as compared to only using points chosen based on the (classical) EIDV method. Also, the proposed modal damping identification method is shown to be relatively insensitive to measurement noise for 1%, 5%, and 10% levels, to apply to mistuned systems, and to require knowledge of only the forced response, the relative forcing, the mistuning, and a finite element model. It was demonstrated that the identification method applied to low dimensional systems and more complicated structures exemplified by the validation blisk.

Chapter IV discussed the hybrid modal damping identification method which offers several benefits as compared to current damping identification techniques. First, the proposed methodology uses a reduced frequency response matrix such that only a subset of all the DOF of the system need to be measured, with another subset being forced. The hybrid damping identification does not require knowledge of the absolute forcing, but can identify this value if the relative forcing is known (from a forcing calibration). An important feature which allows the identification to be accurate is the introduction of the frequency windowing. The windowing can reduce the effects of

measurement noise and also lower the number of required forcing cases. This decrease in data acquisition has a significant impact on the computational cost of preforming the damping identification. In addition, this method can be applied to mistuned systems and uses ROMs. Therefore, the proposed method is also computationally efficient. Results for a validation blisk were presented which show that identifying the modal damping is possible by employing the proposed approach, which uses a ROM, requires measurements at only a few locations per blade, and is effective even in the presence of relative, absolute and bias measurement noise. Next, a comparison of the proposed method with the alternative method in Chapter III shows that the proposed method is less accurate when using the same filter values, however more modal damping values can be identified with the proposed approach. Finally, results of a study are presented which indicate that the damping identification is more sensitive to measurement noise than to forcing errors.

Chapter V introduced a component damping identification method. In contrast to current damping identification methods, this novel method allows the damping to have a meaningful physical interpretation especially for structures with complex geometry. In particular, this type of damping identification enables a more accurate analysis of a damping coating. In addition, the presented formulation can be used to generate the forced response of a mistuned structure with a prescribed component damping for a given harmonic excitation and ranges larger than the identification frequency range. As the forced response method uses ROMs, it is computationally efficient, while eliminating costly experimentation. In addition, the complex interaction between mass or stiffness mistuning and component damping variability can be studied. The application of the proposed method to various situations is explored. Thus, the versatility of the proposed method was illustrated. Results for a validation blisk show that the identification is possible when using ROMs, in the presence of measurement noise, and when both low and high modal density is present. Most importantly,

the dynamics of the structure are captured by the identified component damping. However, the component damping method can be more sensitive to absolute and bias measurement noise than other damping identification methods. A comparison of the proposed method with the hybrid damping identification introduced in Chapter IV reveals that it is possible for the component damping identification to accurately represent the damping of the system with fewer parameters than other methods.

Chapter VI introduced an alternate component damping identification method, which utilizes the reduced frequency response matrix and the known forcing. By applying the method introduced in Chapter V, this method was extended by requiring knowledge of the relative forcing in place of the absolute applied forcing. This method can be applied to mistuned systems and uses ROMs. The hybrid method has the potential to more accurately identify the component damping than the method in Chapter V. This follows from the possibility that the hybrid ability may use more modes and measurement data from resonant conditions which have a larger signal to noise ratio.

7.2 Future Research

The following explores potential topics of interest related to the work herein.

- **Component Damping Identification Improvements**

  The component damping identification in Chapter V is more sensitive to bias and absolute measurement noise than desirable. Examining potential solutions to this issue is suggested for the future. In addition, the identification should be explored and validated for other complex systems.

- **Hybrid Component Damping Identification Results**

  The formulation of the hybrid component damping identification method is provided. Exploring the sensitivity of this work to a ROM and measurement noise

would be beneficial. The focus of this work was on validation using the University of Michigan validation blisk. However, further examination and validation of other systems is recommended to explore any limitations of the damping identification method.

- **Experimental Validation**

  The damping identification methods are validated using numerical data in this work. However, to be applicable for system identification, the methods need to be validated using experimental measurements also. In particular, the input experimental data can be compared to the forced response generated using the identified damping. In addition, the damping identification should be tested on structures with and without damping coatings.

- **Simultaneous Mistuning, Cyclic Modeling Error (CME), and Damping ID**

  Using the following two methods it should be possible to simultaneously identify the mistuning, CME, and (component) damping. Development, implementation, and validation of these methodologies should be preformed both numerically and experimentally.

7.2.1 Simultaneous ID Method 1

The equation of motion can be expressed as

$$\mathbf{M}\ddot{\bar{\mathbf{x}}} + \mathbf{C}\dot{\bar{\mathbf{x}}} + \mathbf{K}\bar{\mathbf{x}} = \mathbf{F}$$

$$\bar{\boldsymbol{\phi}}^T\mathbf{M}\ddot{\bar{\mathbf{x}}} + \bar{\boldsymbol{\phi}}^T\mathbf{C}\dot{\bar{\mathbf{x}}} + \bar{\boldsymbol{\phi}}^T\mathbf{K}\bar{\mathbf{x}} = \bar{\boldsymbol{\phi}}^T\mathbf{F}.$$

Introducing small mistuning, component damping, and harmonic forcing, one ob-

tains

$$-\omega^2\bar{\boldsymbol{\phi}}^T\mathbf{M}\bar{\mathbf{x}} + j\omega\bar{\boldsymbol{\phi}}^T\mathbf{S}^T Bdiag\left[\delta\Gamma^i\left(\boldsymbol{\kappa}^i + \delta\boldsymbol{\kappa}^i\right)\right]\mathbf{S}\bar{\mathbf{x}} + \left(1 + j\omega\Gamma^m\right)\bar{\boldsymbol{\phi}}^T\left(\mathbf{K} + \mathbf{K}^\delta + \mathbf{K}^{cme}\right)\bar{\mathbf{x}} = \bar{\boldsymbol{\phi}}^T\mathbf{F}.$$

Now assuming the mistuning and damping are small such that $\delta\Gamma^i\delta\boldsymbol{\kappa}^i \approx 0$, one obtains

$$-\omega^2\bar{\boldsymbol{\phi}}^T\mathbf{M}\bar{\mathbf{x}} + j\omega\bar{\boldsymbol{\phi}}^T\mathbf{S}^T Bdiag\left[\delta\Gamma^i\boldsymbol{\kappa}^i\right]\mathbf{S}\bar{\mathbf{x}} + \left(1 + j\omega\Gamma^m\right)\bar{\boldsymbol{\phi}}^T\left(\mathbf{K} + \mathbf{K}^\delta + \mathbf{K}^{cme}\right)\bar{\mathbf{x}} = \bar{\boldsymbol{\phi}}^T\mathbf{F}.$$

Now $\bar{\boldsymbol{\phi}}^T\mathbf{M}\bar{\boldsymbol{\phi}} = \mathbf{I}$ so, $\bar{\boldsymbol{\phi}}^T = \bar{\boldsymbol{\phi}}^{-1}\mathbf{M}^{-1}$. Also, convert to modal coordinates such that $\bar{\mathbf{x}} = \bar{\boldsymbol{\phi}}\bar{\mathbf{p}}$. Substituting into the previous equation, one obtains

$$\begin{aligned}
\bar{\boldsymbol{\phi}}^T\mathbf{K}^{cme}\bar{\boldsymbol{\phi}} &= \delta\boldsymbol{\Lambda} \\
\bar{\boldsymbol{\phi}}^{-1}\mathbf{M}^{-1}\mathbf{K}^{cme}\bar{\boldsymbol{\phi}}\bar{\mathbf{p}} &= \delta\boldsymbol{\Lambda}\bar{\mathbf{p}} \\
\mathbf{K}^{cme}\bar{\mathbf{x}} &= \mathbf{M}\bar{\boldsymbol{\phi}}\delta\boldsymbol{\Lambda}\bar{\mathbf{p}}
\end{aligned}$$

So,

$$-\omega^2\bar{\boldsymbol{\phi}}^T\mathbf{M}\bar{\mathbf{x}} + j\omega\bar{\boldsymbol{\phi}}^T\mathbf{S}^T Bdiag\left[\delta\Gamma^i\boldsymbol{\kappa}^i\right]\mathbf{S}\bar{\mathbf{x}} + \left(1 + j\omega\Gamma^m\right)\bar{\boldsymbol{\phi}}^T\left(\mathbf{K} + \mathbf{K}^\delta\right)\bar{\mathbf{x}} + \left(1 + j\omega\Gamma^m\right)\delta\boldsymbol{\Lambda}\bar{\mathbf{p}} = \bar{\boldsymbol{\phi}}^T\mathbf{F}.$$

Rearranging the terms, one obtains

$$\begin{aligned}
j\omega\bar{\boldsymbol{\phi}}^T\mathbf{S}^T Bdiag\left[\delta\Gamma^i\boldsymbol{\kappa}^i\right]\mathbf{S}\bar{\mathbf{x}} + \left(1 + j\omega\Gamma^m\right)\bar{\boldsymbol{\phi}}^T\mathbf{K}^\delta\bar{\mathbf{x}} + \left(1 + j\omega\Gamma^m\right)\delta\boldsymbol{\Lambda}\bar{\mathbf{p}} \\
= \bar{\boldsymbol{\phi}}^T\mathbf{F} + \omega^2\bar{\boldsymbol{\phi}}^T\mathbf{M}\bar{\mathbf{x}} - \left(1 + j\omega\Gamma^m\right)\bar{\boldsymbol{\phi}}^T\mathbf{K}\bar{\mathbf{x}}.
\end{aligned} \tag{7.1}$$

Now from Chapter V,

$$Bdiag\left[\delta\Gamma^i\boldsymbol{\kappa}^i\right]\mathbf{S}\bar{\mathbf{x}} = Bdiag\left[\boldsymbol{\kappa}^i\mathbf{S}^i\right]\left(\mathbf{I}\otimes\bar{\mathbf{x}}\right)\delta\boldsymbol{\Gamma} \tag{7.2}$$

Also note that,

$$\begin{aligned}
\bar{\boldsymbol{\phi}}^T \mathbf{K}^\delta \bar{\boldsymbol{\phi}} \bar{\mathbf{p}} \approx \mathbf{q}^T \bar{\boldsymbol{\phi}}_{CB}^T \mathbf{K}^\delta \bar{\boldsymbol{\phi}}_{CB} \mathbf{q} \bar{\mathbf{p}} &\approx \mathbf{q}^T \boldsymbol{\Lambda}^{\delta,CB} \mathbf{q} \bar{\mathbf{p}} \\
&= \mathbf{q}^T diag\left[\mathbf{q}_i \bar{\mathbf{p}}\right] \delta \boldsymbol{\Lambda}^{CB} \\
\Rightarrow \bar{\boldsymbol{\phi}}^{-1} \mathbf{M}^{-1} \mathbf{K}^\delta \bar{\boldsymbol{\phi}} \bar{\mathbf{p}} &\approx \mathbf{q}^T diag\left[\mathbf{q}_i \bar{\mathbf{p}}\right] \delta \boldsymbol{\Lambda}^{CB} \\
\mathbf{K}^\delta \bar{\mathbf{x}} &\approx \mathbf{M} \bar{\boldsymbol{\phi}} \mathbf{q}^T diag\left[\mathbf{q}_i \bar{\mathbf{p}}\right] \delta \boldsymbol{\Lambda}^{CB},
\end{aligned} \tag{7.3}$$

where $\mathbf{q}_i$ is the i^{th} row of $\mathbf{q}$. Also, the CME term can be expressed as

$$\delta \boldsymbol{\Lambda} \bar{\mathbf{p}} = diag\left[p_i\right] \delta \boldsymbol{\Lambda}^{cme} \tag{7.4}$$

Substituting Eqns. (7.2), (7.3), and (7.4) in Eqn. (7.1), one obtains

$$\begin{aligned}
&j\omega \bar{\boldsymbol{\phi}}^T \mathbf{S}^T B diag\left[\boldsymbol{\kappa}^i \mathbf{S}^i\right] \left(\mathbf{I} \otimes \bar{\mathbf{x}}\right) \delta \boldsymbol{\Gamma} \\
&+ \left(1 + j\omega \Gamma^m\right) \mathbf{q}^T diag\left[\mathbf{q}_i \bar{\mathbf{p}}\right] \delta \boldsymbol{\Lambda}^{CB} \\
&+ \left(1 + j\omega \Gamma^m\right) diag\left[p_i\right] \delta \boldsymbol{\Lambda}^{cme} \\
&= \bar{\boldsymbol{\phi}}^T \mathbf{F} + \omega^2 \bar{\boldsymbol{\phi}}^T \mathbf{M} \bar{\mathbf{x}} - \left(1 + j\omega \Gamma^m\right) \bar{\boldsymbol{\phi}} \mathbf{K} \bar{\mathbf{x}}.
\end{aligned} \tag{7.5}$$

Converting to modal coordinates, one obtains

$$\begin{aligned}
&j\omega \boldsymbol{\Psi}^T B diag\left[\boldsymbol{\kappa}^i \boldsymbol{\Psi}^i\right] \left(\mathbf{I} \otimes \bar{\boldsymbol{\phi}} \bar{\mathbf{p}}\right) \delta \boldsymbol{\Gamma} \\
&+ \left(1 + j\omega \Gamma^m\right) \mathbf{q}^T diag\left[\mathbf{q}_i \bar{\mathbf{p}}\right] \delta \boldsymbol{\Lambda}^{CB} \\
&+ \left(1 + j\omega \Gamma^m\right) diag\left[p_i\right] \delta \boldsymbol{\Lambda}^{cme} \\
&= \bar{\boldsymbol{\phi}}^T \mathbf{F} + \omega^2 \bar{\mathbf{p}} - \left(1 + j\omega \Gamma^m\right) \Lambda_t \bar{\mathbf{p}}.
\end{aligned} \tag{7.6}$$

From Eqn. (7.6), the damping $\delta \boldsymbol{\Gamma}$, mistuning $\delta \boldsymbol{\Lambda}^{CB}$, and CME $\delta \boldsymbol{\Lambda}^{cme}$ can be determined if the applied forcing is known.

7.2.2 Simultaneous ID Method 2

The equation of motion can be expressed as

$$\mathbf{M}\ddot{\mathbf{x}} + \mathbf{C}\dot{\mathbf{x}} + \mathbf{K}\bar{\mathbf{x}} = \mathbf{F}$$

Pre-multiplying by $\boldsymbol{\phi}^T$, one obtains

$$\bar{\boldsymbol{\phi}}^T\mathbf{M}\ddot{\mathbf{x}} + \bar{\boldsymbol{\phi}}^T\mathbf{C}\dot{\mathbf{x}} + \bar{\boldsymbol{\phi}}^T\mathbf{K}\bar{\mathbf{x}} = \bar{\boldsymbol{\phi}}^T\mathbf{F}.$$

Introducing small mistuning, component damping, and harmonic forcing, one obtains

$$\begin{aligned}-\omega^2\bar{\boldsymbol{\phi}}^T\mathbf{M}\bar{\mathbf{x}} + j\omega\bar{\boldsymbol{\phi}}^T\mathbf{S}^T Bdiag\left[\delta\Gamma^i\left(\boldsymbol{\kappa}^i + \delta\boldsymbol{\kappa}^i\right)\right]\mathbf{S}\bar{\mathbf{x}} \\ + \left(1 + j\omega\Gamma^m\right)\bar{\boldsymbol{\phi}}^T\left(\mathbf{K} + \mathbf{K}^\delta + \mathbf{K}^{cme}\right)\bar{\mathbf{x}} = \bar{\boldsymbol{\phi}}^T\mathbf{F}.\end{aligned}$$

Converting to mass normalized modal coordinates $\mathbf{x} = \bar{\boldsymbol{\phi}}\bar{\mathbf{p}}$, one obtains

$$\begin{aligned}&\bar{\boldsymbol{\phi}}^T\mathbf{F} = \\ &\left[-\omega^2\mathbf{I} + j\omega\bar{\boldsymbol{\phi}}^T\mathbf{S}^T Bdiag\left[\delta\Gamma^i\left(\boldsymbol{\kappa}^i + \delta\boldsymbol{\kappa}^i\right)\right]\mathbf{S}\bar{\boldsymbol{\phi}} + \left(1 + j\omega\Gamma^m\right)\bar{\boldsymbol{\phi}}^T\left(\mathbf{K} + \mathbf{K}^\delta + \mathbf{K}^{cme}\right)\bar{\boldsymbol{\phi}}\right]\bar{\mathbf{p}}.\end{aligned}$$

Let $\mathbf{H}$ be the terms inside the brackets so that

$$\mathbf{H}\bar{\mathbf{p}} = \bar{\boldsymbol{\phi}}^T\mathbf{F}.$$

Also, curve fit the same measurement data and create transfer function $\tilde{\mathbf{H}}$ with response $\tilde{\mathbf{x}}$, where $\tilde{\mathbf{H}}$ is written as a linear combination of exponential functions. Then, one obtains

$$\mathbf{H}\bar{\mathbf{x}} = \bar{\boldsymbol{\phi}}^T\tilde{\mathbf{H}}\bar{\boldsymbol{\phi}}\tilde{\mathbf{p}}.$$

The method to determine $\tilde{\mathbf{H}}$ is as follows. First, express the measured response

x_i^f of DOF i, forcing case b, and forcing frequency ω as

$$x_i^f(\omega) = \sum_{k=1}^{n} \frac{\alpha_{k,i}^f e^{j\theta_k}}{\omega_k^2 - \omega^2 + 2\zeta_k \omega \omega_k},$$

where $\alpha_{k,i}^f$ and θ_k are the unknown magnitude and phase relating the forcing to the response for a given mode, ω_k is the unknown natural frequency of mode k, and ζ_k is the unknown modal damping of mode k. Next, from a (to be determined) exponential curve fitting process, the unknowns $\alpha_{k,i}^f$, θ_k, ω_k, and ζ_k are obtained. Converting to modal coordinates $\mathbf{x} = \boldsymbol{\phi}\mathbf{p}$, one obtains

$$\mathbf{p}^f(\omega) = \sum_{k=1}^{n} \boldsymbol{\phi}^{-*} \frac{\boldsymbol{\alpha}_k^f e^{j\theta_k}}{\omega_k^2 - \omega^2 + 2\zeta_k \omega \omega_k}$$

Finally, $\tilde{\mathbf{H}}$ can be constructed for the same forcing cases, but at any frequency ω.

Letting $\bar{\mathbf{p}} = \tilde{\mathbf{p}} + \bar{\mathbf{p}}_{noise}$, one obtains

$$\mathbf{H}(\tilde{\mathbf{p}} + \bar{\mathbf{p}}_{noise}) = \bar{\boldsymbol{\phi}}^T \tilde{\mathbf{H}} \bar{\boldsymbol{\phi}} \tilde{\mathbf{p}}.$$

Assuming that $\mathbf{H}\bar{\mathbf{p}}_{noise} << \mathbf{H}\tilde{\mathbf{p}} \approx \bar{\boldsymbol{\phi}}^T \tilde{\mathbf{H}} \bar{\boldsymbol{\phi}} \tilde{\mathbf{p}}$, one obtains

$$\mathbf{H}\tilde{\mathbf{p}} \approx \bar{\boldsymbol{\phi}}^T \tilde{\mathbf{H}} \bar{\boldsymbol{\phi}} \tilde{\mathbf{p}}.$$

As this equation holds for all $\tilde{\mathbf{p}}$,

$$\mathbf{H} = -\omega^2 \mathbf{I} + j\omega \bar{\boldsymbol{\phi}}^T \mathbf{S}^T Bdiag\left[\delta\Gamma^i \left(\boldsymbol{\kappa}^i + \delta\boldsymbol{\kappa}^i\right)\right] \mathbf{S}\bar{\boldsymbol{\phi}} + \left(1 + j\omega\Gamma^m\right) \bar{\boldsymbol{\phi}}^T \left(\mathbf{K} + \mathbf{K}^\delta + \mathbf{K}^{cme}\right) \bar{\boldsymbol{\phi}}$$
$$\approx \bar{\boldsymbol{\phi}}^T \tilde{\mathbf{H}} \boldsymbol{\phi}.$$

Assuming the mistuning and damping are small such that $\delta\Gamma^i\delta\boldsymbol{\kappa}^i \approx 0$, one obtains

$$\begin{aligned} &-\omega^2\mathbf{I} + j\omega\bar{\boldsymbol{\phi}}^T\mathbf{S}^T Bdiag\left[\delta\Gamma^i\boldsymbol{\kappa}^i\right]\mathbf{S}\bar{\boldsymbol{\phi}} + (1+j\omega\Gamma^m)\,\bar{\boldsymbol{\phi}}^T\left(\mathbf{K}+\mathbf{K}^\delta+\mathbf{K}^{cme}\right)\bar{\boldsymbol{\phi}} \\ &= \bar{\boldsymbol{\phi}}^T\tilde{\mathbf{H}}\bar{\boldsymbol{\phi}}. \end{aligned} \tag{7.7}$$

Now, $\bar{\boldsymbol{\phi}}^T\mathbf{K}^{cme}\bar{\boldsymbol{\phi}} = \delta\boldsymbol{\Lambda}$. So,

$$-\omega^2\mathbf{I}+j\omega\bar{\boldsymbol{\phi}}^T\mathbf{S}^T Bdiag\left[\delta\Gamma^i\boldsymbol{\kappa}^i\right]\mathbf{S}\bar{\boldsymbol{\phi}}+(1+j\omega\Gamma^m)\,\bar{\boldsymbol{\phi}}^T\left(\mathbf{K}+\mathbf{K}^\delta\right)\bar{\boldsymbol{\phi}}+(1+j\omega\Gamma^m)\,\delta\boldsymbol{\Lambda} = \bar{\boldsymbol{\phi}}^T\tilde{\mathbf{H}}\boldsymbol{\phi}.$$

Rearranging,

$$\begin{aligned} j\omega\bar{\boldsymbol{\phi}}^T\mathbf{S}^T Bdiag\left[\delta\Gamma^i\boldsymbol{\kappa}^i\right]\mathbf{S}\bar{\boldsymbol{\phi}} + (1+j\omega\Gamma^m)\,\bar{\boldsymbol{\phi}}^T\mathbf{K}^\delta\bar{\boldsymbol{\phi}} + (1+j\omega\Gamma^m)\,\delta\boldsymbol{\Lambda} \\ = \bar{\boldsymbol{\phi}}^T\tilde{\mathbf{H}}\boldsymbol{\phi} + \omega^2\mathbf{I} - (1+j\omega\Gamma^m)\,\boldsymbol{\Lambda}_t. \end{aligned} \tag{7.8}$$

Now from Chapter V, one obtains

$$Bdiag\left[\delta\Gamma^i\boldsymbol{\kappa}^i\right]\mathbf{S}\bar{\boldsymbol{\phi}} = Bdiag\left[\boldsymbol{\kappa}^i\boldsymbol{\Psi}^i\right]Bdiag\left(\delta\Gamma^i\mathbf{I}\right) = Bdiag\left[\boldsymbol{\kappa}^i\boldsymbol{\Psi}^i\right]\delta\boldsymbol{\Gamma}, \tag{7.9}$$

where $\boldsymbol{\Psi} = \mathbf{S}\bar{\boldsymbol{\phi}}$. Also, $\bar{\boldsymbol{\phi}}^T\mathbf{K}^\delta\bar{\boldsymbol{\phi}} \approx \mathbf{q}^T\bar{\boldsymbol{\phi}}_{CB}^T\mathbf{K}^\delta\bar{\boldsymbol{\phi}}_{CB}\mathbf{q} \approx \mathbf{q}^T\boldsymbol{\Lambda}^{\delta,CB}\mathbf{q}$. So,

$$\bar{\boldsymbol{\phi}}^T\mathbf{K}^\delta\bar{\boldsymbol{\phi}} \approx \mathbf{q}^T\sum_i \mathbf{q}_i diag\left[\Lambda_i^{\delta,CB}\right] = \mathbf{q}^T\sum_i \mathbf{q}_i\mathbf{I}\Lambda_i^{\delta,CB} \tag{7.10}$$

where $\mathbf{D}_i$ is a matrix containing the i^{th} row of $\mathbf{D}$ (with the rest zeros) and $\Lambda_i^{\delta,CB}$ is the mistuning of the i^{th} blade.

Substituting Eqns. (7.9) and (7.10) in Eqn. (7.8), one obtains

$$\begin{aligned} & j\omega\bar{\boldsymbol{\Psi}}^T Bdiag\left[\boldsymbol{\kappa}^i\boldsymbol{\Psi}^i\right]\delta\boldsymbol{\Gamma} \\ & +\left(1+j\omega\Gamma^m\right)\mathbf{q}^T\sum_i \mathbf{q}_i\mathbf{I}\Lambda_i^{\delta,CB} \\ & +\left(1+j\omega\Gamma^m\right)\delta\boldsymbol{\Lambda} \\ & =\bar{\boldsymbol{\phi}}^T\tilde{\mathbf{H}}\boldsymbol{\phi}+\omega^2\mathbf{I}-\left(1+j\omega\Gamma^m\right)\boldsymbol{\Lambda}_t. \end{aligned} \tag{7.11}$$

From Eqn. (7.11), the damping $\delta\boldsymbol{\Gamma}$, mistuning $\Lambda_i^{\delta,CB}$, and CME $\delta\boldsymbol{\Lambda}$ can be determined if the transfer function is fitted with exponential functions.

APPENDICES

APPENDIX A

Simple Case of Isolated Modes

From Chapter II, in mistuned modal coordinates

$$(1+j\gamma)\left[\mathbf{p}_i - \alpha_k \mathbf{p}_k\right] = \tilde{\mathbf{K}}^{-1}_{mist_{m\times m}} \tilde{\mathbf{M}}_{m\times m} \left[\omega_i^2 \mathbf{p}_i - \alpha_k \omega_k^2 \mathbf{p}_k\right]. \tag{A.1}$$

The following shows that for isolated modes and for responses measured at the half power points, Eqn. A.1 reduces to the single DOF half-power method. First, assume that the forced response for an isolated mode has been measured. For the mistuned system, $\tilde{\mathbf{K}}^{-1}_{mist_{m\times m}} \tilde{\mathbf{M}}_{m\times m}$ is a diagonal matrix containing elements corresponding to $\frac{1}{\omega_{n_v}^2}$, where ω_{n_v} is the v^{th} mistuned natural frequency in the frequency range of interest. Hence, for two measurements ($i = 1$ and $k = 2$), Eqn. A.1 becomes

$$\begin{aligned}(1+j\gamma)\left[\mathbf{p}_1 - \alpha_2 \mathbf{p}_2\right]_{m\times 1} = \\ diag\left[\frac{1}{\omega_{n_v}^2}\right]_{m\times m} \left[\omega_1^2 \mathbf{p}_1 - \alpha_2 \omega_2^2 \mathbf{p}_2\right]_{m\times 1}.\end{aligned} \tag{A.2}$$

As the forced response is for an isolated mode, all entries in $\mathbf{p}_1$ are approximately zero, except for one entry. The same applies for $\mathbf{p}_2$. Therefore, Eqn. (A.2) can be

rewritten as

$$[p_1 - \alpha_2 p_2](1 + j\gamma) = \frac{1}{\omega_n^2}\left[\omega_1^2 p_1 - \alpha_2 \omega_2^2 p_2\right],$$

where p_1 and p_2 correspond to the non-zero entries, and ω_n is the corresponding mistuned natural frequency of the isolated mode. Pre-multiplying by the mistuned eigenvector corresponding to the isolated mode $\mathbf{\Psi}_{m\times 1}$, one obtains

$$(1 + j\gamma)[\mathbf{x}_1 - \alpha_2 \mathbf{x}_2] = \frac{1}{\omega_n^2}\left[\omega_1^2 \mathbf{x}_1 - \alpha_2 \omega_2^2 \mathbf{x}_2\right]. \tag{A.3}$$

Pre-multiplying Eqn. (A.3) by $[\mathbf{x}_1 - \alpha_2 \mathbf{x}_2]^T$ and taking the imaginary part of both sides, after some algebraic manipulations one obtains

$$\begin{aligned}\gamma = Im\Bigg\{ & \frac{1}{\omega_n^2}\Big([\mathbf{x}_1 - \alpha_2 \mathbf{x}_2]^T [\mathbf{x}_1 - \alpha_2 \mathbf{x}_2]\Big)^{-1} \\ & [\mathbf{x}_1 - \alpha_2 \mathbf{x}_2]^T \left[\omega_1^2 \mathbf{x}_1 - \alpha_2 \omega_2^2 \mathbf{x}_2\right]\Bigg\}.\end{aligned} \tag{A.4}$$

Equation (A.4) is a least squares solution to the damping identification for an isolated mode. Since the mode is isolated, the physical measurements in vectors $\mathbf{x}_1$ and $\mathbf{x}_2$ are proportional to p_1 and p_2 respectively. Hence, measuring multiple DOF does not provide more information than measuring a single DOF. Consider that the measured DOF from $\mathbf{x}_1$ is x_1 and the measured DOF from $\mathbf{x}_2$ is x_2. Equation (A.4) becomes

$$\gamma = Im\left\{\frac{\omega_1^2 x_1 - \alpha_2 \omega_2^2 x_2}{\omega_n^2 (x_1 - \alpha_2 x_2)}\right\}.$$

Assuming that the force applied at ω_1 is the same as the force applied at ω_2 (i.e. considering that $\alpha_2 = 1$), one obtains

$$\gamma = Im\left\{\frac{\omega_1^2 - \omega_2^2\left(\frac{x_2}{x_1}\right)}{\omega_n^2\left(1 - \frac{x_2}{x_1}\right)}\right\}. \tag{A.5}$$

When measurements at the half-power points are used, Eqn. (A.5) is equivalent to the half-power method. To show this equivalence, a brief derivation of the half-power points for a single DOF system follows. The equation of motion for a single DOF system is

$$m\ddot{x} + (1 + j\gamma)\, kx = F.$$

Assuming harmonic forcing and response, one obtains

$$x = \frac{F/m}{\omega_n^2 - \omega^2 + j\gamma\omega_n^2}, \tag{A.6}$$

and

$$|x| = \frac{|F|/m}{\omega_n^2 \sqrt{\left[1 - \left(\frac{\omega}{\omega_n}\right)^2\right]^2 + \gamma^2}}, \tag{A.7}$$

where $|\cdot|$ denotes a magnitude, ω is the excitation frequency, and $\omega_n = \sqrt{\frac{k}{m}}$ is the natural frequency. When $\omega = \omega_n$, $|x| = \frac{|F|/m}{\omega_n^2 \gamma}$. Next, one may assume that the forcing is constant and choose responses at the half-power points, where the response amplitude is $\frac{1}{\sqrt{2}}$ times the resonant response. Substituting into Eqn. (A.7) and solving for the half-power frequencies, one obtains $\omega_1 = \omega_n\sqrt{1-\gamma}$ and $\omega_2 = \omega_n\sqrt{1+\gamma}$. Substituting these frequencies into Eqn. (A.6), one obtains the ratio of the responses at the half-power points

$$\frac{x_2}{x_1} = \frac{\omega_n^2 - \omega_n^2\,(1-\gamma) + j\gamma\omega_n^2}{\omega_n^2 - \omega_n^2\,(1+\gamma) + j\gamma\omega_n^2} = \frac{1+j}{-1+j} = -j. \tag{A.8}$$

Now, assume the half-power frequencies are known for an isolated mode. Substi-

tuting Eqn. (A.8) into Eqn. (A.5), one obtains

$$\gamma = Im\left\{\frac{\omega_1^2 + j\omega_2^2}{\omega_n^2\,(1+j)}\right\} = \frac{\omega_2^2 - \omega_1^2}{2\omega_n^2}. \tag{A.9}$$

Thus, for cases where γ is small (such as blisks), Eqns. (A.5) and (A.9) become

$$\gamma = \frac{\omega_2^2 - \omega_1^2}{2\ \omega_n^2} = \frac{\omega_2 - \omega_1}{\omega_n}\frac{\omega_2 + \omega_1}{2\omega_n} \approx \frac{\omega_2 - \omega_1}{\omega_n}. \tag{A.10}$$

Equation (A.10) is the same result as the half-power method for a single DOF system. Therefore, for an isolated mode with measured half-power points and constant forcing, the proposed method reduces to the well-known half-power method.

APPENDIX B

Mode Window Calculation

An estimated frequency window is desired to select the mistuned modes which significantly participate in the response in the measurement window $[\omega_l^t, \omega_u^t]$. Figure B.1 shows the general principle behind the mode window. All modes in or close

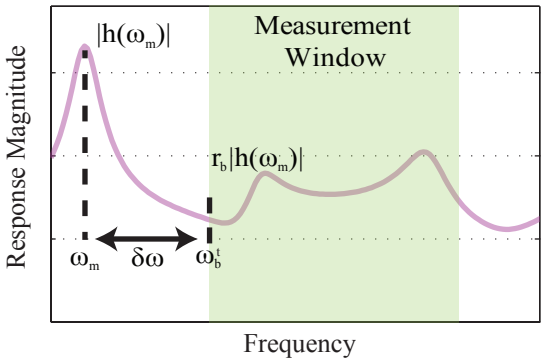

Figure B.1: Mode window description

to this range will likely participate. Thus, we focus on finding how far in frequency a mode should be from ω_l^t or ω_u^t to *not* participate. To determine that, we consider the response of a fictitious mode located at ω_m. The response of this mode is small at frequency ω_b^t (where ω_b^t is either ω_l^t or ω_u^t) when $\delta\omega$ is large enough. Therefore, we compute ω_b^t so that the magnitude of the response of the fictitious mode at ω_b^t is less than a fraction r_b of the magnitude of the response of the same mode at ω_m.

Assuming that the damping is small, the response at ω_m is close to the maximal (resonant) response. The magnitude of the responses of the fictitious mode at ω_m and $\omega_m + \delta\omega = \omega_b^t$ are given by

$$|h(\omega_m)| = |F|/|2j\zeta\omega_m^2|, \text{ and } |h(\omega_b^t)| = \frac{|F|}{|-\omega_b^{t2} + 2j\zeta\omega_m\omega_b^t + \omega_m^2|}, \tag{B.1}$$

where ζ is the damping of the fictitious mode (an estimated value of the damping for the system), and F is the magnitude of the applied forcing. For $|h(\omega_m + \delta\omega)|$ to be a fraction r_b of $|h(\omega_m)|$, one obtains

$$\begin{aligned} r_b = \frac{|h(\omega_m + \delta\omega)|}{|h(\omega_m)|} &= \frac{|2j\zeta\omega_m^2|}{|-\omega_b^{t2} + 2j\zeta\omega_m\omega_b^t + \omega_m^2|} \\ &= 2\zeta\omega_m^2/\sqrt{\left(\omega_m^2 - \omega_b^{t2}\right)^2 + 4\zeta^2\omega_m^2\omega_b^{t2}}. \end{aligned} \tag{B.2}$$

Following some algebraic manipulations, Eqn. (B.2) gives an equation for ω_b^t as a function of r_b

$$\frac{\omega_b^t}{\omega_m} = \sqrt{1 - 2\zeta\left(\zeta \mp \sqrt{1/r_b^2 - 1 + \zeta^2}\right)}. \tag{B.3}$$

Since damping is small, $\zeta^2 < r^2$ and $\mathcal{O}(\zeta^2) \approx 0$. One obtains

$$\omega_m = \frac{\omega_b^t\sqrt{1 + 2\zeta^2 \pm 2\zeta\sqrt{1/r_b^2 - 1 + \zeta^2}}}{1 - \mathcal{O}(\zeta^2)} \approx \omega_b^t\sqrt{1 \pm 2\zeta\sqrt{1/r_b^2 - 1}}. \tag{B.4}$$

Equation (B.4) can be used for $\omega_b^t = \omega_l^t$ and $r_b = 1/r_l$, and separately for $\omega_b^t = \omega_u^t$ and $r_b = 1/r_u$ to obtain the values in Eqn. (4.24).

BIBLIOGRAPHY

BIBLIOGRAPHY

[1] Holland, D. E., Castanier, M. P., Ceccio, S. L., Epureanu, B. I., and Filippi, S., 2010. "Testing and calibration procedures for mistuning identification and traveling wave excitation of blisks". *Journal of Engineering for Gas Turbines and Power,* **132**(4), p. 042502.

[2] Penny, J. E. T., Friswell, M. I., and Garvey, S. D., 1994. "Automatic choice of measurement locations for dynamic testing". *AIAA Journal,* **32**(2), pp. 407–414.

[3] Joshi, A., and Epureanu, B., 2011. "Reduced-order models for blade-to-blade damping variability in mistuned blisks". In Proceedings of ASME Turbo Expo, ASME.

[4] Sum, K. S., and Pan, J., 2002. "On the steady-state and the transient decay methods for the estimation of reverberation time". *Journal of the Acoustical Society of America,* **112**(6), pp. 2583–2588.

[5] Liang, J., 2005. "Identifying Coulomb and viscous damping from free-vibration acceleration decrements". *Journal of Sound and Vibration,* **282**(3-5), pp. 1208–1220.

[6] Lancaster, P., 1961. "Expressions for damping matrices in linear vibration problems". *Journal of the Aerospace Sciences,* **28**(3), p. 256.

[7] Adhikari, S., 2002. "Lancaster's method for damping identification revisited". *Journal of Vibration and Acoustics,* **124**(4), pp. 617–627.

[8] Adhikari, S., 2006. "Damping modelling using generalized proportional damping". *Journal of Sound and Vibration,* **293**(1-2), pp. 156–170.

[9] Chen, S.-L., Liu, J.-J., and Lai, H.-C., 2009. "Wavelet analysis for identification of damping ratios and natural frequencies". *Journal of Sound and Vibration,* **323**(1-2), pp. 130–147.

[10] Staszewski, W., 1997. "Identification of damping in MDOF systems using time-scale decomposition". *Journal of Sound and Vibration,* **203**(2), pp. 283–305.

[11] Tan, J.-B., Liu, Y., Wang, L., and Yang, W.-G., 2008. "Identification of modal parameters of a system with high damping and closely spaced modes by combining continuous wavelet transform with pattern search". *Mechanical Systems and Signal Processing,* **22**(5), pp. 1055 – 1060.

[12] Slavic, J., and Boltear, M., 2011. "Damping identification with the morlet-wave". *Mechanical Systems and Signal Processing,* **25**(5), pp. 1632 – 1645.

[13] Li, X. Y., and Law, S. S., 2009. "Identification of structural damping in time domain". *Journal of Sound and Vibration,* **328**(1-2), pp. 71–84.

[14] Roemer, M. J., and Mook, D. J., 1992. "Mass, stiffness, and damping matrix identification: An integrated approach". *Journal of Vibration and Acoustics,* **114**(3), pp. 358–363.

[15] Adhikari, S., and Phani, A. S., 2009. "Experimental identification of generalized proportional viscous damping matrix". *Journal of Vibration and Acoustics,* **131**(1), p. 011008.

[16] Adhikari, S., and Woodhouse, J., 2001. "Identification of damping: Part 1, viscous damping". *Journal of Sound and Vibration,* **243**(1), pp. 43–61.

[17] Adhikari, S., and Woodhouse, J., 2001. "Identification of damping: Part 2, non-viscous damping". *Journal of Sound and Vibration,* **243**(1), pp. 63–88.

[18] Adhikari, S., and Woodhouse, J., 2002. "Identification of damping: Part 3, symmetry-preserving methods". *Journal of Sound and Vibration,* **251**(3), pp. 477–490.

[19] Adhikari, S., and Woodhouse, J., 2002. "Identification of damping: Part 4, error analysis". *Journal of Sound and Vibration,* **251**(3), pp. 491–504.

[20] Minas, C., and Inman, D. J., 1991. "Identification of a nonproportional damping matrix from incomplete modal information". *Journal of Vibration and Acoustics,* **113**(2), pp. 219–224.

[21] Ibrahim, S., 1983. "Dynamic modeling of structures from measured complex-modes". *AIAA Journal,* **21**(6), pp. 898–901.

[22] Alvin, K. F., Peterson, L. D., and Park, K. C., 1997. "Extraction of normal modes and full modal damping from complex modal parameters". *AIAA Journal,* **35**(7), pp. 1187–1193.

[23] Andrianne, T., and Dimitriadis, G., 2012. "Damping identification of lightly damped linear dynamic systems using common-base proper orthogonal decomposition". *Mechanical Systems and Signal Processing,* **28**(0), pp. 492 – 506.

[24] Khalil, M., Adhikari, S., and Sarkar, A., 2007. "Linear system identification using proper orthogonal decomposition". *Mechanical Systems and Signal Processing,* **21**(8), pp. 3123 – 3145.

[25] Pilkey, D., and Inman, D., 1997. "An iterative approach to viscous damping matrix identification". In Proceedings of the 15th International modal analysis

conference - IMAC, vols I and II, Vol. 3089 of *Proceedings of the Society of Photo-optical Instrumentation Engineers (SPIE)*, Soc Exptl Mech Inc, pp. 1152–1157. 15th International Modal Analysis Conference - Current Horizon for Structural Damage Detection (IMAC), Orlando, FL, Feb 03-06, 1997.

[26] Chen, S. Y., Ju, M. S., and Tsuei, Y. G., 1996. "Estimation of mass, stiffness and damping matrices from frequency response functions". *Journal of Vibration and Acoustics,* **118**(1), pp. 78–82.

[27] Chen, S. Y., 2005. "A system matrices reduction method for damped systems". *JSME International Journal, Series C,* **48**(4), pp. 681–687.

[28] Lee, J. H., and Kim, J., 2001. "Development and validation of a new experimental method to identify damping matrices of a dynamic system". *Journal of Sound and Vibration,* **246**(3), pp. 505–524.

[29] Kim, K.-S., Kang, Y. J., and Yoo, J., 2008. "Structural parameters identification using improved normal frequency response function method". *Mechanical Systems and Signal Processing,* **22**(8), pp. 1858 – 1868.

[30] Fritzen, C., 1986. "Identification of mass, damping, and stiffness matrices of mechanical systems". *Journal of Vibrations Acoustics, Stress, and Reliabilty in Design - Transactions of the ASME,* **108**(1), pp. 9–16.

[31] Phani, A. S., and Woodhouse, J., 2007. "Viscous damping identification in linear vibration". *Journal of Sound and Vibration,* **303**(3-5), pp. 475–500.

[32] Langhe, K. D., and Sas, P., 1996. "Statistical analysis of the power injection method". *The Journal of the Acoustical Society of America,* **100**(1), pp. 294–303.

[33] Bloss, B. C., and Rao, M. D., 2005. "Estimation of frequency-averaged loss factors by the power injection and the impulse response decay methods". *Journal of the Acoustical Society of America,* **117**(1), pp. 240–249.

[34] Prandina, M., Mottershead, J., and Bonisoli, E., 2009. "An assessment of damping identification methods". *Journal of Sound and Vibration,* **323**, pp. 662–676.

[35] Ming, R., 2005. "An experimental comparison of the sea power injection method and the power coefficient method". *Journal of Sound and Vibration,* **282**(3-5), pp. 1009–1023.

[36] Fahy, F., and Ruivo, H., 1997. "Determination of statistical energy analysis loss factors by means of an input power modulation technique". *Journal of Sound and Vibration,* **203**(5), pp. 763–779.

[37] Cotoni, V., Langley, R. S., and Shorter, P. J., 2008. "A statistical energy analysis subsystem formulation using finite element and periodic structure theory". *Journal of Sound and Vibration,* **318**(4-5), pp. 1077–1108.

[38] Mace, B., 2005. "Statistical energy analysis: coupling loss factors, indirect coupling and system modes". *Journal of Sound and Vibration,* **279**(1-2), pp. 141–170.

[39] Yap, F., and Woodhouse, J., 1996. "Investigation of damping effects on statistical energy analysis of coupled structures". *Journal of Sound and Vibration,* **197**(3), pp. 351–371.

[40] Yang, M.-T., and Griffin, J. H., 1997. "A normalized modal eigenvalue approach for resolving modal interaction". *Journal of Engineering for Gas Turbines and Power,* **119**(3), pp. 647–650.

[41] Saito, A., Epureanu, B. I., Castanier, M. P., and Pierre, C., 2010. "Node sampling for nonlinear vibration analysis of structures with intermittent contact". *AIAA Journal,* **48**(9), pp. 1903–1915.

[42] D'Souza, K., Saito, A., and Epureanu, B. I., (submitted for publication). "Reduced order modeling for nonlinear analysis of cracked mistuned multi-stage bladed disk systems". *AIAA Journal*.

[43] Marinescu, O., Epureanu, B. I., and Banu, M., (submitted for publication). "Reduced-order models of mistuned cracked bladed disks". *Journal of Vibration and Acoustics*.

[44] D'Souza, K., and Epureanu, B. I., (submitted for publication). "A statistical characterization of the effects of mistuning in multi-stage bladed disks". *Journal of Turbomachinery*.

[45] Yang, M.-T., and Griffin, J. H., 2001. "A reduced-order model of mistuning using a subset of nominal system modes". *Journal of Engineering for Gas Turbines and Power,* **123**(4), pp. 893–900.

[46] Feiner, D. M., and Griffin, J. H., 2002. "A fundamental model of mistuning for a single family of modes". *Journal of Turbomachinery,* **124**(4), pp. 597–605.

[47] Feiner, D., and Griffin, J., 2004. "Mistuning identification of bladed disks using a fundamental mistuning model–part i: Theory". *Journal of Turbomachinery,* **126**(1), pp. 150–158.

[48] Lim, S., Bladh, R., Castanier, M. P., and Pierre, C., 2007. "Compact, generalized component mode mistuning representation for modeling bladed disk vibration". *AIAA Journal,* **45**(9), pp. 2285–2298.

[49] Madden, A., Castanier, M., and Epureanu, B., 2009. "Reduced-order model construction procedure for robust mistuning identification of blisks". *AIAA Journal,* **46**(11), pp. 2890–2898.

[50] Mignolet, M., Rivas-Guerra, A., and Delor, J., 2001. "Identification of mistuning characteristics of bladed disks from free response data–part i". *Journal of Engineering for Gas Turbines and Power,* **123**(2), pp. 395–403.

[51] Lim, S.-H., 2005. "Dynamic analysis and design strategies for mistuned bladed disks". PhD thesis, The University of Michigan, Ann Arbor.

[52] Judge, J., Pierre, C., and Ceccio, S., 2009. "Experimental mistuning identification in bladed disks using a component-mode-based reduced-order model". *AIAA Journal,* **47**(5), pp. 1277–1287.

[53] Holland, D., Epureanu, B., and Filippi, S., 2010. "Damping identification for mistuned blisks". In Proceedings of the ASME International Design Engineering Technical Conferences, American Society of Mechanical Engineers, pp. 1–12.

[54] Rösel, R., 1973. "On the interpretation of structural damping". *Journal of Applied Mathematics and Mechanics / Zeitschrift fr Angewandte Mathematik und Mechanik,* **53**, pp. 329–332.

[55] Holland, D., Epureanu, B., and Filippi, S., 2012. "Structural damping identification for mistuned bladed disks and blisks". *Journal of Vibration and Acoustics,* **134**(2), pp. 1–3.

[56] Holland, D., Rodgers, J., and Epureanu, B., (submitted for publication). "Measurement point selection and modal damping identification for bladed disks". *Mechanical Systems and Signal Processing.*

[57] Allemang, R., 2003. "The modal assurance criterion - Twenty years of use and abuse". *Sound and Vibration,* **37**(8), pp. 14–23.

[58] Judge, J. A., 2002. "Experimental investigations of the effects of mistuning on bladed disk dynamics". PhD thesis, The University of Michigan, Ann Arbor.

[59] Holland, D., and Epureanu, B., (to be submitted for publication). "Hybrid modal damping identification for bladed disks". *Mechanical Systems and Signal Processing.*